

Review

Contemporary Developments in Ferrocene Chemistry: Physical, Chemical, Biological and Industrial Aspects

Umair Rauf ¹, Ghulam Shabir ¹, Saba Bukhari ¹, Fernando Albericio ^{2,3,*} and Aamer Saeed ^{1,*}

- ¹ Department of Chemistry, Quaid-I-Azam University, Islamabad 45320, Pakistan; urauf@chem.qau.edu.pk (U.R.); shabirg@yahoo.com (G.S.); sababukhari021@gmail.com (S.B.)
- ² Peptide Science Laboratory, School of Chemistry and Physics, University of KwaZulu-Natal, Westville, Durban 4000, South Africa
- ³ CIBER-BBN, Networking Centre on Bioengineering, Biomaterials and Nanomedicine, Department of Organic Chemistry, University of Barcelona, 08028 Barcelona, Spain
- * Correspondence: albericio@ukzn.ac.za (F.A.); asaeeed@qau.edu.pk (A.S.)

Abstract: Ferrocenyl-based compounds have many applications in diverse scientific disciplines, including in polymer chemistry as redox dynamic polymers and dendrimers, in materials science as bioreceptors, and in pharmacology, biochemistry, electrochemistry, and nonlinear optics. Considering the horizon of ferrocene chemistry, we attempted to condense the neoteric advancements in the synthesis and applications of ferrocene derivatives reported in the literature from 2016 to date. This paper presents data on the progression of the synthesis of diverse classes of organic compounds having ferrocene scaffolds and recent developments in applications of ferrocene-based organometallic compounds, with a special focus on their biological, medicinal, bio-sensing, chemosensing, asymmetric catalysis, material, and industrial applications.

Keywords: ferrocene; synthesis; applications; asymmetric catalysis; chemosensors; bioreceptors



Citation: Rauf, U.; Shabir, G.; Bukhari, S.; Albericio, F.; Saeed, A. Contemporary Developments in Ferrocene Chemistry: Physical, Chemical, Biological and Industrial Aspects. *Molecules* **2023**, *28*, 5765. <https://doi.org/10.3390/molecules28155765>

Academic Editor: Andrea Penoni

Received: 8 June 2023

Revised: 26 July 2023

Accepted: 26 July 2023

Published: 30 July 2023



Copyright: © 2023 by the authors. Licensee MDPI, Basel, Switzerland. This article is an open access article distributed under the terms and conditions of the Creative Commons Attribution (CC BY) license (<https://creativecommons.org/licenses/by/4.0/>).

1. Introduction

Ferrocene is an organometallic compound consisting of two cyclopentadienyl rings bound to a central iron atom. On account of its unique electronic and structural properties, ferrocene has found a wide range of applications in various fields, such as fuel additives to improve their performance and reduce emissions; electrochemical sensors to detect the presence of various molecules and ions in solutions, including glucose, dopamine, and heavy metals; catalysts in various organic reactions, including oxidation, hydrogenation, and cross-coupling reactions; and medicinal chemistry in the development of anticancer, antiviral, and antimicrobial drugs. Ferrocene derivatives have been used to synthesize a wide range of materials, including polymers, liquid crystals, and nanoparticles, with diverse electronic and magnetic properties. Ferrocene is used as a potential electrode material in redox flow batteries due to its reversible redox behavior and high stability, and as a lubricant to improve the performance and longevity of engines and industrial machinery. The discovery of ferrocene and its structural characterization initiated an explosive rebirth of organometallic chemistry [1]. Nowadays, ferrocene derivatives have received much consideration owing to their outstanding properties like thermal and photochemical inertness and their exceptional and stable electrochemical properties due to an electron donor–acceptor conjugated structure and an efficient redox couple of $\text{Fe}^{2+}/\text{Fe}^{3+}$ [2–4]. The development of ferrocene unveiled new horizons of chemistry that are deeply rooted in the interpretation of its structure, way of bonding, and chemical inertness, and paved the way for the escalating field of organometallic chemistry itself [5]. Ferrocene and its derivatives are laurel molecules, and the synthesis of this sandwich system—specifically its flavors, utilization in homogeneous catalysis as a novel resource, including its usage in polymer chemistry, and also as a fuel additive—has triggered the hasty advancement of this family

of compounds over the past sixty years [6–8]. Polymers with pendant ferrocene units are a marvelous family of organometallic polymers elevating substantial attention, chiefly owing to their idiosyncratic properties and the high chemical inertness of ferrocene [9]. These polymeric materials, either as ferrocenyl or ferrocendiyl groups, deliver various effects including conducting, redox, optoelectronic, catalytic, and biological effects with potential for applications such as radiation absorbers, combustion regulators, highly effective non-toxic medicinal substances, components of various redox systems, etc. [10]. Ferrocene-grafted polymers can easily migrate from the propellant system through diffusion as well as by surface migration. This migration leads to further abolishing the propellant homogeneity and allows higher combustion rates only on the surface of the propellant rather than the whole propellant [11]. Recent trends led to the development of established drugs by metallocene-appended organometallic moieties through drug reprofiling strategy as a proxy of the chemotherapy of tachyphylaxis in cancer and many tropical diseases [12]. The substitution of the phenyl or hetero-aryl group with a ferrocene scaffold in organic molecules afforded a momentous alteration not only in the physicochemical properties of drugs, but also ameliorated the potential of biologically active ligands. Moreover, the success of ferrocene owes to its intrinsic solidity in air, heat, and light, as well as low toxicity, low cost, and reversible redox properties. In the presence of oxidizing agents, the oxidation of ferrocene to ferrocenium cation occurs, which is characterized by the naked eye, i.e., red coloration. The well-known application of this oxidized ferrocene comprises sensing, corrosion inhibition, and drug delivery in cancer therapy [13–15]. Indeed, based on an extensive database of knowledge regarding ferrocene, numerous articles have been published in several fields concerning applications like water treatment, lithography, information storage, molecular logics, pharmacology, agriculture, biosensors, chemosensors, analytical applications, etc., during 2010–2020. Also, ferrocene derivatives are leading targets primarily for power conversion, and their thermo- and electrochemical applications have been extensively studied due to astonishing features like high thermal stability, higher photoconductivity, and the better chemical stability of ferrocene derivatives [16].

In the past ten years, due to the iron chemistry of ferrocene derivatives, there has been a spate of review articles on the synthesis and applications of ferrocenyl conjugates, which include the research areas of materials science, asymmetric catalysis [17], electrochemistry, and bio-organometallics [18,19]. Saeed et al. reviewed the synthesis, biological activities, and some important applications of ferrocene derivatives [20]. X. Zhai et al. published a review on recent research progress in the synthesis, properties, and applications of ferrocene-based derivatives and polymers with azobenzene [21]. In 2017, a review article with the title “Ferrocene-based redox-responsive polymer gels: Synthesis, structures and applications” was published by Jialiang and co-workers [22]. Similarly, A. Khan and colleagues presented another review on the synthesis and applications of ferrocene-based electro- and photo-responsive materials in 2018 [23]. During 2015–2019, more focused reviews seemed to cover medicinal outlooks including anti-malarial and anticancer activities of ferrocene derivatives [24], antimicrobial activities of ferrocene conjugates [25], tetrazole-based ferrocenyl compounds as anti-tuberculosis agents [26], and the anti-infective potential of ferrocene derivatives [27].

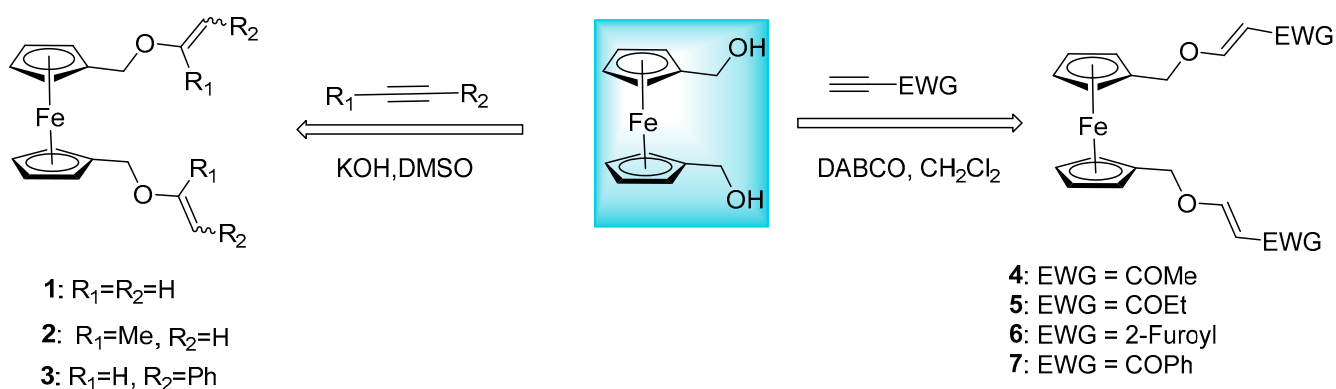
The aim of our work is to provide a comprehensive review of recent trends in synthetic strategies of ferrocene derivatives and their versatile pharmacological, agricultural, biosensing, chemosensing, biological, electrochemical, industrial, and materials science applications, covering the period from 2016 to the start of 2023.

2. Synthesis of Different Ferrocene-Based Compounds

2.1. Synthesis of Ferrocenyl Ethers

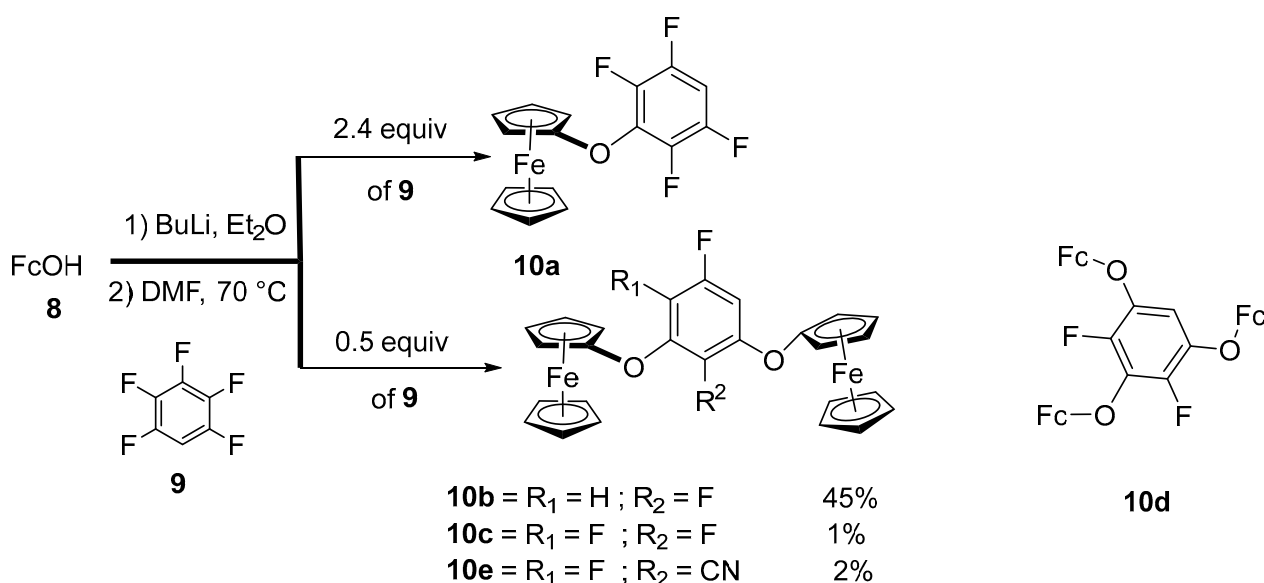
Ferrocene-containing aliphatic and aromatic ethers are of special interest due to their beauty and electrochemical properties, but their synthesis has always been difficult. To respond to this challenge, Oparina and co-workers introduced a novel nucleophilic addition reaction of ferrocene 1,1-bis(hydroxymethyl) to different alkyne derivatives (Scheme 1).

This base-catalyzed addition could be performed on acetylene, propyne, phenylethyne, alkyl propionates, and acylacetylenes to obtain various divinyl ferrocenyl ethers with a remarkable yield value in the range of 73–98% [28].



Scheme 1. Synthesis of ferrocene-based diethenyl ethers.

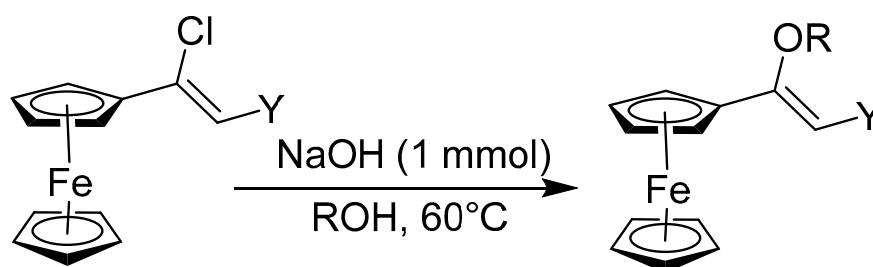
In a relevant work, multi-ferrocenyl aryl ethers of general type $C_6H_{0-3}F_{1-5}(OFc)_{1-5}$ were synthesized through base-catalyzed nucleophilic aromatic substitution reaction on aryl fluorides. Preparation of mono-, di-, and trisubstituted fluorobenzene was simply carried out through the replacement of one, two, and three fluorine atoms by FcO, respectively (Scheme 2). Further tetra and penta (FcO)-substituted arenes were also prepared by the same procedure and identified by spectroscopic analysis, and XRD confirmed their substitution patterns [29].



Scheme 2. Synthesis of ferrocenyl aryl ethers.

It has been reported that different primary alcohols and ferrocene chlorovinyl derivatives can form C-O bonds easily, leading to the production of ferrocenyl vinyl ethers (Scheme 3). The approach that is being offered has a high yield and provides the products quickly. For a variety of primary alcohols, functionalized ferrocenyl chlorovinyl derivatives (-CHO, -CN, and C(CN)₂) were shown to be well tolerated. All the ferrocenated vinyl ethers are novel and have not been previously reported. When the optical metal-detecting capabilities of the 1,2- and 1,3-diol-derived vinyl ether derivatives were examined, selectivity for Cu²⁺ ions was found. Among all the other metal ions put to the test, the

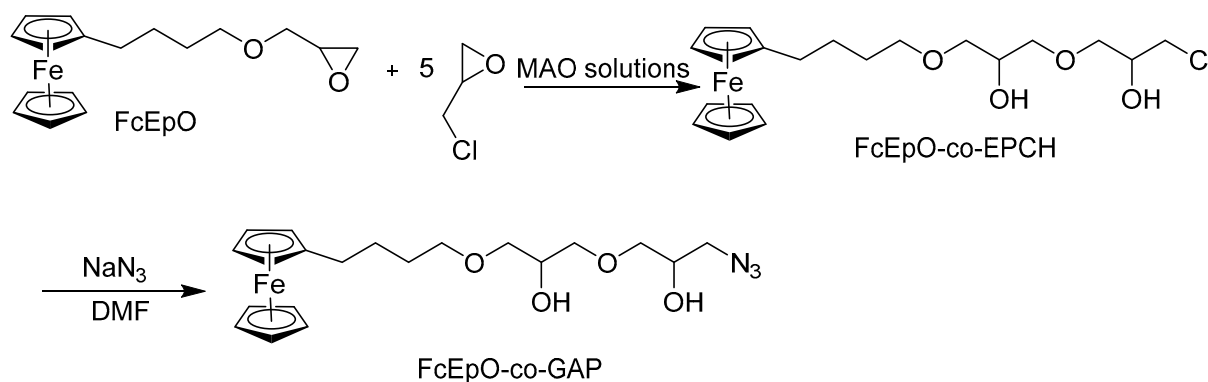
ferrocenated malenonitrile-containing vinyl ether showed high sensitivity and selectivity toward Cu^{2+} [30].



R= Aliphatic, Diols, Benzylic,
Heteroaromatic

Scheme 3. Synthesis of ferrocene-substituted vinyl ethers.

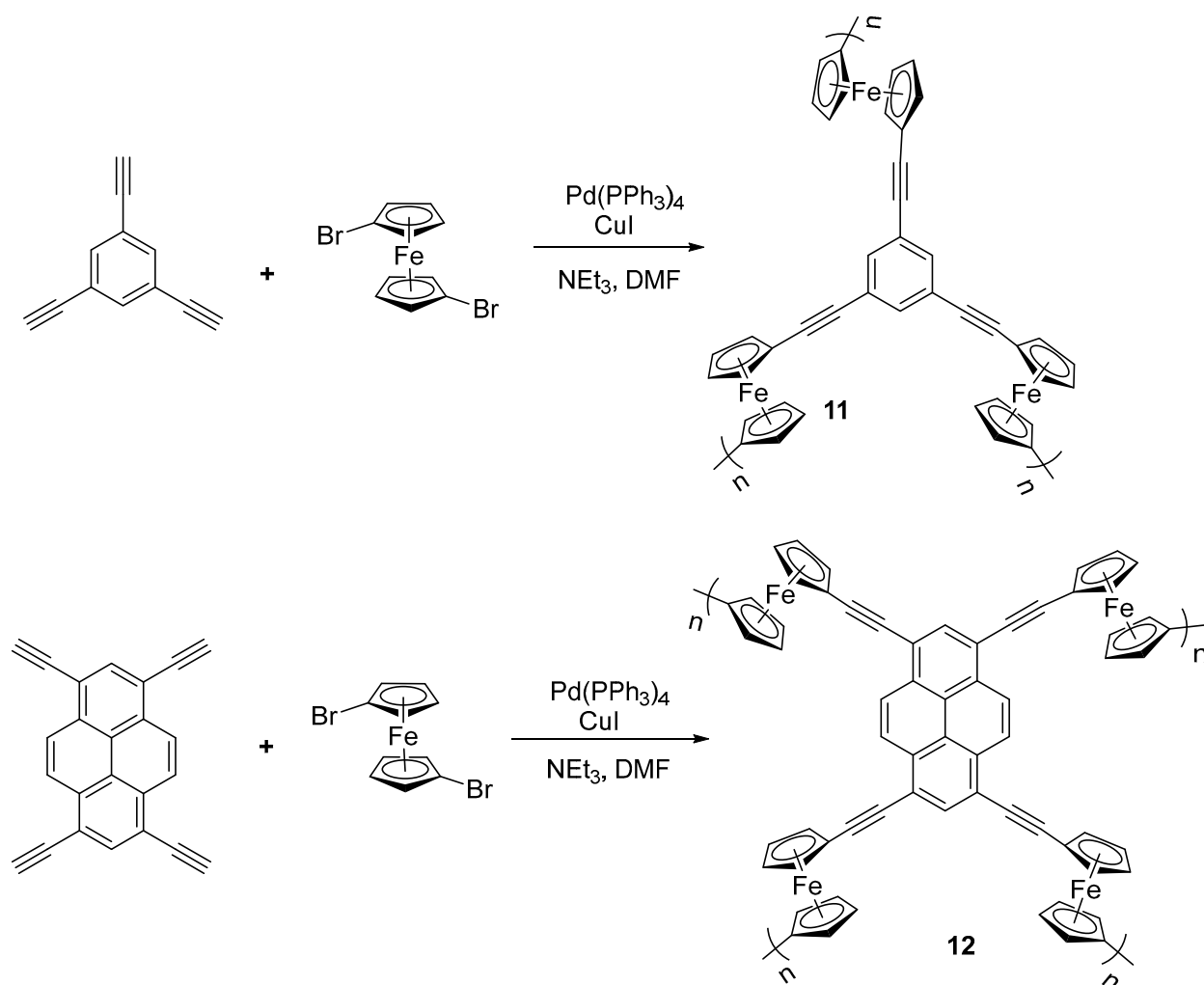
By polymerizing 2-[(4-ferrocenylbutoxy) methyl] oxirane (FcEpo) using toluene solution of methylaluminoxane (MAO) as the catalyst, poly(ferrocenyl glycidyl ether) was synthesized. In order to create another ferrocenyl-based poly, 2-[(4-ferrocenylbutoxy) methyl] oxirane and epichlorohydrin were copolymerized (epichlorohydrin). GAP, a ferrocenyl-based poly (glycidyl azide), was created by treating sodium azide with this copolymer in a room-temperature DMF solvent (Scheme 4). By using FT-IR, ^1H NMR, UV-VIS, TGA, DSC, and GPC analysis, the synthesized ferrocenyl-based polymers were evaluated for their characteristics [31].



Scheme 4. Synthesis of poly (FcEpo-co-EPCH) and poly (FcEpo-co-GAP).

2.2. Synthesis of Alkynylated Ferrocenes

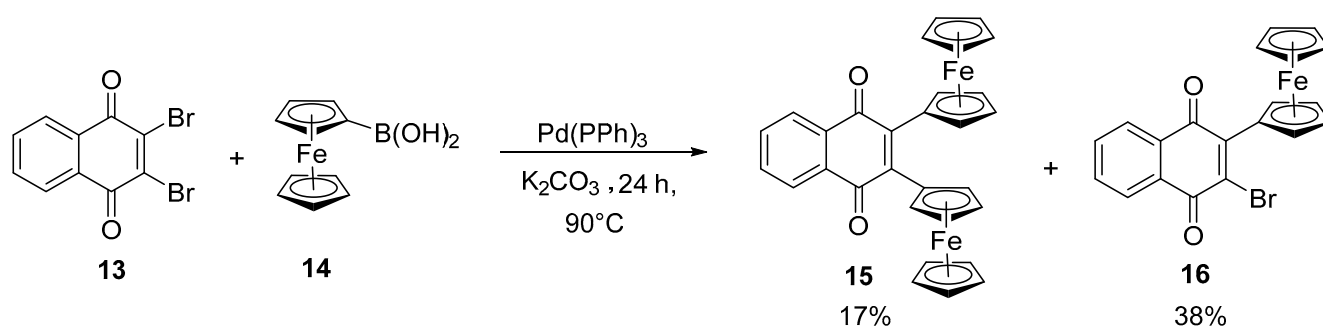
In a promising work, ferrocene was grafted to microporous polymers of 1,3,5-triethynyl benzene and 1,3,6,8-tetraethynyl analogs using Pd-catalyzed Sonogashira Hegihara cross-coupling chemistry (Scheme 5). The molecular structures of these compounds were confirmed by FTIR and ^{13}C NMR spectroscopy, and the presence of iron was confirmed through X-ray photoelectron spectroscopy. These synthesized compounds exhibited higher thermal stability, porosity, and variable ferromagnetic properties [32].



Scheme 5. Synthesis of ferrocene-functionalized triethynyl and tetraethynyl benzene.

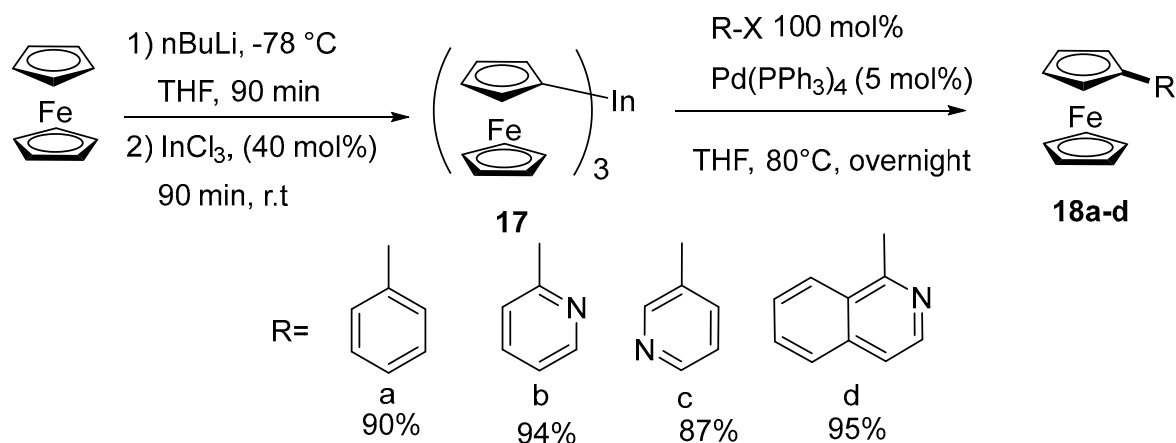
2.3. Synthesis of Vinyl and Aryl-Substituted Ferrocene

Ertas and co-workers used the Pd-assisted Suzuki–Miyaura coupling method to synthesize ferrocenyl–naphthoquinone derivatives, and their structure was characterized by ^1H NMR and ^{13}C NMR spectroscopy (Scheme 6). This coupling reaction was also performed through microwave irradiation, but the yield was not as effective as compared with the reported protocol. Furthermore, the reported compound **16** was thought to be the first innovative ferrocene-based H_2O_2 chemosensor [33].



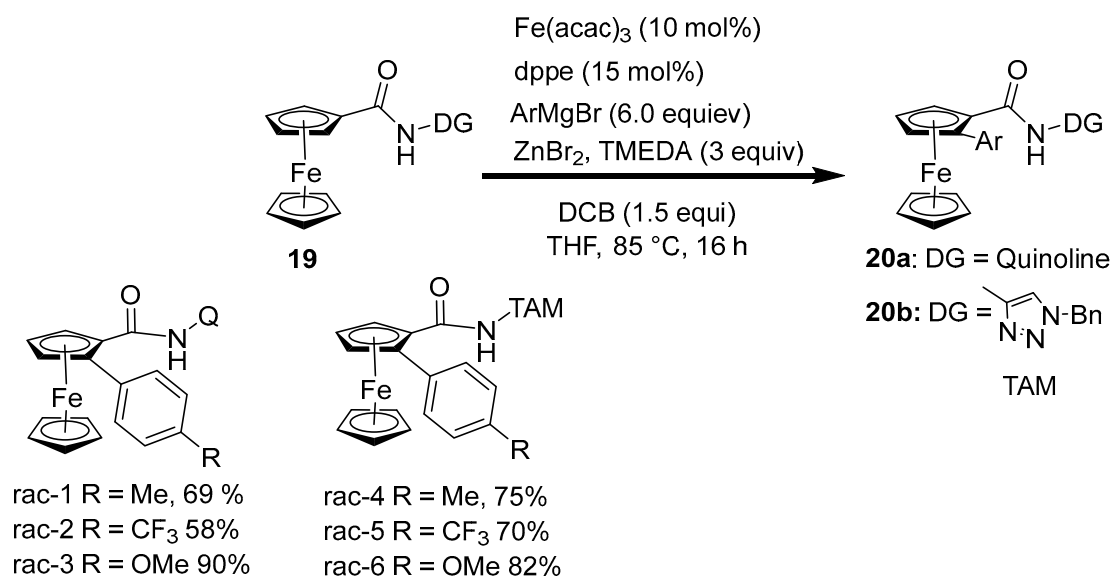
Scheme 6. Suzuki–Miyaura coupling reaction.

Mato described a procedure for the preparation of mono and planer asymmetric disubstituted ferrocenyl conjugates by using tri-ferrocenylindium intermediate followed by a Pd-assisted cross-coupling reaction [34]. Under mild conditions, a series of organic electrophiles were treated with Fc_3In (**17**) for the synthesis of monosubstituted ferrocenyl compounds **18**_{a-d}. Plane chiral disubstituted ferrocenyl conjugates were also prepared by the same coupling mechanism (Scheme 7).



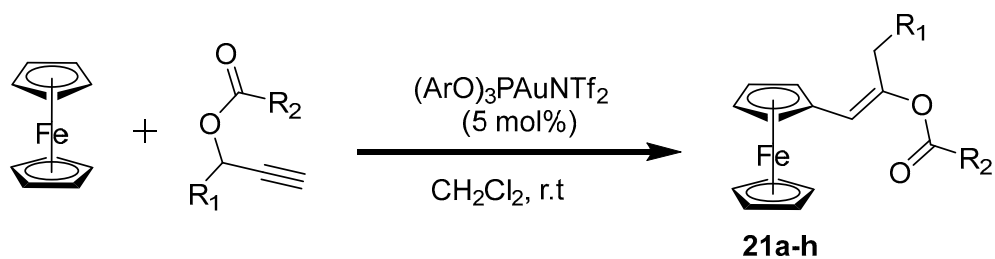
Scheme 7. Synthesis of mono-substituted ferrocene derivatives through coupling reaction.

In an advanced work, Schmiel and co-authors reported a novel procedure for the ortho-substitution of ferrocenyl units by C–H activation using sp^2 – sp^2 coupling reactions [35]. The excellent yield of methylation and ethylation was observed, while stereoselective phenylation of **20a** and **20b** with asymmetric ligand resulted in a remarkable yield of a product with 46% of ee (Scheme 8).



Scheme 8. Synthesis of ortho-substituted ferrocenyl conjugates.

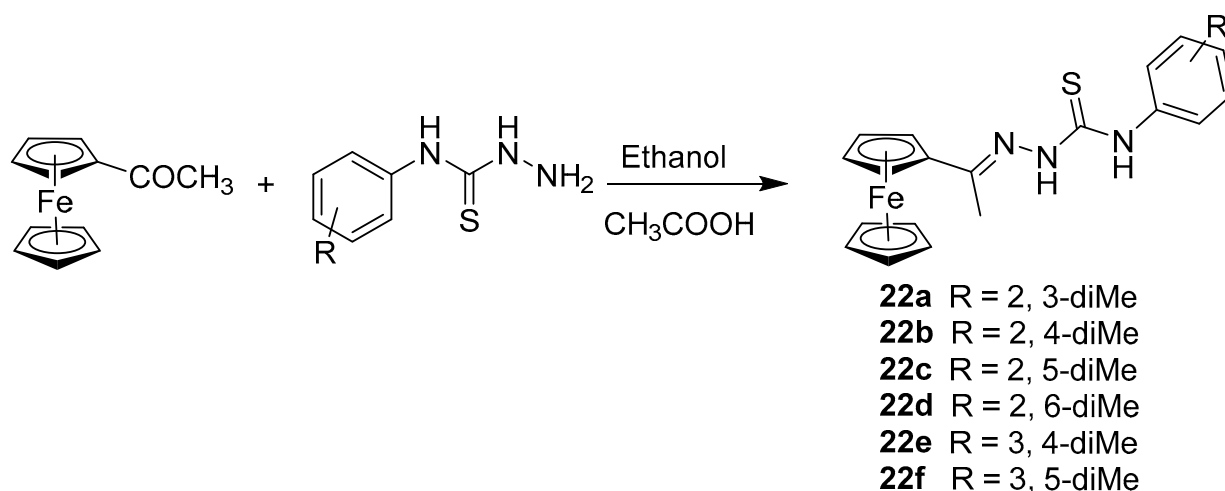
Lopez's group focused their research on the development of a novel gold-catalyzed C–H activation reaction of ferrocene-appended prop-2-ynoic acid [36]. The reaction proceeded through the substitution of ferrocene by capturing vinyl gold carbenoid, generated from propargylic ester. Isotopic labeling experiments described the mechanism as an electrophilic substitution reaction in which 1–2 rearrangements produced metal vinyl carbene that acts as an electrophile that was attacked by ferrocene derivatives via C–H activation (Scheme 9).



| Entry | R ₁ | R ₂ |
|-------|----------------|----------------|
| a | Ph | Me |
| b | Ph | t-But |
| c | Ph | Ph |
| d | 4-Me-Ph | Me |
| e | 3-Me-Ph | Me |
| f | 2-Me-Ph | Me |
| g | 4-MeO-Ph | Me |
| h | 4-F-Ph | Me |

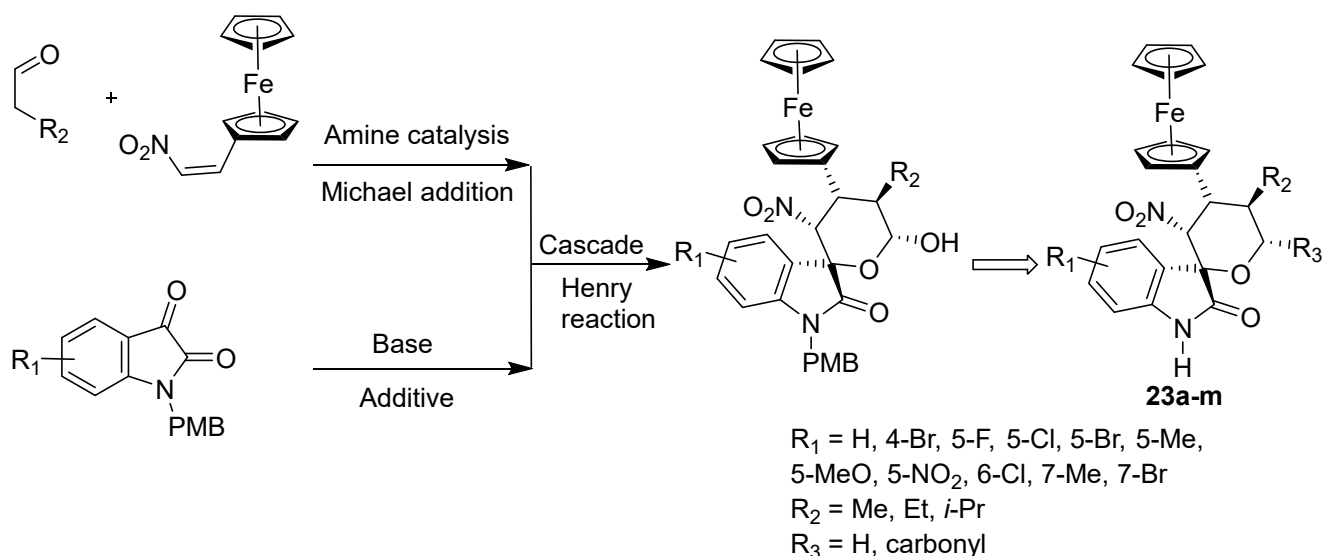
Scheme 9. Synthesis of ferrocene-based prop-2-ynoic acid derivatives.

Ferrocene and its derivatives represent a crucial class of organometallic compounds with significant biological activity. By condensing acetyl ferrocene with variously substituted thiosemicarbazides, six new ferrocene-based thiosemicarbazones have been created (Scheme 10). Furthermore, the theoretical features for putative antiviral properties of produced compounds were investigated using cutting-edge computational docking methodology. The Mpro protein of SARS-CoV-2, an essential protein for viral replication, was docked with all six chemicals [37].



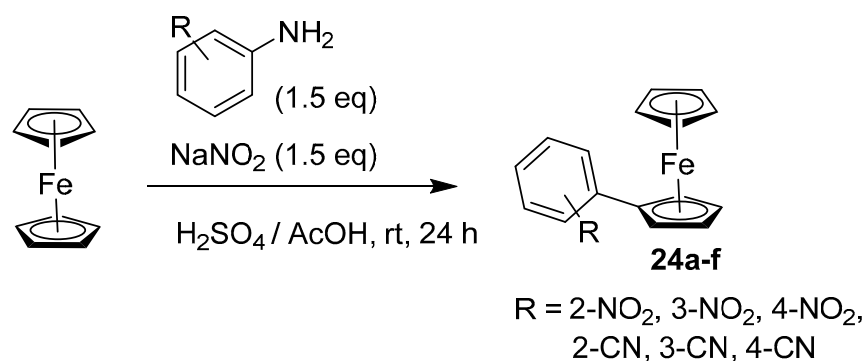
Scheme 10. Synthesis of ferrocene-based thiosemicarbazones.

Organocatalysis was used to create several spirooxindole–ferrocene hybrids with four or five contiguous chiral centers. Additionally, mechanistic studies revealed that compound **23d** enhanced oxidative damage, caused apoptosis, and reduced MDM2-mediated p53 degradation (Scheme 11). According to molecular docking research, **23d** attaches to MDM2 by imitating the Trp23 and Leu26 residues of p53. This research may serve as a foundation for the creation of innovative, multipurpose MDM2 inhibitors. The research of other derivatives from this library and the application of organocatalysis in the creation of novel molecules may result in the discovery of new potential lead compounds for cancer-targeted therapy [37].



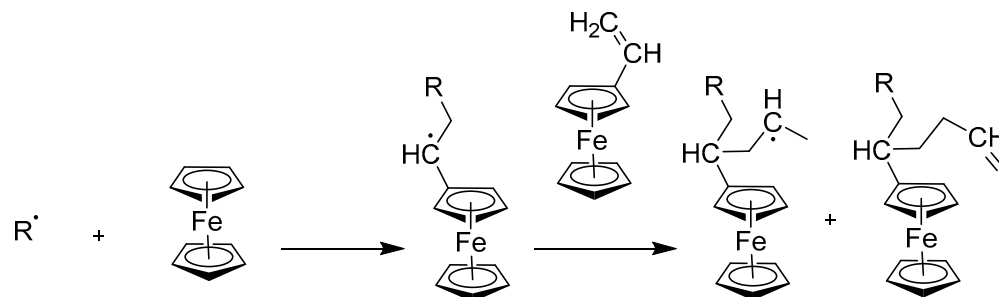
Scheme 11. Asymmetric synthesis of chiral spirocyclic oxindole–ferrocene hybrids.

Ferrocene is a typical organometallic compound, which has a sandwich structure with strong hydrophobicity and stability. In this study, the nitro- and cyanophenylferrocene series' physicochemical characteristics were identified, and their biological activity as androgen receptor (AR) antagonists was assessed (Scheme 12). Inferring that the hydrophobicity of ferrocene is ideal for its use as a hydrophobic core structure of nuclear receptor ligands, ferrocene derivatives showed hydrophobicity parameter values in the range of 2.54 to 3.23, depending on the substituents. The synthetic ferrocene derivatives demonstrated AR-antagonistic action, and 3-nitrophenylferrocene **24a** was the most effective of these, with an IC_{50} value of 0.28 M. As AR antagonists, the discovered compounds might be suitable for further structural development. These results confirm the usefulness of organometallic substances as structural options for drug discovery [38].



Scheme 12. Synthesis of phenyl ferrocene derivatives.

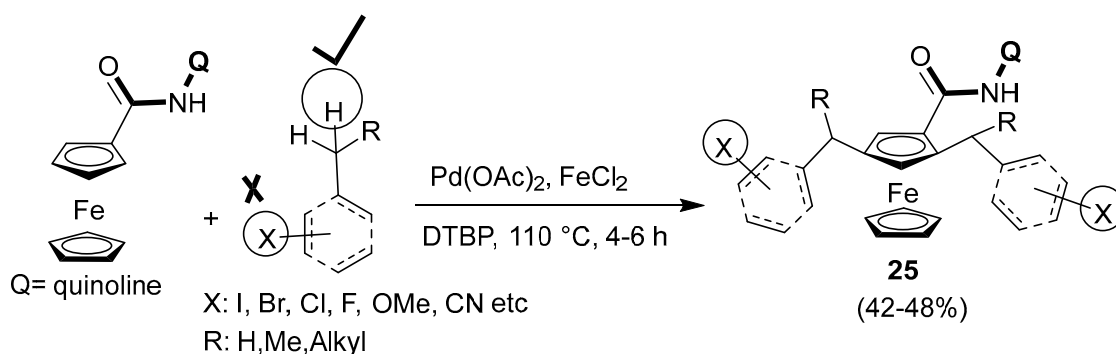
Effective composite solid propellants have low-pressure exponents and a consistent burning rate (BR). The addition of burning rate catalysts (BRCs) to the propellant system is one of the finest options for achieving the optimal performance of propellants (Scheme 13). BRCs are incredibly significant in composite propellants because of their unique ability to increase the operating effectiveness of solid propellants. Numerous beneficial varieties of BRCs were synthesized for this purpose. Ferrocene-based compounds are a well-known type of BRC due to their superior ignition. However, the practical application of this new family of beneficial compounds as an ideal BRC is constrained by their significant migration and diffusion propensity during storage operations of composite solid propellants [39].



Scheme 13. Synthesis of poly (vinyl-Fc) by FRP of vinyl-Fc.

2.4. Synthesis of Alkyl and N-Heteroatom-Substituted Ferrocene Derivatives

Satter and Kumar reported a new pathway for C-C bond formation between ferrocene and other alkyl or aryl substituents catalyzed by hybrid transition metal catalysts [40]. The reported work indicated an innovative sp^2 - sp^3 coupling reaction for the first time where the C-H bond was coupled for new C-C bond formation, chiefly directed by ligands (Scheme 14). The reaction could be a useful approach for the synthesis of ferrocene-functionalized biologically active drugs.

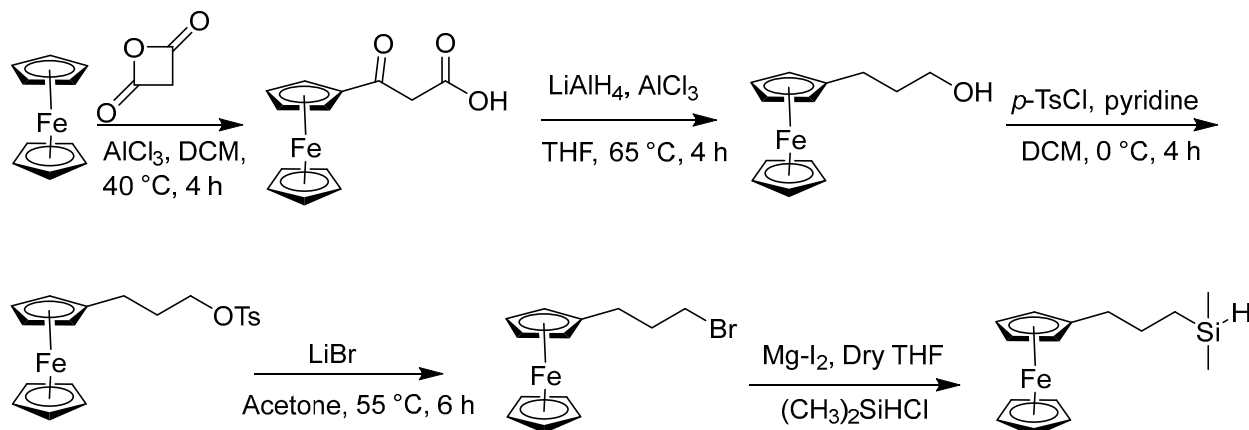


Scheme 14. Alkylation of ferrocenyl compounds by means of Pd-Fe hybrid catalyst.

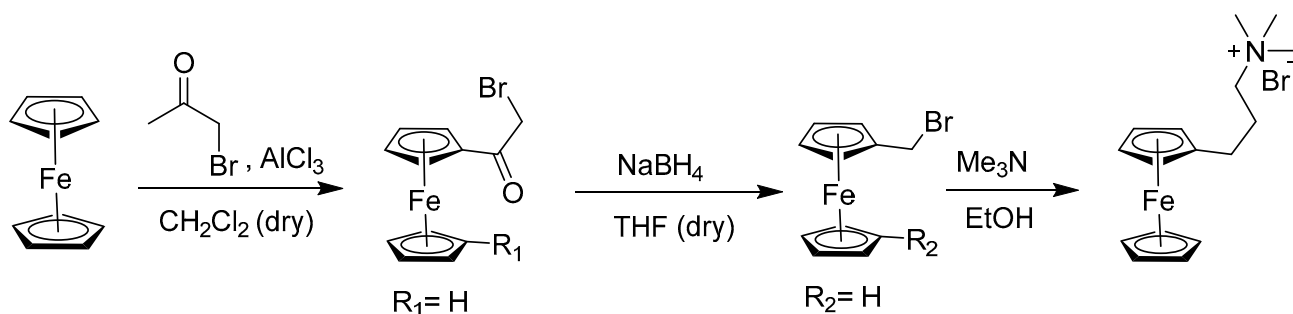
The synthesis of thiol, silyl, and halogen derivatives of alkyl-ferrocene was made simple and affordable. In this procedure, ferrocene is functionalized with terminal carboxylic acid using cyclic anhydrides as a precursor to be purified using an acid-base workup. With good to exceptional yields, the synthetic technique uses moderate reaction conditions (Scheme 15). To create polymeric binders with a faster burn rate for usage in composite solid propellant for aerospace applications, the ferrocene-alkyl silane and ferrocene-alkyl-thiol are covalently grafted to the pendent vinylic groups of HTPB [41].

By utilizing the redox reactions of water-soluble organic molecules, an aqueous organic flow battery (AOFB) holds immense potential as an energy storage solution for fluctuating renewable electricity (Scheme 16). The absence of suitable organic molecules for catholytes is impeding current progress; however, it is yet unknown how catholyte structure affects battery longevity. In water, six ferrocene derivatives with specifically tuned chemical structures go through reversible redox processes, and the redox potentials of these energized

forms are inversely related to their LUMO energies. In symmetric and complete flow cells, the stability of the ferrocene derivatives was assessed. Calculations using density function theory (DFT) and actual findings show that the localized LUMO density on Fe causes a rapid capacity fading, with BQHFc having the lowest LUMO density [42].



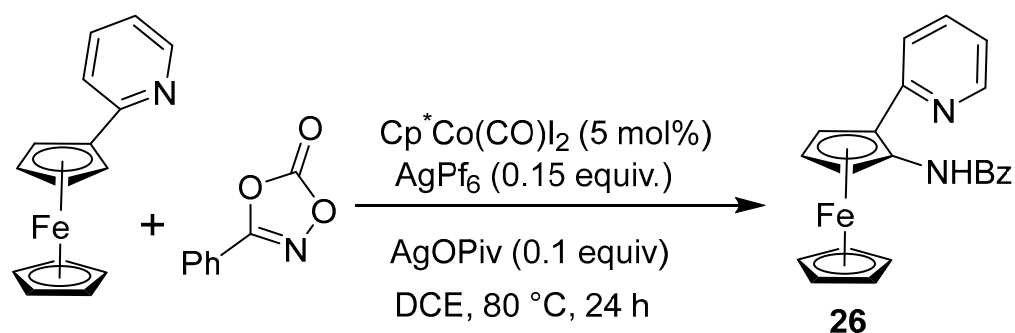
Scheme 15. Schematic representation for the synthesis of *n*-(dimethylsilane)alkyl ferrocene.



Scheme 16. Synthetic route for the ferrocene derivatives.

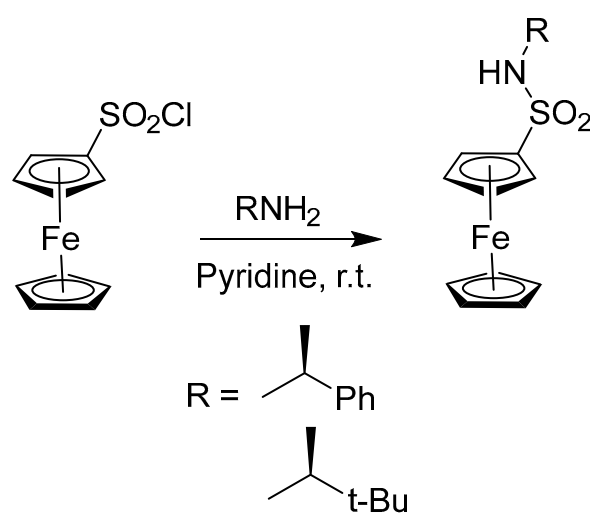
2.5. Synthesis of Ferrocenyl Derivative Directly Bonded with Heteroatom

Recent research reported the synthesis of cyclopentyl cobalt (III)-assisted carbon–heteroatom coupling reaction on a gram scale, using pyridylferrocene and dioxazolones under soft conditions with an impressive yield of 96% (Scheme 17). These ferrocene-based compounds could be used as effective catalysts due to the presence of N, N-bidentate ligands. Further, the replacement of the directing group could increase the efficiency of the reaction column, and the absolute configuration of selected enantiomers was determined by X-ray crystallographic analysis [43].



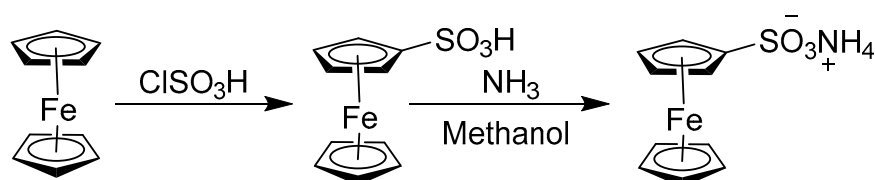
Scheme 17. Cyclopentyl cobalt (III)-assisted synthesis of N-substituted ferrocene derivatives.

The *ortho*-directed lithiation of chiral ferrocene sulfonamides, followed by a reaction with electrophilic reactants, was used to synthesize a number of 1,2-disubstituted planar chiral ferrocenes (Scheme 18). The various diastereoisomers could be separated in pure form, and the planar 1,2-functionalized ferrocene sulfonamides were produced in good yields. The planar chirality-relevant relative configurations of the chemical groups in positions 1 and 2 were recovered from NMR measurements, and the absolute configuration was established by X-ray crystallography. Modern quantum chemical algorithms were used to record, assign, and interpret experimental ECD and VCD spectra, allowing for an impartial examination of the several structural elements that influence the overall spectroscopic properties [44].



Scheme 18. Synthesis of chiral ferrocene sulfonamides.

The synthesis and application of redox-active organic species in aqueous redox flow batteries offer numerous opportunities for extensive and sustainable energy storage, which is necessary for sustainable development. Here, a stable and simple-to-synthesize sulfonated ferrocene derivative known as ferrocene ammonium sulfonate is disclosed. In zinc hybrid flow batteries, it served as a catholyte. With the electrolyte adjusted, the battery demonstrated good efficiency and capacity retention. After 100 continuous charge/discharge cycles with a current density of 20 mA/cm² and a supporting electrolyte of 0.5 M NaCl + 0.5 M NH₄Cl, the capacity retention achieved 92.55% (Scheme 19). This battery design proposes a concept for developing low-cost materials and improving capacity retention [45].

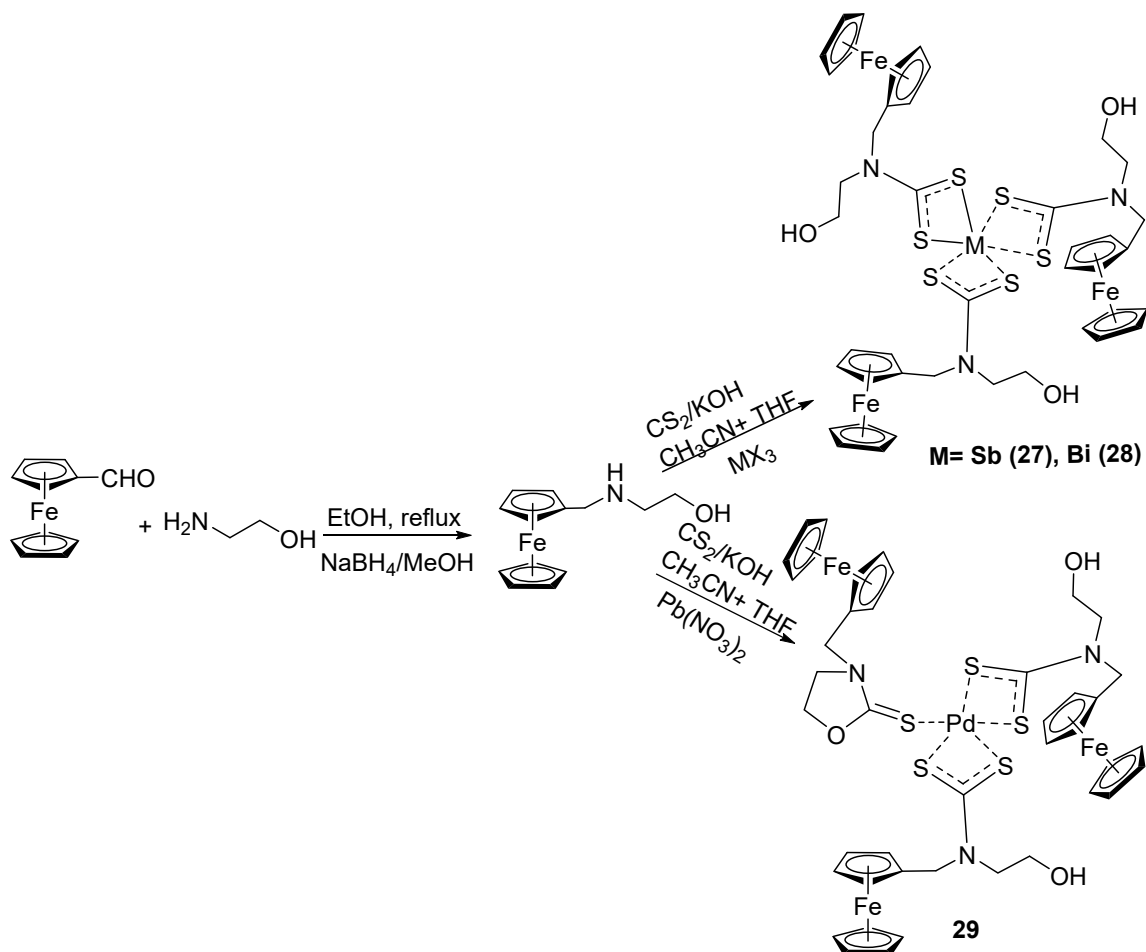


Scheme 19. Synthetic route of Fc-SO₃NH₄.

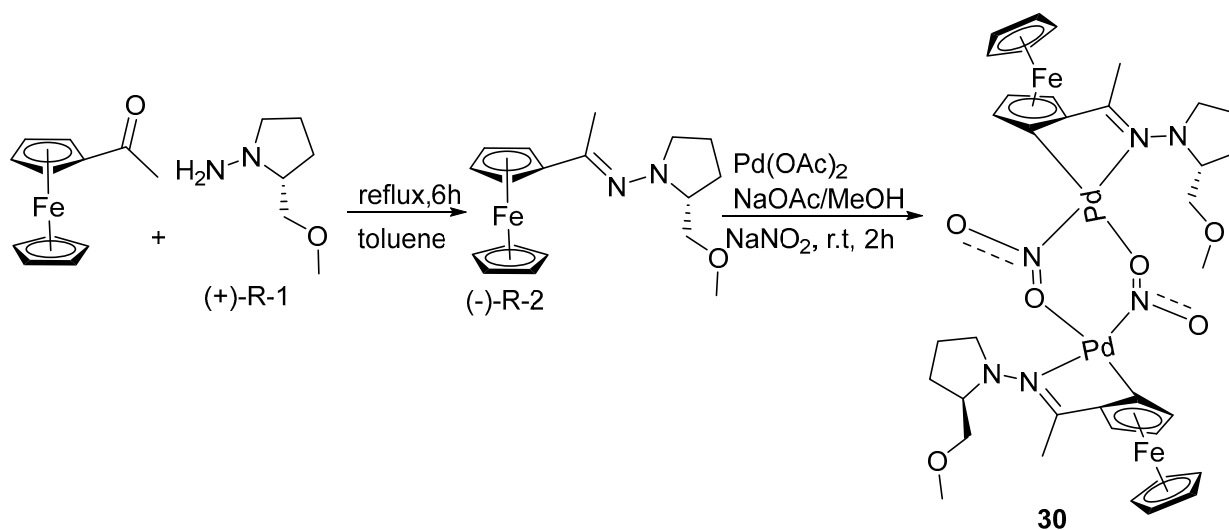
2.6. Synthesis of Ferrocene-Conjugated Metal Complexes

Three ferrocenyl-functionalized metal complexes (27–29) were synthesized using a newly reported synthetic procedure in which the ferrocene nucleus was converted to carbamate precursors that further developed into thiazolidine-containing metal complexes (Scheme 20). The geometry of these organometallic complexes was confirmed by spectroscopic studies and the XRD approach. All three complexes found their applications in the biological system, especially in a bacterial metabolic pathway study [46].

Gao and colleagues reported a rapid and efficient method for the synthesis of an advanced ferrocene-functionalized cyclopalladated complex by the reaction of acetyl ferrocene and chiral amines that produced orange-colored chiral ferrocenyl hydrazones that further reacted with Pd(OAc)₂ and generated red-colored cyclopalladated product **30** (Scheme 21). Biological screening revealed that the potency of the cyclic organometallic complex was 93-fold greater than the usual anticancer drug cisplatin [47].

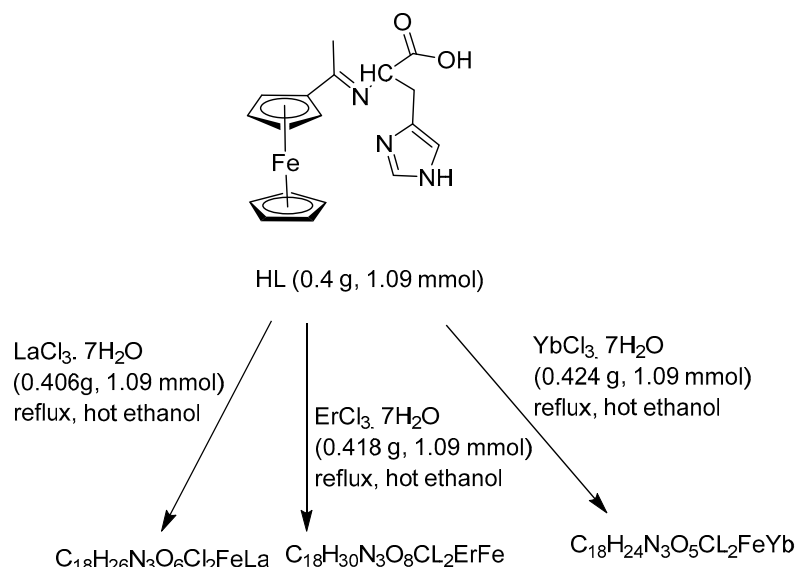


Scheme 20. Synthesis of ferrocene-grafted metal complexes.



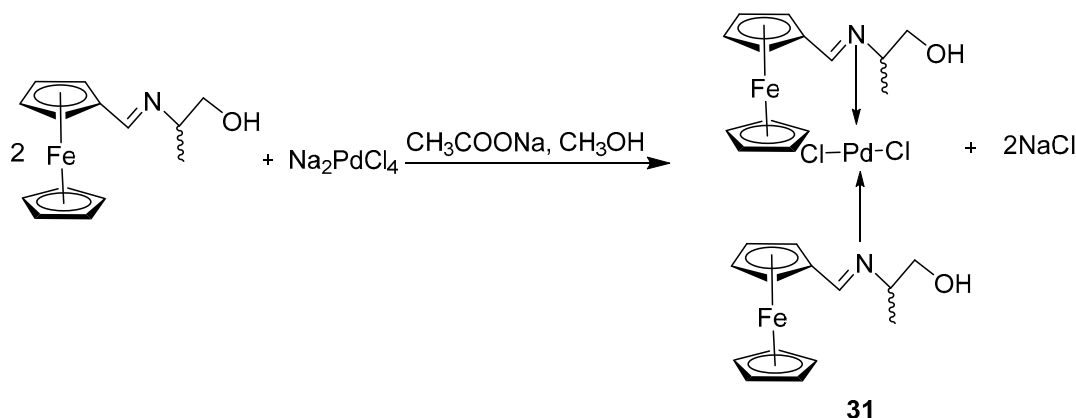
Scheme 21. Synthesis of ferrocene-based cyclopalladated complex.

As the primary components of proteins, amino acids are essential to all major biological processes. Schiff bases are biologically active molecules with a variety of pharmacological functions. Their La (III), Er (III), and Yb (III) metal complexes were accomplished as shown in Scheme 22. Different spectroscopic techniques, such as elemental analysis, FT-IR, mass, UV-Vis spectra, thermal analysis (TG), and scanning electron microscopy (SEM), were used to describe these metal complexes. The complexes were discovered to have octahedral geometry using the elemental analysis data, with the formula $[M(L)(H_2O)_2Cl]Cl \cdot nH_2O$ ($M = La(III), n = 2; Er(III), n = 4; \text{and } Yb(III), n = 1$). According to what has been determined, carboxylic oxygen, imidazole nitrogen, and azomethine nitrogen play a role in the ligand's mono-negative tridentate form of binding to the metal ions [48].



Scheme 22. Synthesis of lanthanides metal complexes.

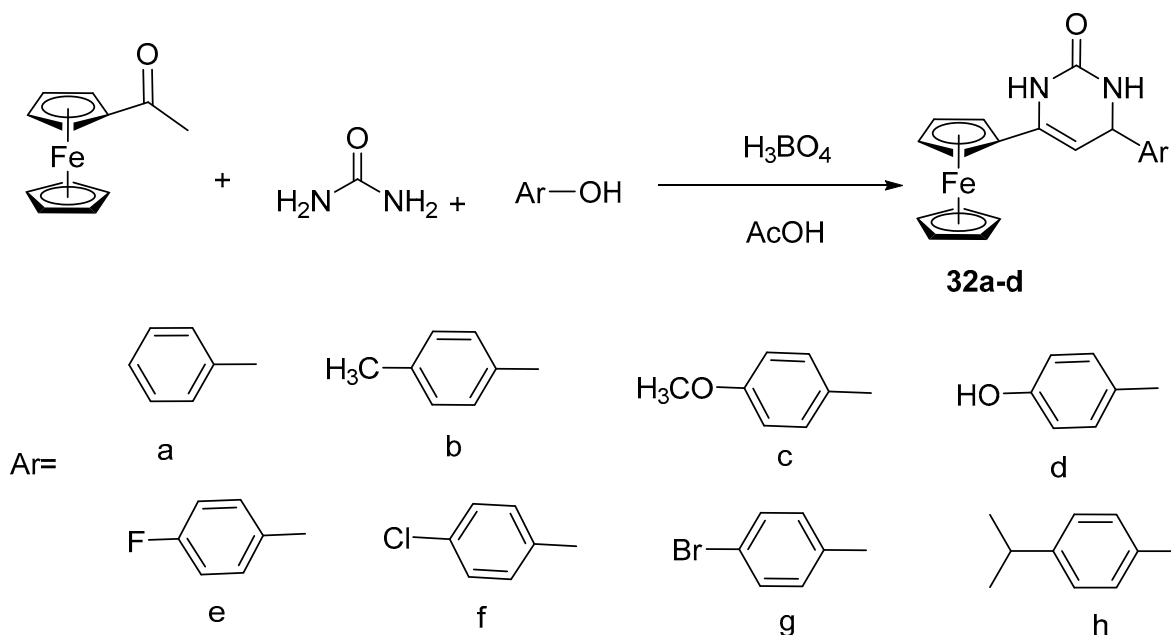
A two-step process was used to produce an organic bimetallic complex with a cross configuration. The combination of ferrocene carboxaldehyde and DL-alaninol produced the ferrocene–palladium (II) complex, which in turn formed the ferrocene–Schiff base (Scheme 23). The crystal structure revealed that two motifs exist as a racemate and have a trans structure opposite to cisplatin. Compound **31** was found to be less hazardous to normal cells and to effectively decrease the viability of many tumor cell lines, with efficacy up to 20-fold better than cisplatin. The induction of caspase-3-dependent apoptosis *in vitro* served as the mechanism of antiproliferation actions. Molecular docking was used to predict that the biological target of the synthesized compound was XIAP, which showed it was bound to the BIR3 protein [49].



Scheme 23. Synthesis of bimetallic complex with cross configuration.

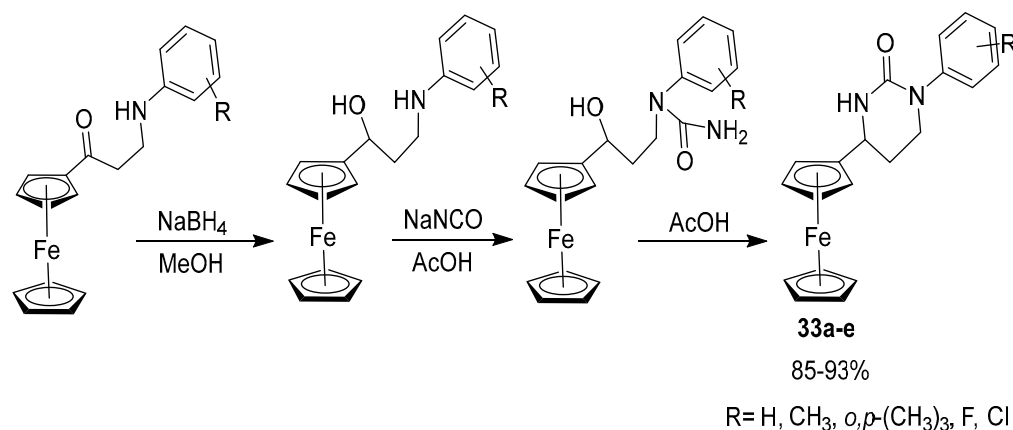
2.7. Synthesis of Ferrocene-Based Cyclic Urea

In a recent study, a highly efficient, cost-effective, and environmentally benign protocol named “Biginelli Reaction” was utilized for the preparation of various para-substituted phenyl-6-ferrocenyl 3,4-dihydropyrimidine derivatives (**32a–d**) [50]. In a one-pot reaction, various substituted benzaldehyde units, acylated ferrocene, and urea components were mixed, and different products with different ranges of yield were isolated and characterized by spectroscopic analysis (Scheme 24). Biological assays proved these compounds as promising candidates for drug testing.



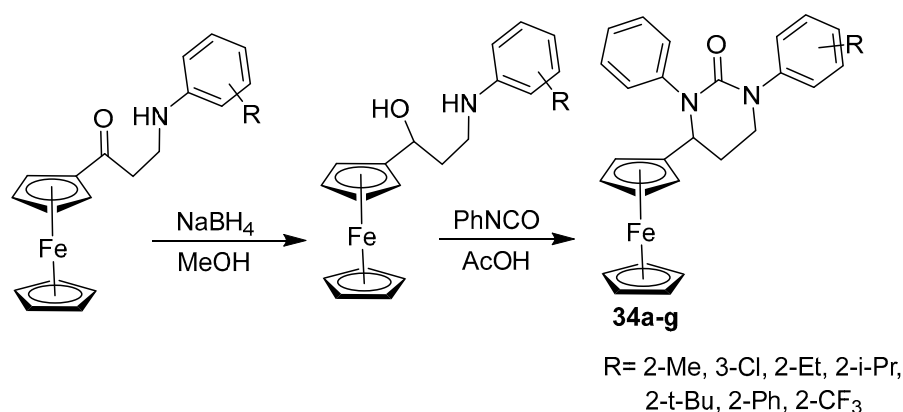
Scheme 24. Synthesis of 3,4-dihydropyrimidines via Biginelli reaction.

A process for synthesizing tetrahydropyrimidin-2(1H)-ones that contain ferrocene by starting with the appropriate 3-arylamino-1-ferrocenylpropan-1-ols and sodium cyanate (NaOCN) in the presence of glacial acetic acid was exercised. An intramolecular cyclization of 1,3-hydroxyurea produced in situ afforded eleven 1,3-amino alcohols containing ferrocene moiety, and the desired 1-aryl-4-ferrocenyltetrahydropyrimidin-2(1H)-ones (**33a–e**) were produced in good to high yields (up to 93%) (Scheme 25). Every product has been purified to a high level (>95%). A thorough structural characterization of the novel compounds, carried out using IR and NMR spectroscopy, is also described [51].



Scheme 25. A synthetic strategy to 1-aryl-4-ferrocenyltetrahydropyrimidin-2(1H)-ones.

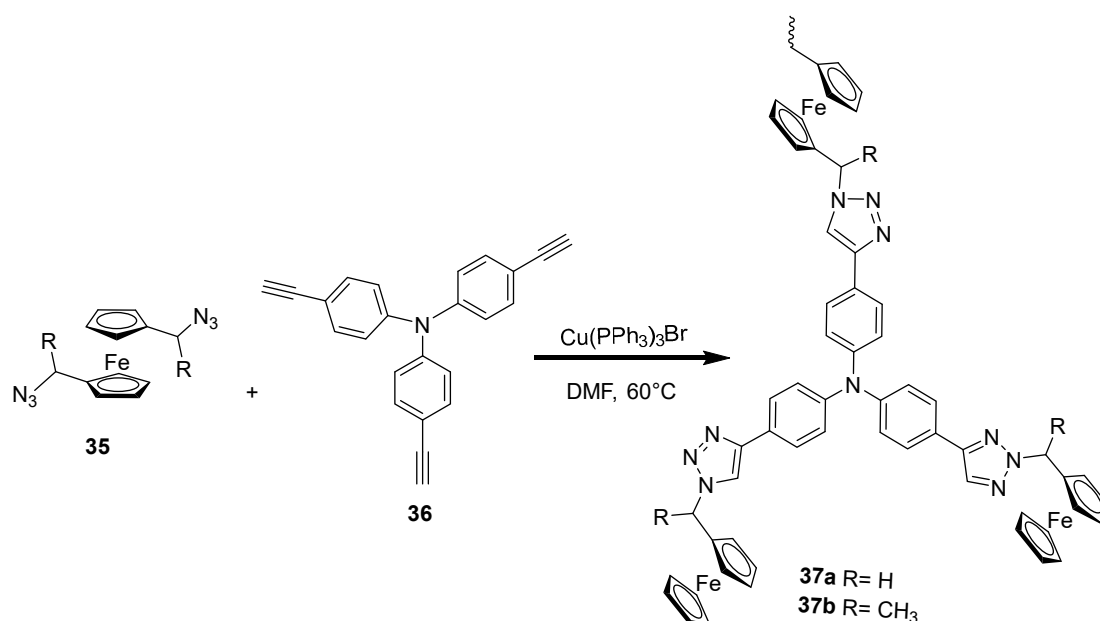
Atropoisomerism is a term used to describe a stereochemical phenomenon caused by impeded rotation around bonds in nonplanar molecules. An easy-to-perform synthesis and thorough characterization of novel atropisomeric ferrocene-containing six-membered cyclic ureas (**34a–g**) is reported. This work was motivated by the intriguing biological/medical characteristics of six-membered cyclic ureas and “atropoisomers-things that rotate.” Two atropoisomers of the same compound’s crystal structure are also described. These two architectures’ molecular structural characteristics and intermolecular interactions have been compared and thoroughly examined. It is interesting to note that while having conformation and geometrical properties that are relatively comparable, these two isomers create significantly distinct crystal packing (Scheme 26) [52].



Scheme 26. Substrate scope of synthesis of 1-aryl-4-ferrocenyl-3-phenyltetrahydropyrimidin-2(1H)-ones.

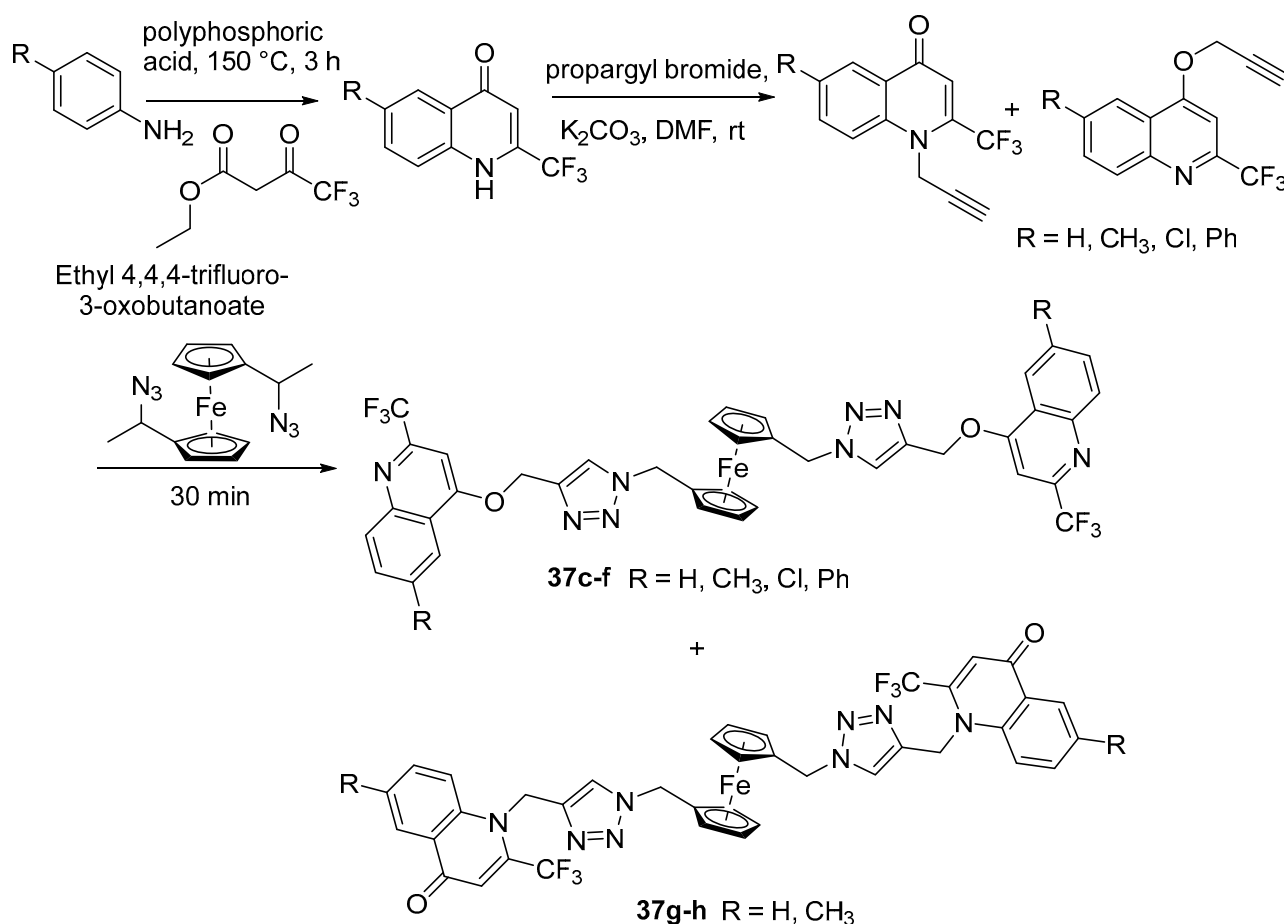
2.8. Synthesis of Ferrocene-Based Heterocyclic Derivatives

The group of Li and Chi have developed an elegant method for the construction of two ferrocene-branched poly-triazoles (**37a–b**) by treating ferrocene-based diazides (**35**) and tris (4-ethynylphenyl) amine (**36**) in the presence of a copper catalyst (Scheme 27). Owing to the ferrocene scaffold present inside poly-triazole-based polymers, two nanocomposites were prepared using carbonization or destructive distillation. Both polymeric materials also exhibited the saturation magnetization potential that proved the remarkable standard of these polymers for ultra-advanced technological applications [53].



Scheme 27. Synthesis of ferrocene-branched polytriazoles.

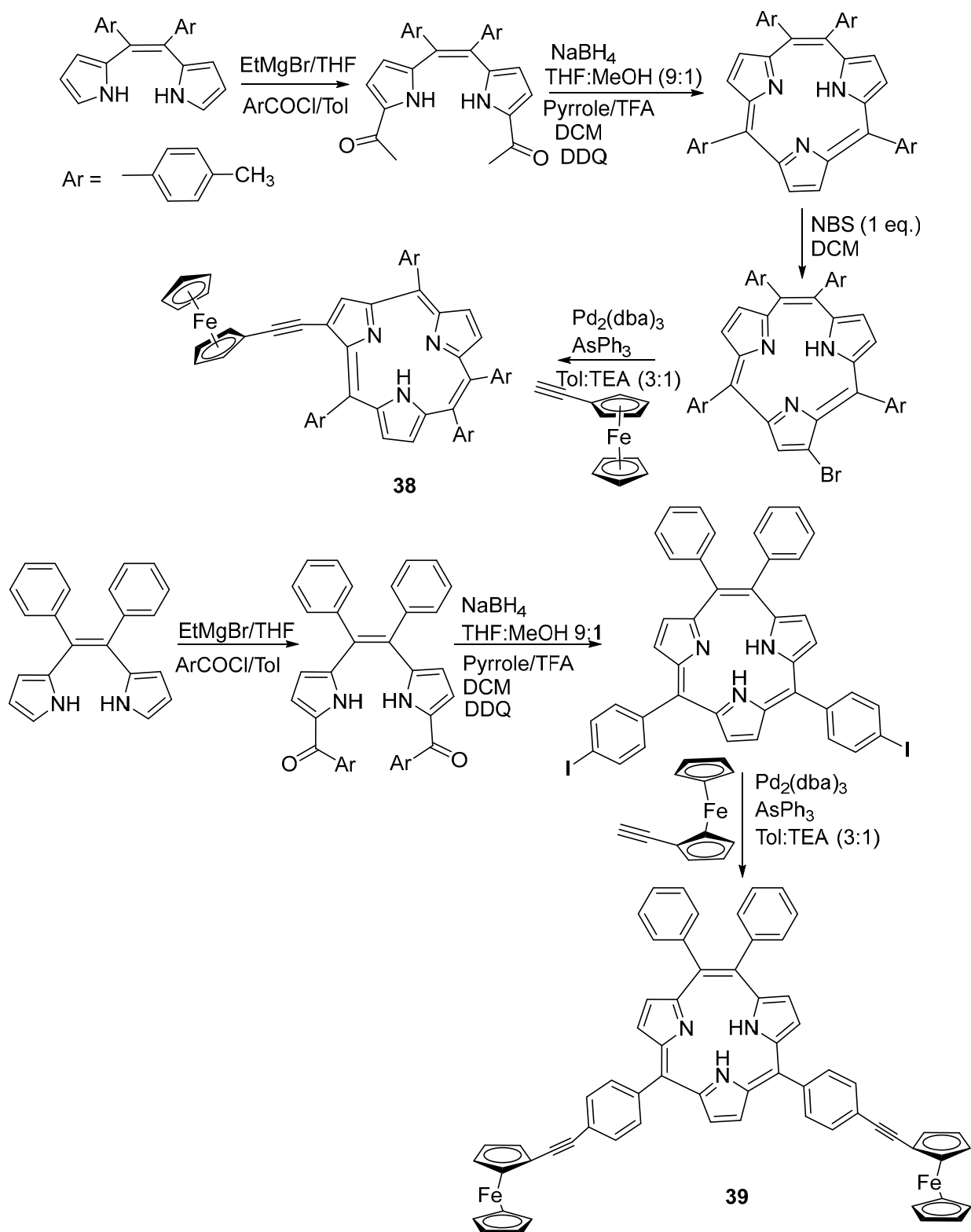
Maracic et al. conducted the synthesis of a series of novel bis-triazole containing 1,1'-disubstituted ferrocene conjugates (**37c–h**) attached with N-1 and O-4 alkylated quinolone and quinoline by the liquid-assisted grinding (LAG) mechanochemical method in copper-catalyzed azide–alkyne cycloaddition (CuAAC) in higher yields and with a shorter reaction time compared to a conventional method, thus proving the superiority of mechanochemistry versus conventional synthesis (Scheme 28). The antiproliferative effects of bis-quinoline and bis-quinolone ferrocene derivatives on five tumor cell lines and two non-tumor cell lines were investigated [54].



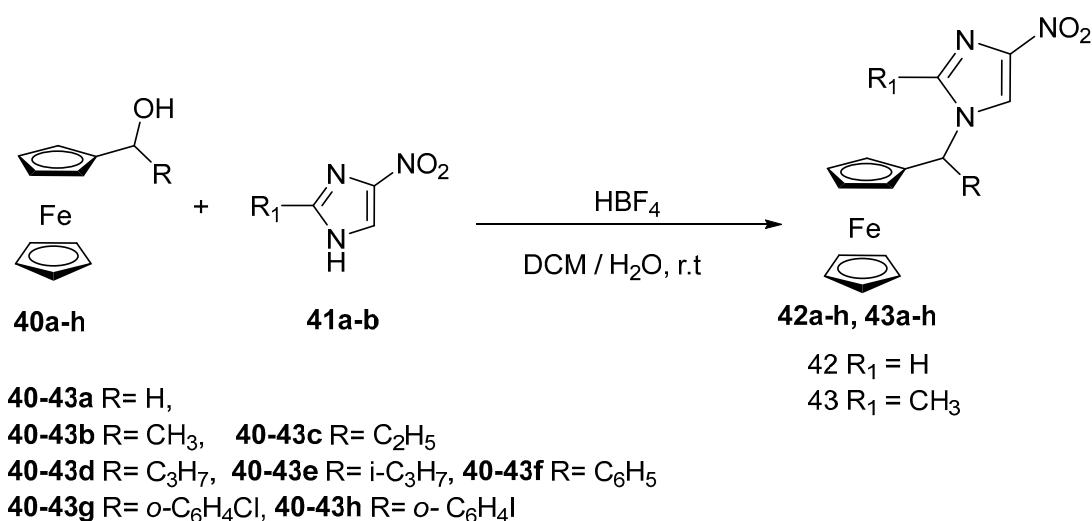
Scheme 28. Mechanochemical synthesis and antiproliferative activity of novel ferrocene quinoline/quinolone hybrids containing bis-triazoles.

In addition, the synthesis of ferrocene-functionalized triphyrin analogs has been attempted using the Pd-promoted coupling reaction between substituted triphyrin and ethynyl ferrocene subunits under lenient conditions [55]. Further mechanistic study revealed that there was a strong affinity between triphyrins and ferrocenyl units in the diad (**38**) when compared with the triad (**39**). Both conjugates were thought to be promising candidates for evolutionary development in molecular device applications (Scheme 29).

Another interesting example regarding ferrocenyl heterocycles was the synthesis of ferrocene-grafted nitroimidazoles **42** in which a regiospecific reaction occurred between α -hydroxy ferrocene **40** and nitroimidazole precursor **41** in the presence of HBF_4 (Scheme 30). The resulting racemic mixture was resolved by HPLC containing amylose or cellulose-based chiral stationary phase. Cytotoxicity assay of these derivatives revealed the anticancer activity of only compound **42b** against murine solid tumor system Ca755 cancer cells [56].

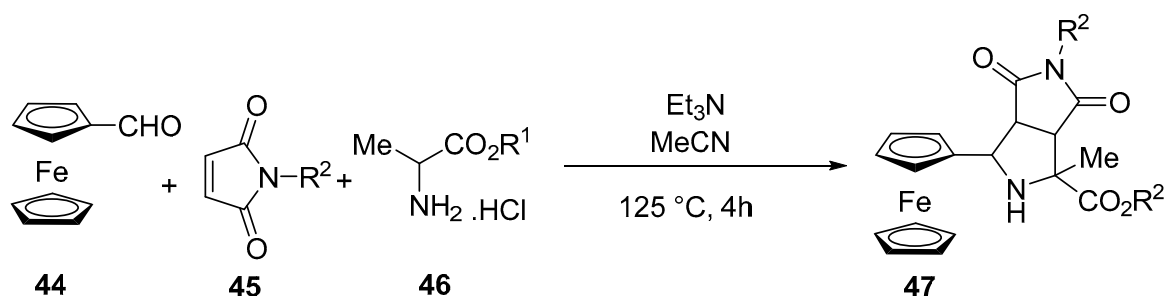


Scheme 29. Synthesis of ferrocenyl-substituted triphyrin derivatives.



Scheme 30. Regiospecific synthesis of ferrocene-functionalized nitroimidazoles.

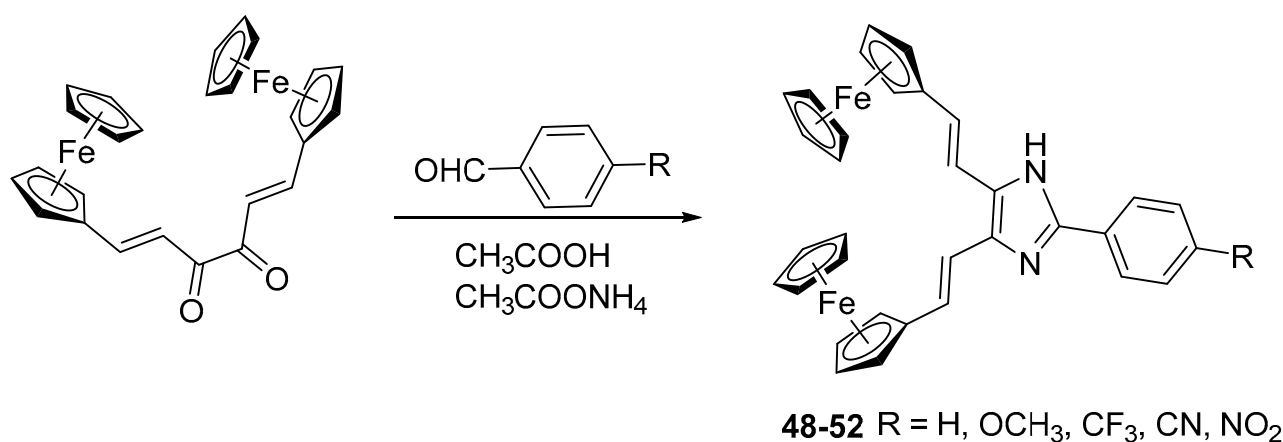
Zhang and co-workers introduced an innovative 1,3 dipolar cycloaddition protocol to synthesize a ferrocene-based substituted pyrrolidine system. In this novel approach, azomethine yields were generated through the in situ reaction of α -amino acid ester and ferrocene-functionalized carbaldehyde that further reacted with *N*-substituted maleimide to give a pyrrolidine product (Scheme 31). Moreover, the structures of these compounds were elucidated by ¹H NMR and high-resolution mass spectral data [57].



| R ₁ | R ₂ | Product | Yield % | R ₁ | R ₂ | Product | Yield % |
|----------------|----------------|------------|---------|----------------|----------------|------------|---------|
| Et | Bn | 47a | 89 | Me | Bn | 47f | 91 |
| Et | Me | 47b | 93 | Me | Me | 47g | 93 |
| Et | Et | 47c | 91 | Me | Et | 47h | 95 |
| Et | Ph | 47d | 84 | Me | Ph | 47i | 82 |
| Et | Cy | 47e | 85 | Me | Cy | 47j | 85 |

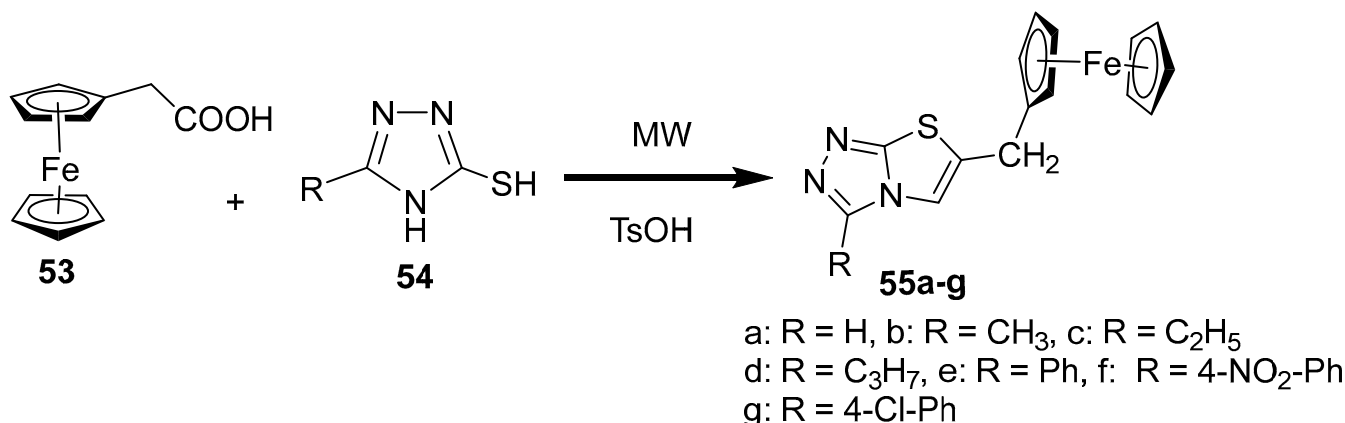
Scheme 31. Synthesis of ferrocene-substituted pyrrolidine via dipolar cycloaddition reaction.

The synthesis of ferrocenyl imidazole derivatives occurs through the Debus–Radziszewski condensation reaction in which 1,6-bis-ferrocene-hexa-1,5-diene-3,5-dione is condensed with *p*-substituted benzaldehyde, demonstrated by Selvam and co-workers (Scheme 32). These imidazole derivatives displayed second-order NLO properties confirmed by SHG analysis [58].



Scheme 32. Synthesis of ferrocenyl imidazole derivatives.

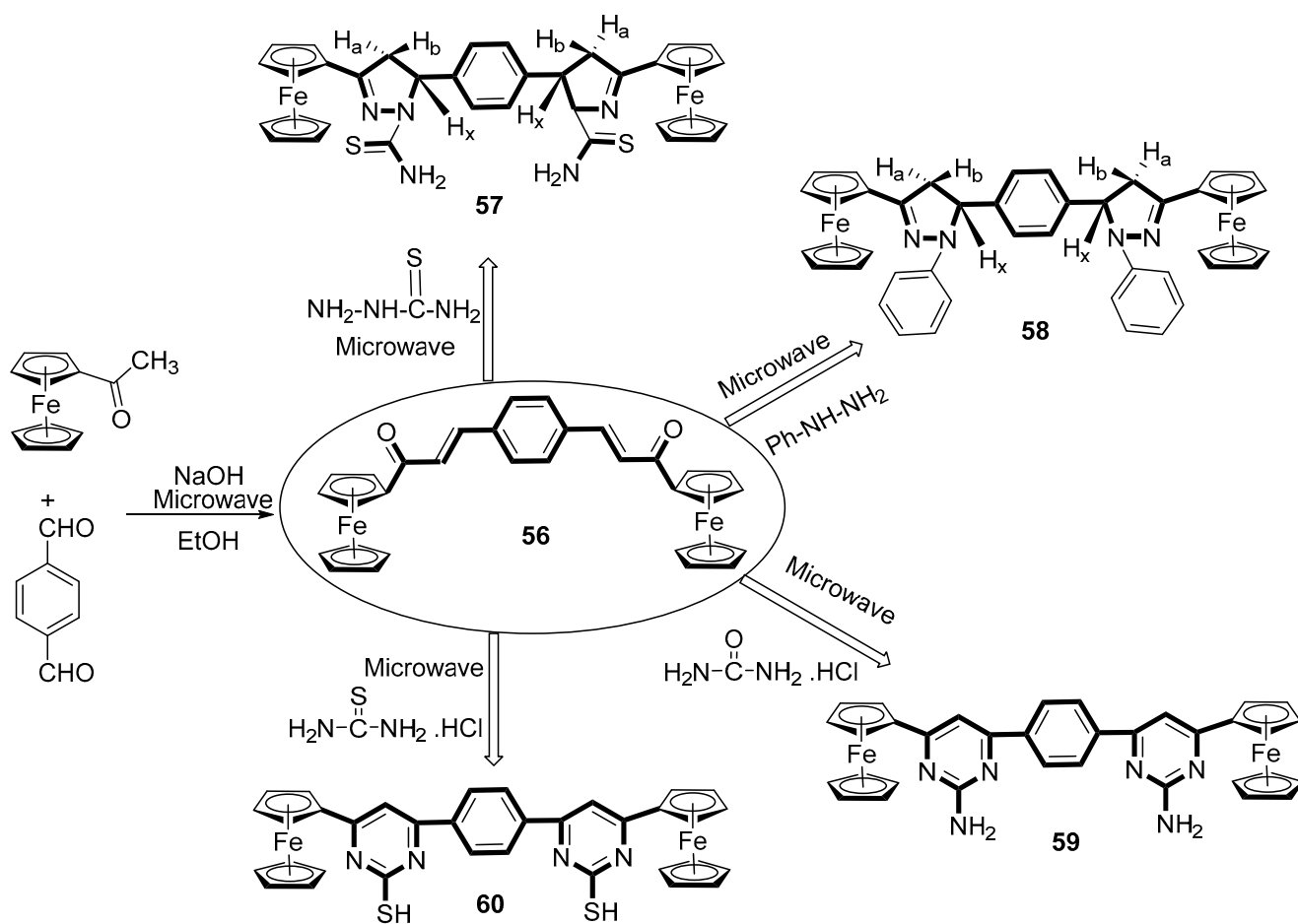
A microwave-assisted procedure for the synthesis of various ferrocene-functionalized triazole derivatives has been reported by Liu and co-authors [59]. The reaction between 2-amino-5-substituted-1,3,4-thiadiazole and α -bromoacetylferrocene as substrates in the presence of *p*-toluenesulfonic acid under microwave irradiation offered high yields of ferrocenylimidazo [2,1-*b*]-1,3,4-thiadiazoles (Scheme 33). The reported synthetic method seems to be useful in terms of reduced time for synthesis, higher rate of reaction, and greater % yields.



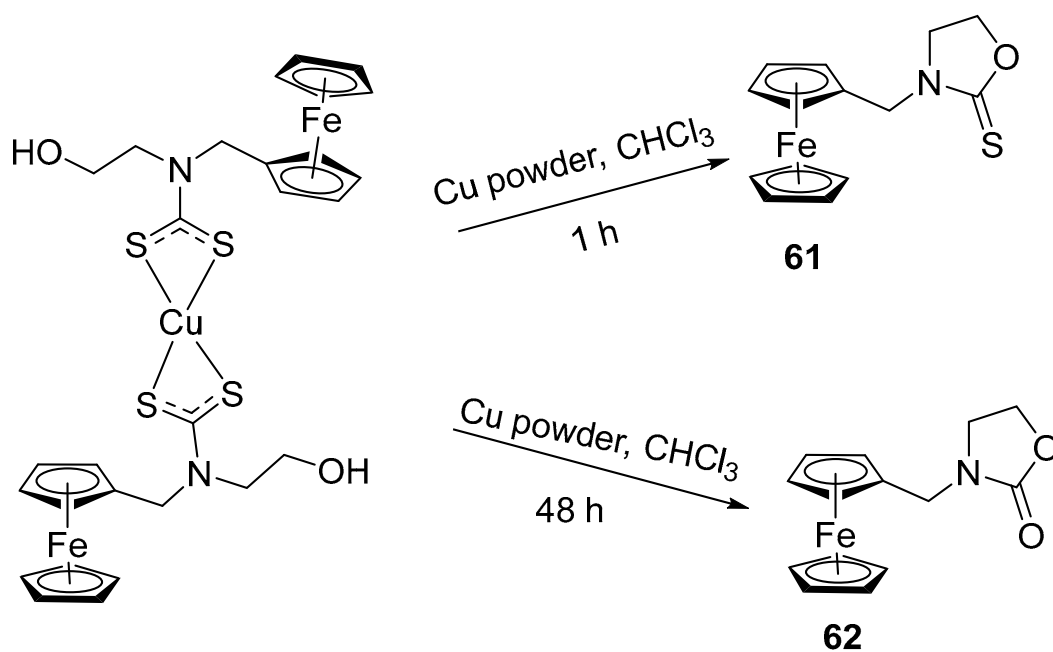
Scheme 33. Microwave-assisted synthesis of ferrocenylthiazoles.

Khan et al. reported microwave-assisted synthesis of macromolecules containing ferrocenyl bis-pyrazoline (57, 58) and bis-pyrimidine (59, 60) derivatives by treating ferrocenyl bis-chalcone 56 with thiosemicarbazide, phenylhydrazine, guanidine hydrochloride, and thiourea (Scheme 34). Targeted compounds were further characterized by IR, ¹H NMR, ¹³C NMR, mass spectrometry, and combustion analysis [60].

Different reaction conditions afforded the formation of two different products with different yields, characterized by X-ray crystallography and spectroscopic analysis (Scheme 35).



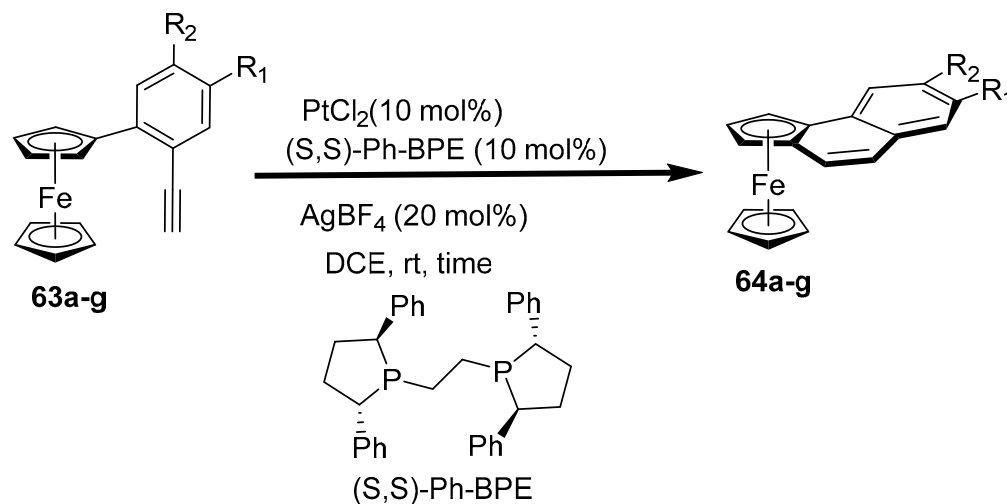
Scheme 34. Microwave-supported synthesis of ferrocenyl bis-pyrazolines and bis-pyrimidine derivatives.



Scheme 35. Synthesis of ferrocene-based oxazolidine-2-thione and ferrocene-based oxazolidine.

2.9. Synthesis of Ferrocene-Fused Cyclic Derivatives

Shibata and co-workers explored platinum chloride as a useful catalyst for enantioselective synthesis of a ferrocene-fused aromatic system through cycloisomerization of 2-ethynyl-1 ferrocenyl benzene precursor (Scheme 36). The mechanistic study revealed that C–H activation did not occur in the rate-determining step and the reaction proceeded through the activation of the alkyne nucleus via protonation of π cloud of chiral Pt complex followed by a 6-endo-dig cyclization reaction [61].

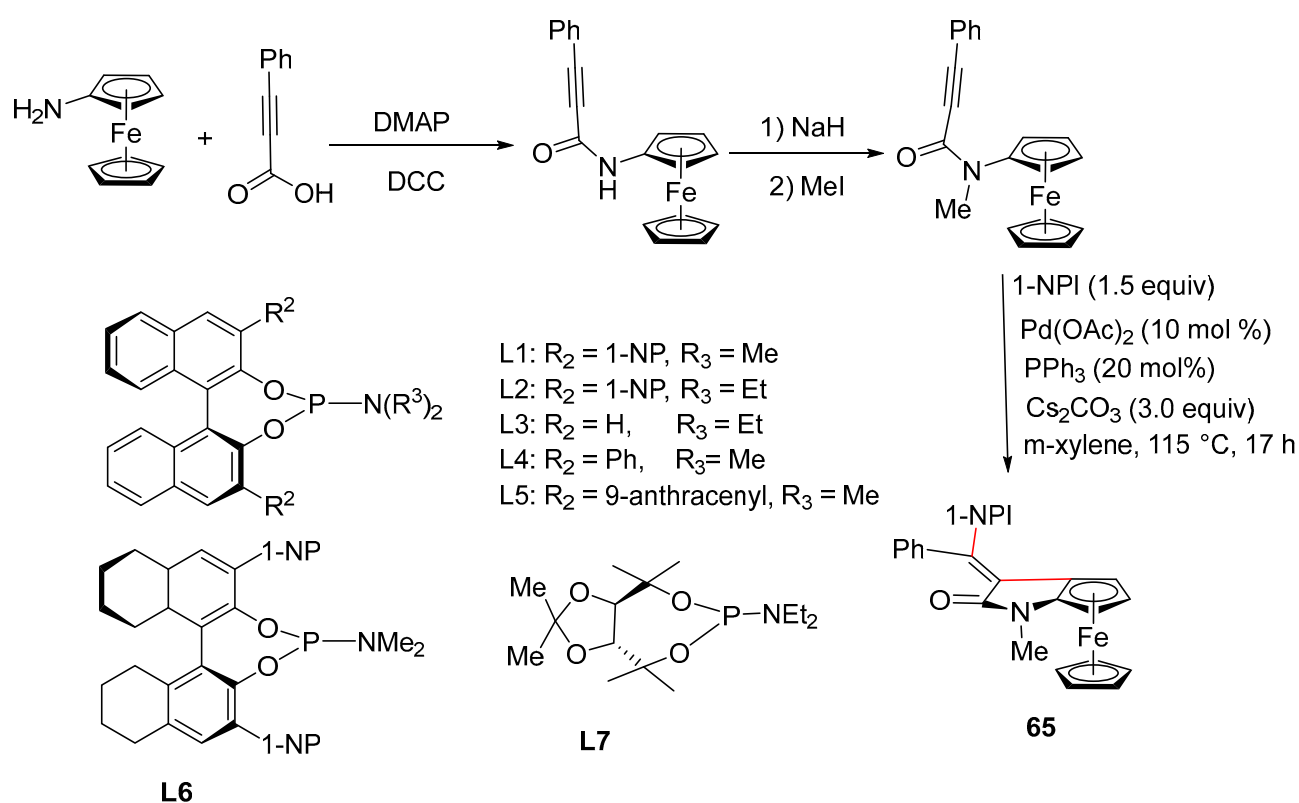


| entry | | R ₁ | R ₂ | time/h | yield % | ee % |
|-------|------------|-----------------|----------------|--------|-----------------|------|
| 1 | 63b | Me | H | 21 | 64b , 82 | 97 |
| 2 | 63c | MeO | H | 22 | 64c , 70 | 80 |
| 3 | 63d | Cl | H | 15 | 64d , 89 | 75 |
| 4 | 63e | F | H | 15 | 64e , 93 | 88 |
| 5 | 63f | CF ₃ | H | 20 | 64f , 69 | 18 |
| 6 | 63g | H | Cl | 18 | 64g , 62 | 94 |

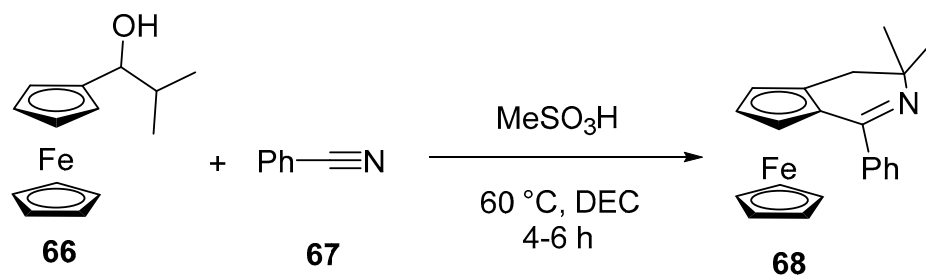
Scheme 36. Asymmetric synthesis of ferrocene-fused aromatic compounds.

Recently, a new protocol has been safely scaled up based on Pd-catalyzed intramolecular tandem cyclization of ferrocene analogs with substituted alkyne, to form novel asymmetric planar ferrocene [1,2-*d*] pyrrolidines [62]. This Pd (0)-catalyzed tandem intermolecular syn-carbopalladation of *N*-ferrocenyl propionamide with aryl iodides had been appreciated, fabricating planar asymmetric ferrocene [1,2-*d*] pyrrolinones in virtuous yields. Moreover, using BINOL-based phosphoramidite ligands, up to 95% ee was attained (Scheme 37).

The Ritter reaction was used for the preparation of 3,4-dihydroferrocenyl[*c*]pyridine racemates by Rozhkova et al. [63]. In this newly planned strategy, 2-methyl-1-ferrocenyl propane-1-ol was treated with substituted nitriles in the existence of a methyl sulfonic acid catalyst (Scheme 38). The targeted racemates were successfully resolved by preparatory HPLC on a chiral cell OD-H column and the absolute configuration of each enantiomer was determined by X-ray crystallographic studies.



Scheme 37. Synthesis of ferrocene [1,2-*d*] pyrrolinones.



Scheme 38. Synthesis of dihydro ferrocenyl pyridine derivatives.

3. Applications of Ferrocene Derivatives

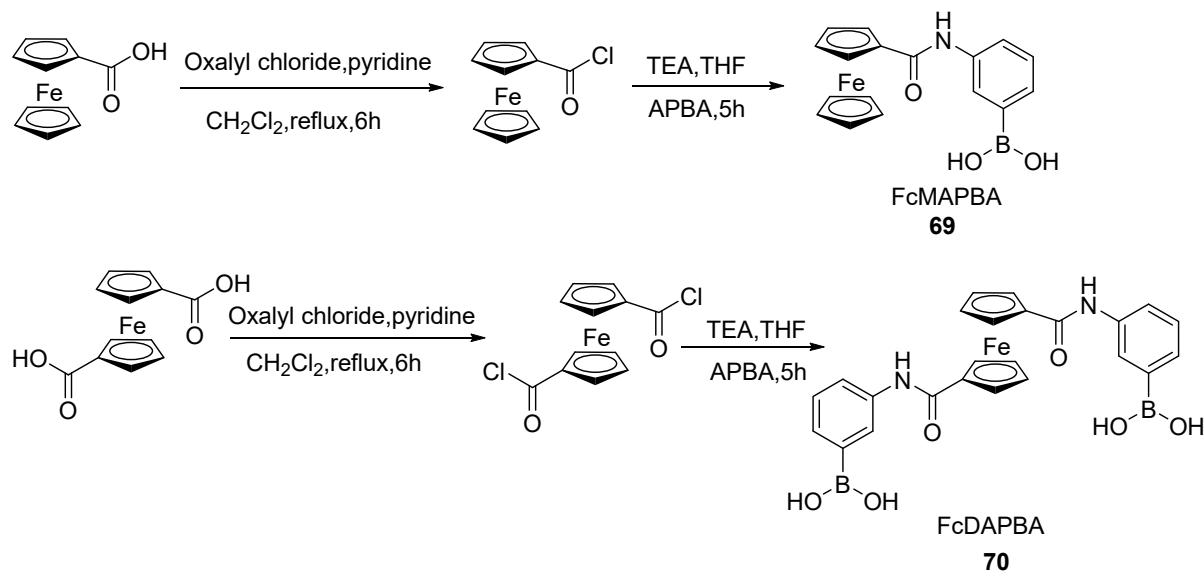
The application of metallocene-functionalized compounds has become a research topic of growing interest in recent years. Ferrocenes have been used as chemical intermediates, antiknock additives to gasoline, lubricants, and for other uses, but a primary application is related to catalysis [64]. Ferrocene is also currently being investigated as an active pharmacological agent against many notorious diseases like cancer, malaria, and other bacterial infections. Here, we tried to review applications of ferrocene derivatives embracing several fields like materials science, industry, agriculture, biology, medicine, electrochemistry, etc.

3.1. Materials Science Applications

Ferrocene retains an iron synthetic chemistry which includes a 3D structure that permits the synthesis of many derivatives, outstanding thermal stabilities [65,66], and rapid dissolution in common organic solvents [67]. Thanks to these imperative features, ferrocene derivatives have been used in a wide number of materials science applications; so diverse are they that it is problematic to classify these into a coherent manuscript. Thus, this is a general outline of some specific applications of ferrocene-functionalized compounds, including NLO devices, functional materials in electrochemical sensors, electron beam lithography, and electrochromic applications.

3.1.1. Biosensing Potential of Saccharides

By considering the binding affinities, biocompatibility, and host–guest molecule recognition capacity of amides, Saleem et al. synthesized ferrocene-appended phenylboronic amino acid and diaminophenyl boronic acid (APBA) derivatives and evaluated their saccharide sensing activity using spectroscopic analysis (Scheme 39). The neighboring environment of the boronic acid binding site and the linking ferrocene unit enhanced the binding abilities of tetrahedral boron. Further, ferrocene's electrochemical response signified a substantial step towards effective and robust artificial bioelectronic affinity receptors [68].



Scheme 39. Total synthesis of ferrocene-based aminophenyl and diaminophenyl boronic acid.

In a different work, Rabti and co-authors designed an innovative ferrocene-grafted (rGO) electrode, prepared by drop-casting ferrocene-based graphene against a polyester surface (Figure 1a). The freshly synthesized ω -azidodiethylene-glycol- α -ferrocenyl esters (agFc) and rGO nanosheets generated extremely aqueous soluble agFc–rGO nanosheets through cycloaddition (Figure 1b). Further, biological interactions with glucose oxidase for glucose recognition were accomplished using bioelectrode, offering evidence for latent biosensing use [69].

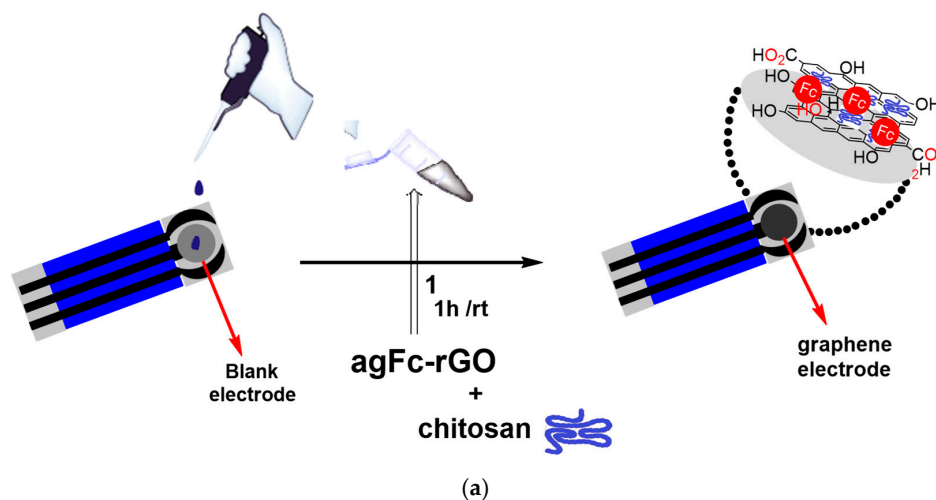


Figure 1. Cont.

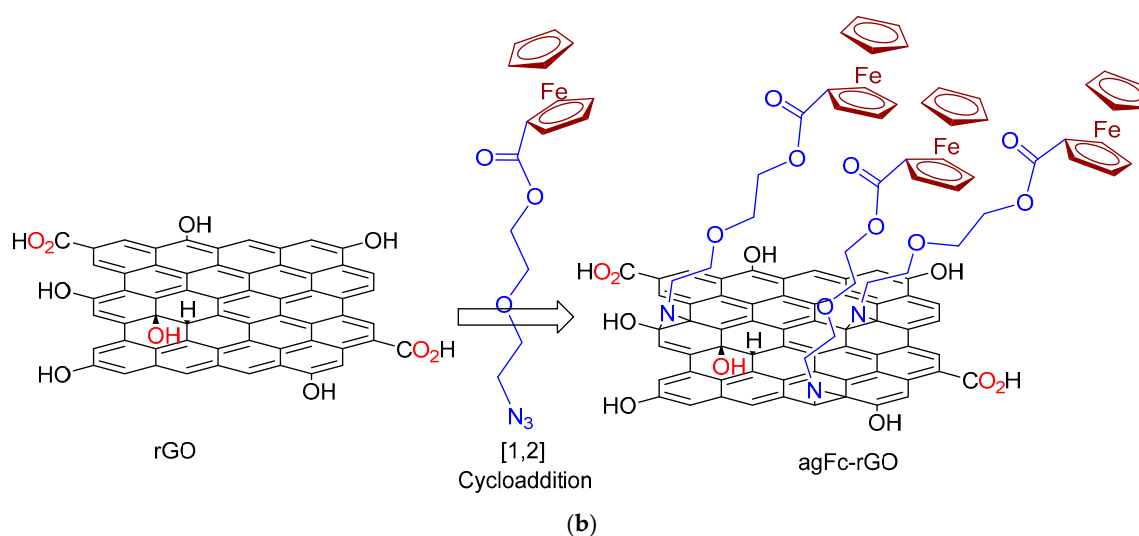


Figure 1. (a) Ferrocene-grafted (rGO) electrode preparation by drop-casting ferrocene-based graphene (b) Synthesis of ω -azidodiethylene-glycol- α -ferrocenyl esters (agFc) and rGO nanosheets from agFc-rGO nanosheets through cycloaddition reaction.

3.1.2. Anion Biosensors

Various analytical methods were reported in the literature for the detection of superoxide anion, but all fail to provide *in vivo* and *in vitro* monitoring. These issues were resolved by fabricating highly selective hydrogel structures in which ferrocene units were associated with superoxide dismutase into a poly diacrylate hydrogen matrix for the synthesis of SOD-Fc-PEG-based electrodes [68]. The polymeric solution was emulated by optical lithography in Au microelectrodes assembled onto the surface of glass slides (Figure 2). Such reproducible biosensing materials were used for the diagnosis of carcinoma anion cells that release superoxide anions, with LOD of 0.001 μM and sensitivity of 1.41 $\text{Na}^+ 4 \text{ M}/\text{mm}^2$.

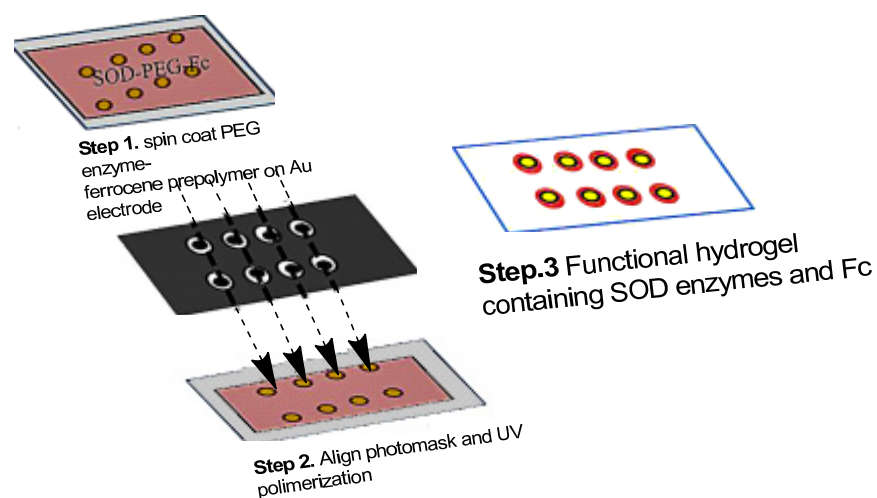


Figure 2. Biosensing chip comprising eight micropatterned gold electrodes.

3.1.3. Hydrogen Peroxide Biosensor

In a providential work, Dong's group developed an electrochemical biosensor based on chitosan-immobilized enzymes and a β -cyclodextrin-containing ferrocene complex for the biological detection of H_2O_2 [70]. A CTS-CAT/ β -CD-FE-grafted electrode was constructed by conglomerating CTS-CAT with β -CD-Fe complex onto the surface of a glassy carbon electrode and used for the electrochemical evaluation of hydrogen peroxide (Figure 3). Further, the inclusion of ferrocene units offered great durability to the β -cyclodextrin complex.

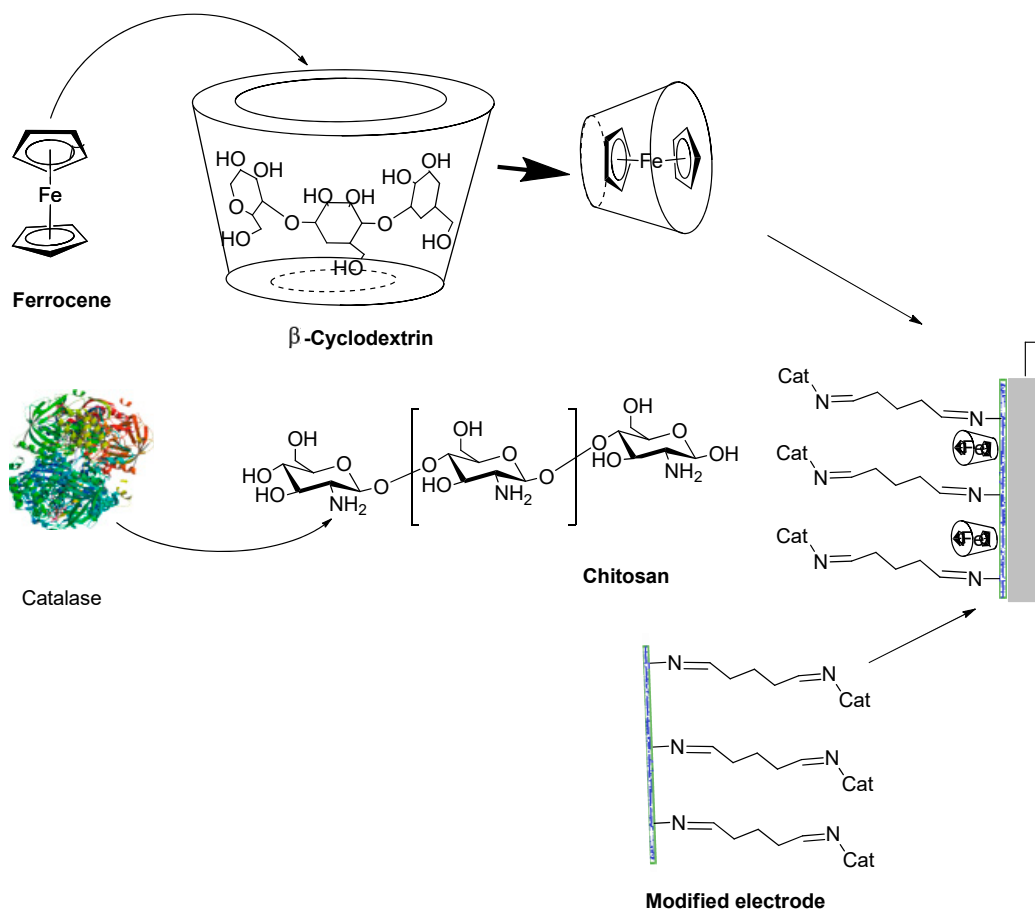


Figure 3. Schematic illustration of the CTS-CAT/β-CD-FE amalgamated electrode.

3.1.4. Peptide Biosensors

Xia Lu and co-workers invented a new fluorescent nano-bioaptamer sensor assimilating a β-cyclodextrin-modified quantum dot luminescent probe and applied it to find the (PDGF)-BB factor that showed significant fluorescence quenching (Figure 4). The reason for this quenching phenomenon was initiated by the Fc unit that recognized the host-guest interaction, followed by the blockage of photoexcited electron transport between Fc and CDs supported by DNA that reduced fluorescence. This ferrocene-marked adapter served as a sensitive and selective biological receptor for detecting platelet-derived growth factor BB [71].

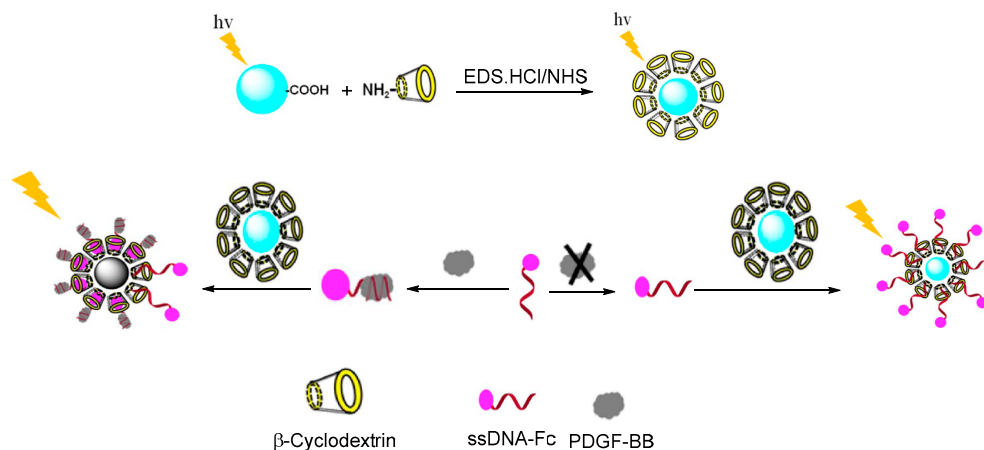


Figure 4. Sensing procedure of the proposed β-CD-CD fluorescent nanoprobe for PDGF-BB detection.

3.1.5. Chemosensing Applications

The astonishing stability, easy functionalization, and distinctive redox behavior of the ferrocene nucleus have led to expeditious research in molecular recognition studies. Recently, Preet and Arora with their colleagues combined the electrochemical activity of ferrocene with the chemical ligation potential of organosilanes via the preparation of ferrocene-tailed, chalcone-based organosilanes from ethynylferrocene precursor (**71**) using click chemistry [72]. The resultant ligands were examined for their ion sensing potential and exhibited their sensing ability for Cu^{2+} ion on the addition of EDTA with the reversal of the sensing phenomenon. Moreover, the presence of the ferrocene nucleus offered a diverse signaling sensor that was helpful in the naked-eye revelation of Cu^{+1} ion within a limit of detection of $10 \mu\text{M}$ (Figure 5).

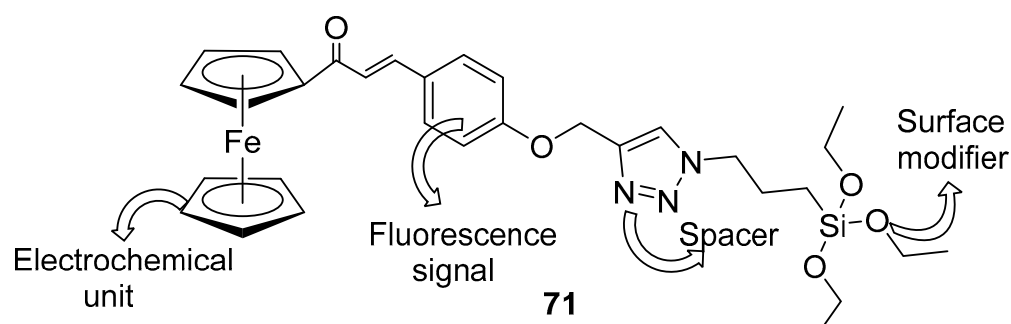


Figure 5. Molecular design of the chemosensor.

Another research group constructed two highly selective ferrocene-based chemosensing materials without the inclusion of nitrogen atoms for the chemoselective detection of Cu^{2+} and Hg^{2+} ions [73]. Compound **72** showed remarkable detection aptitude for Hg^{+} via optical and electrochemical signals with a lower value of detection limit that further confirmed its sensor potential. Further, ferrocene-functionalized sulfone **73** also demonstrated highly selective detection toward Cu^{2+} with the detection limit approaching $5.22 \times 10^{-7} \text{ M}$ (Figure 6).

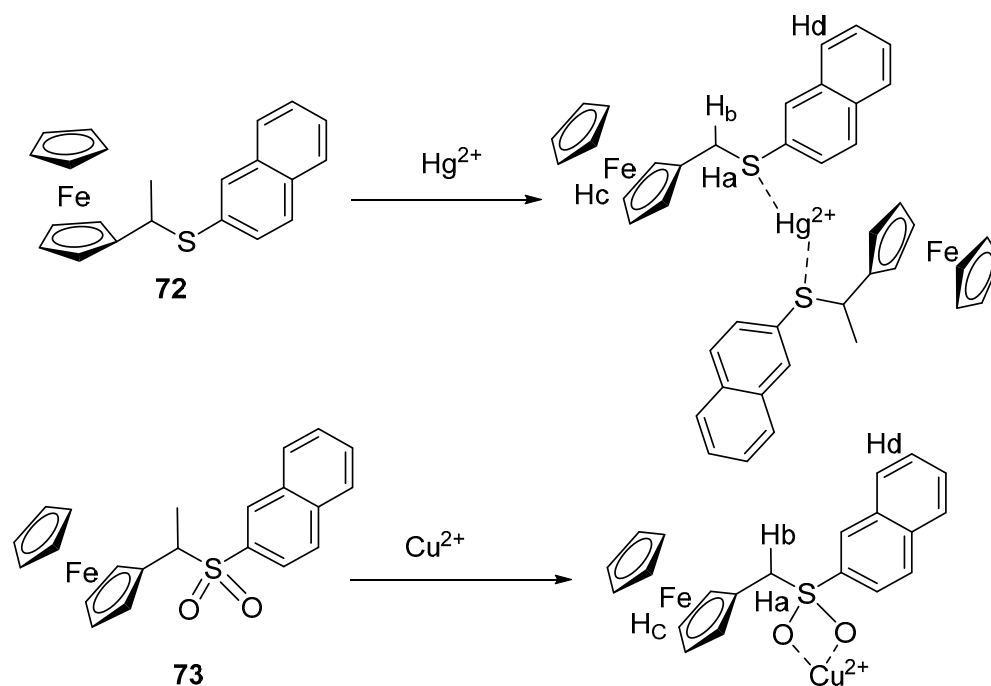


Figure 6. Possible binding mode of Hg^{2+} and Cu^{1+} ions with the receptors.

In a more recent work, a ferrocene-grafted chemosensor was proposed and assessed for its selectivity in the detection of Al^{3+} cations [74]. Mechanistic study revealed that the probe compound captured the Al^{3+} and enhanced the fluorescence intensity 200 times. Various characterization techniques confirmed the formation of a complex between compound **74** and Al^{3+} , and were successfully used to find out the Al^{3+} content in environmental samples (Figure 7).

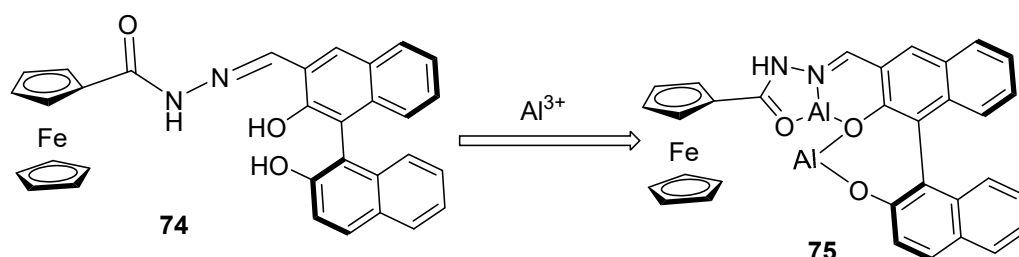


Figure 7. Proposed metal complex and its molecular model.

Finally, the method employed by Atasen explained the sensing potential of Be^{2+} by ion pair formation with ferrocenyl naphthoquinones radicals and dianions [75]. Cyclic voltammetric analysis revealed that the sensitivity effect was more pronounced in the case of Be^{2+} among all alkaline earth metals that formed an ion pair with Fc-cnq-1a and could selectively sense the ultra-trace amount of Be^{2+} (LOD 3.6 ppb). The proposed mechanism of the ion pair formation reaction between Be^{2+} ion and Fc-cnq-1a is depicted in Figure 8.

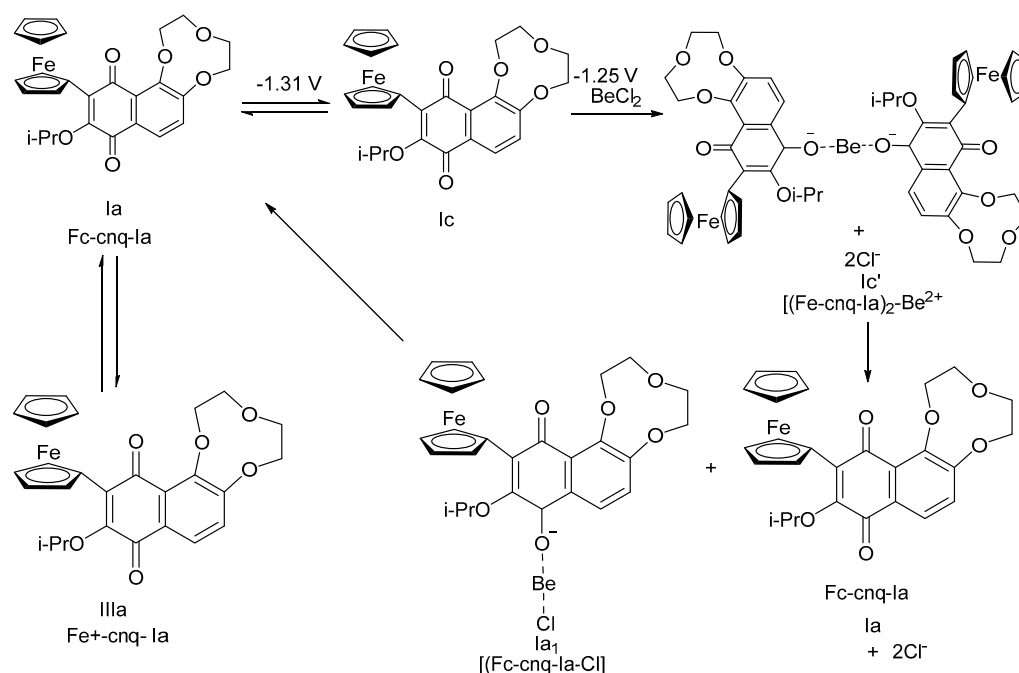


Figure 8. Proposed mechanism for ion pair formation between Be^{2+} ion and Fc-cnq-1a.

Anion recognition and anion sensing are of special interest not only because of their significant roles in biological systems but also because they can work in both organic and aqueous media. The group of Hosseinzadeh and Maliji recently reported the synthesis of an innovative tetra ferrocene-triazole-amide-based Calix [4] arene and described it as an efficient optical and electrochemical anion sensor [76]. CV and proton nuclear magnetic resonance titration tests disclosed the selective and ultrasensitive behavior of compound **79** for F^- with a detection limit of $2.98 \mu\text{M}$. The above-reported outcomes could be open-and-shut proof of the efficiency of a newly synthesized compound as a sensitive moiety for F^- anion (Figure 9).

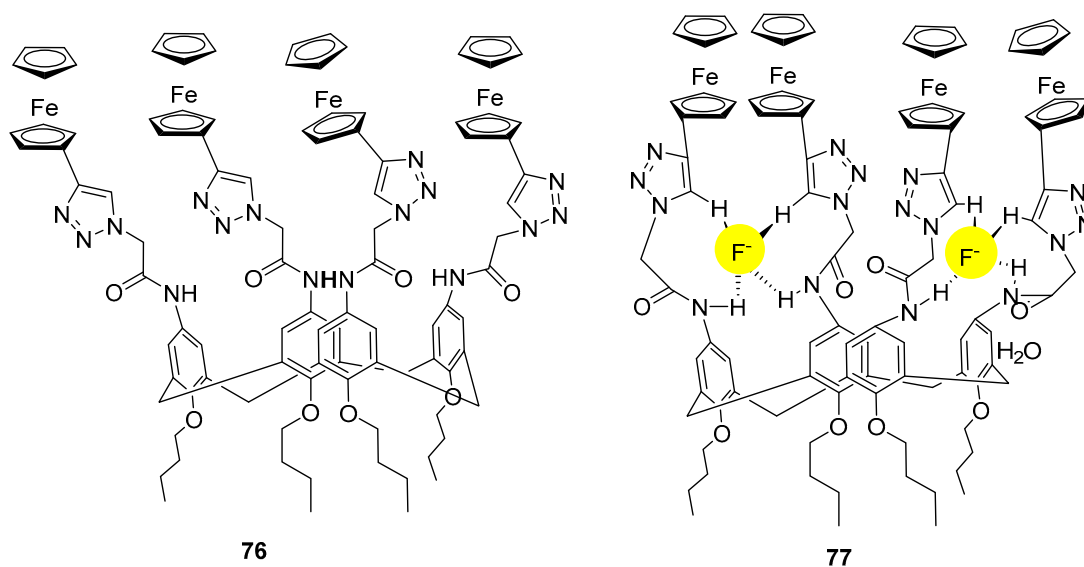


Figure 9. Structure of the synthesized receptor and its proposed binding mode with F^- .

Wu and co-workers designed four phenanthroimidazole derivatives with ferrocene scaffolds and examined their anion recognition properties towards twelve common anions such as F^- , Cl^- , Br^- , SO_4^{2-} , OAc^- , etc. [77]. Investigation of these common anions via spectroscopy studies indicated that compounds **78b** and **78d** sensed $B_4O_7^{2-}$ specifically and the sensing potential was realized through the naked eye, 1H NMR, and various titration experiments, concluding that the binding force between $B_4O_7^{2-}$ and **78b** was hydrogen bonding (Figure 10).

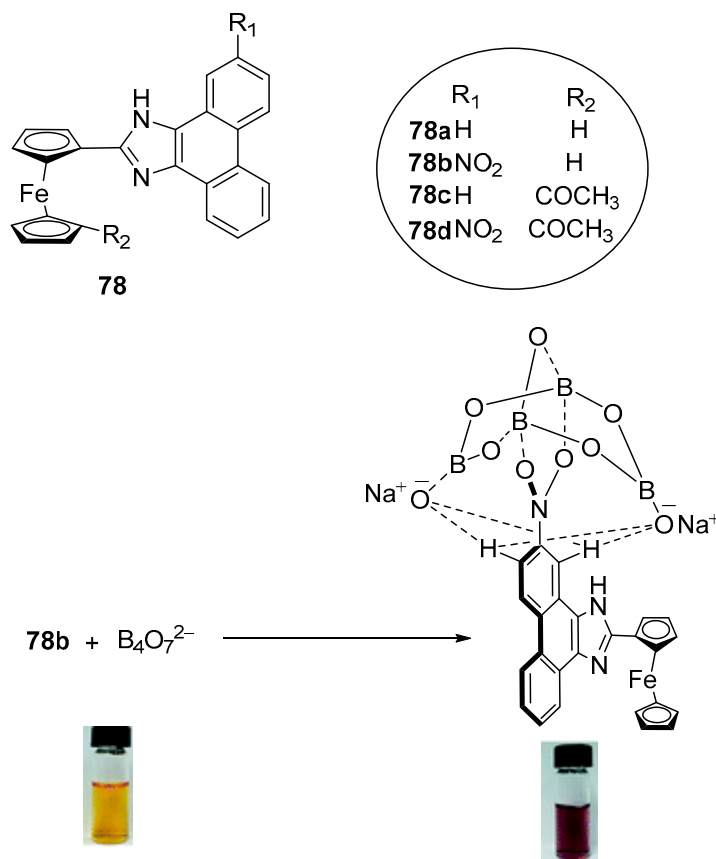


Figure 10. Structure and mode of complexation of synthesized receptor **78b**.

Another interesting example was reported in Feng's publication where the author designed a degradable electrochemical sensing system for the determination of nitrite moiety in pickle juice [78]. Nitrite is a commonly used food preservative, but a side effect was also reported as it reacted with amino acids and produced a carcinogenic effect [79]. A carbon electrode was developed by installing ferrocenyl derivatives on the surface of screen-printed electrodes; characterization techniques realized that the sensitivity and stability of the reported sensor were brilliant, with R.S.D lower than 2.1% (Figure 11).

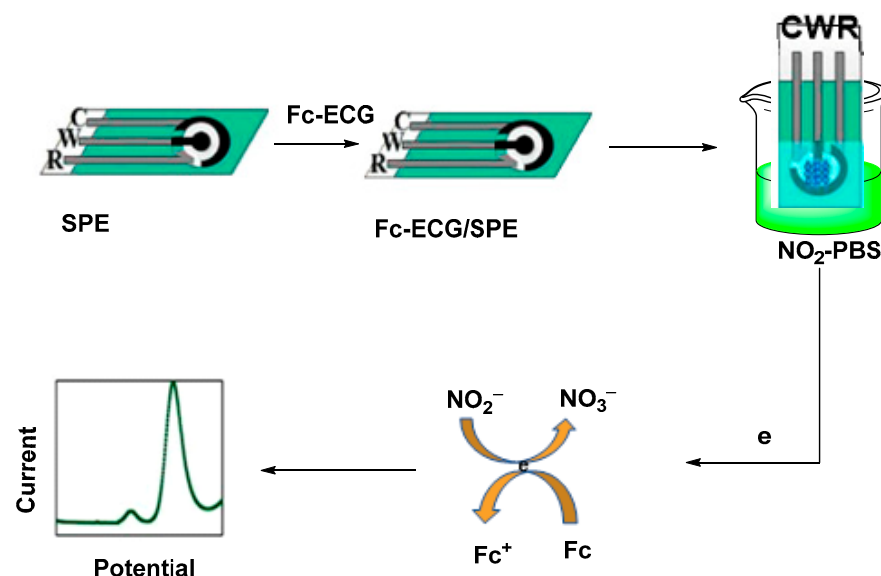


Figure 11. Assembly of Fc-ECG electrochemical sensor for nitrite recognition by DPV.

In an advanced work, Zaleskaya and co-authors fabricated ion pair sensing materials, having benzo crown ether and ferrocene-functionalized squaramide as the cation accepting center and anion welcoming center [80]. Receptors **79** and **80** were observed to be stronger candidates that could sense negative ions more efficiently in the company of positively charged species. This research offered a huge platform for the measurement of salt content in a real-life situation in which an appropriate amount of salt is required (Figure 12).

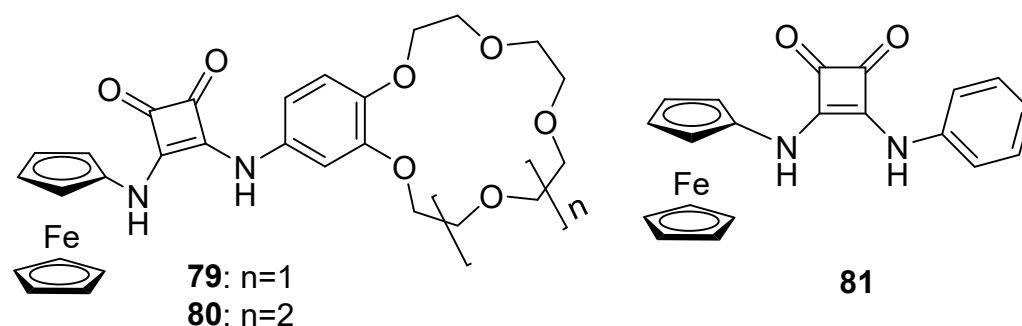


Figure 12. Structures of new ion pair sensors based on squaramide scaffold.

3.1.6. Electron Beam Lithographic Application

Ferrocene-grafted organic–inorganic hybrids are an innovation category of homo polymeric resists, and the recently synthesized poly-(TPMA) and poly-(FEMA-CO-TPMA) were studied for their large-scale micro/nanolithographic functions [81]. These copolymers also behaved like light resists when exposed to an electron beam lithography device for arranging nano-marked characters. The ultra-sensitivity and contrast of 2% poly (FEMA)-CO-TPMA **82** resulted from ferrocene's inclusion, which elevated the sensitivity and resolution scale of the polymer in comparison to **83** (Figure 13).

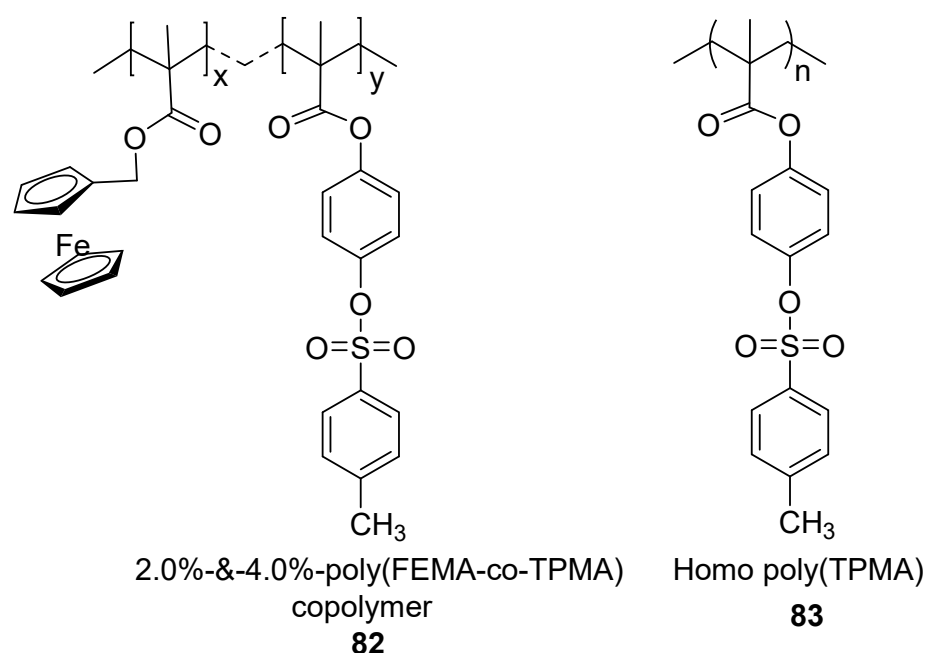
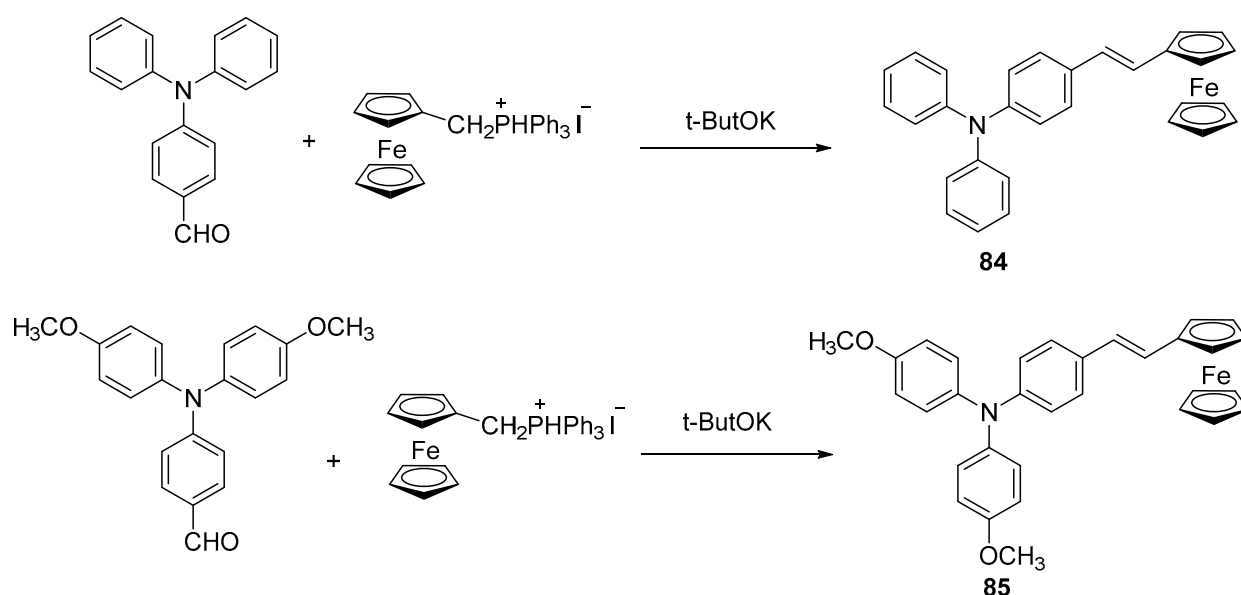


Figure 13. Chemical structures of ferrocene-bearing non-ionic poly-aryl tosylates.

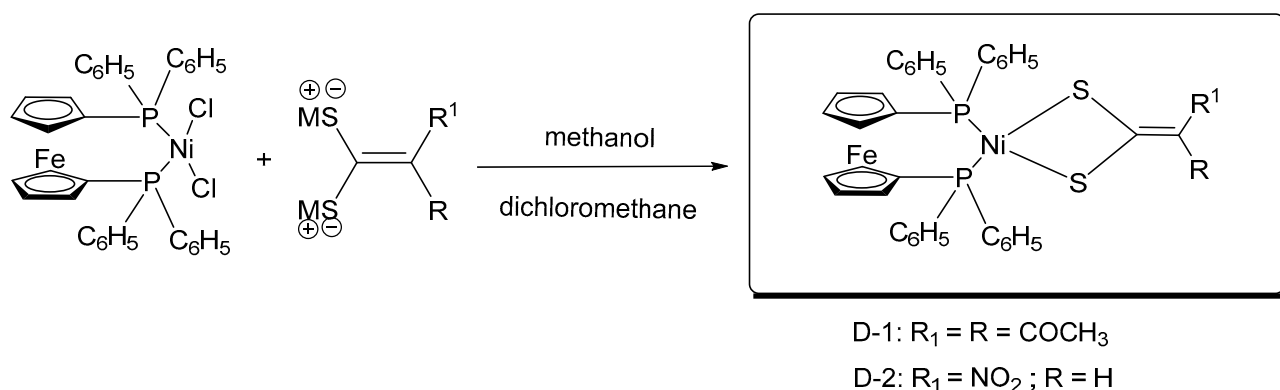
3.1.7. Nonlinear Optics Applications of Ferrocene-Based Conjugates

Relying on the merits of triphenylamine and ferrocenes as building blocks, novel compounds based on *N,N*-diphenyl-4-*E*-[(1-ferrocenyl)ethenyl] aniline (**84**) and *N,N*-diethoxyphenyl-4-*E*-[(1-ferrocenyl)ethenyl] aniline (**85**) were designed and synthesized, and a detailed study of these organometallic analogs revealed their NLO potential (Scheme 40). The cyclic voltammogram and ON/OFF aperture Z-scan measurements confirmed the third-order nonlinear optical (NLO) properties of these reported compounds, considered to be the result of their extended conjugation system [82]. Further, optically switching properties of these derivatives were also examined, which further confirmed their novelty.



Scheme 40. Synthesis of ferrocene-based conjugates with third-order nonlinear optical (NLO) properties.

In the same vein, Pielak's group reported the first- and second-order nonlinear optical properties of ferrocene-linked indolino-oxazolidine derivatives through scattering techniques, which showed that the β factor for NLO properties and β -POF/ β -CF value



Scheme 41. Synthetic route for the preparation of sensitizers.

Incorporating ferrocenyl groups into meso-substituted porphyrins with various donor substituents affords three metallo ligands: ZnP_1 , ZnP_2 , and ZnP_3 [85]. Self-aggregated zinc porphyrins and a linker, ZnPA, were utilized as sensitizers in dye-sensitized solar cells. It was observed that the photocurrent transformation potential of self-aggregated units was high; particularly, an amide bridge and ferrocene-based zinc porphyrin (ZnP_1) solar cell exhibited maximum photocurrent turning capacity compared with its derivatives (Figure 16).

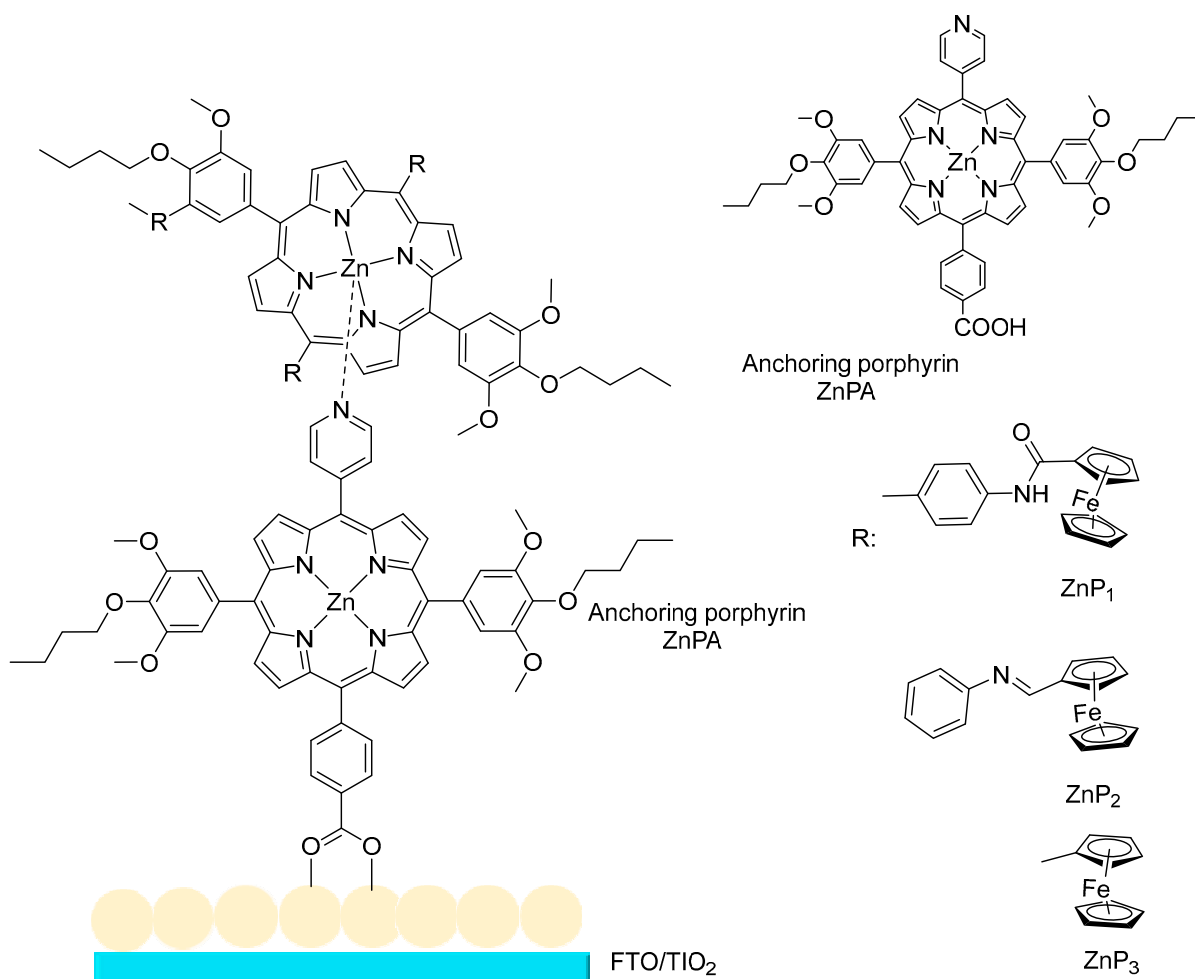


Figure 16. The complete aggregation method of accumulation on TiO_2 electrode surface.

3.1.9. Supercapacitor Applications

An advanced cobalt-graded poly-catenated metal–organic framework was constructed by Rajak's group and its electrochemical properties were extensively studied [86]. The synthesized framework (88) was applied with a binder to modify a glassy carbon electrode and evaluated its supercapacitor performance with or without a binder group. Detailed analysis was performed with a binder containing a modified glassy carbon electrode, which exhibited the superb value of capacitance and stability of that metal–organic framework onto the surface of the electrodes (Figure 17).

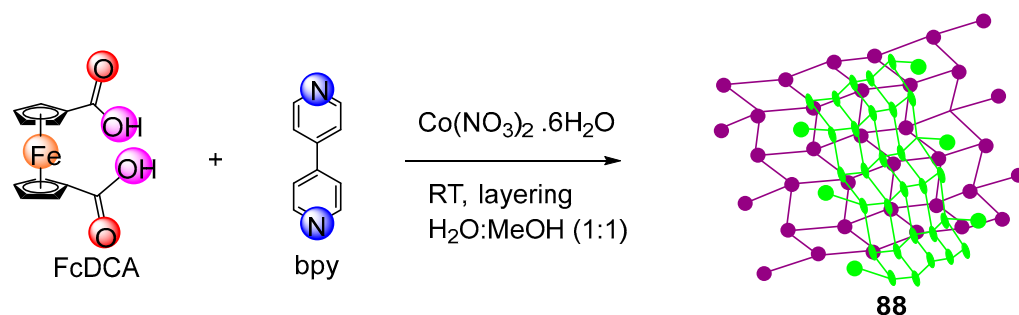


Figure 17. Synthesis of cobalt-based inclined polycatenated MOF.

Teimuri et al. developed a typical supercapacitor hinged on a glassy carbon electrode, mutated with graphene-oxide-loaded ferrocene through ring-opening polymerization (Figure 18). The amalgamated polyFc was impaired on glassy carbon, and its electrochemical potential was noticed through CV, GCD, and EIS techniques. All these characterization techniques revealed that the modified material showed excellent electrochemical features as a supercapacitor electrode with a high capacitance value of 200 Fg^{-1} [87].

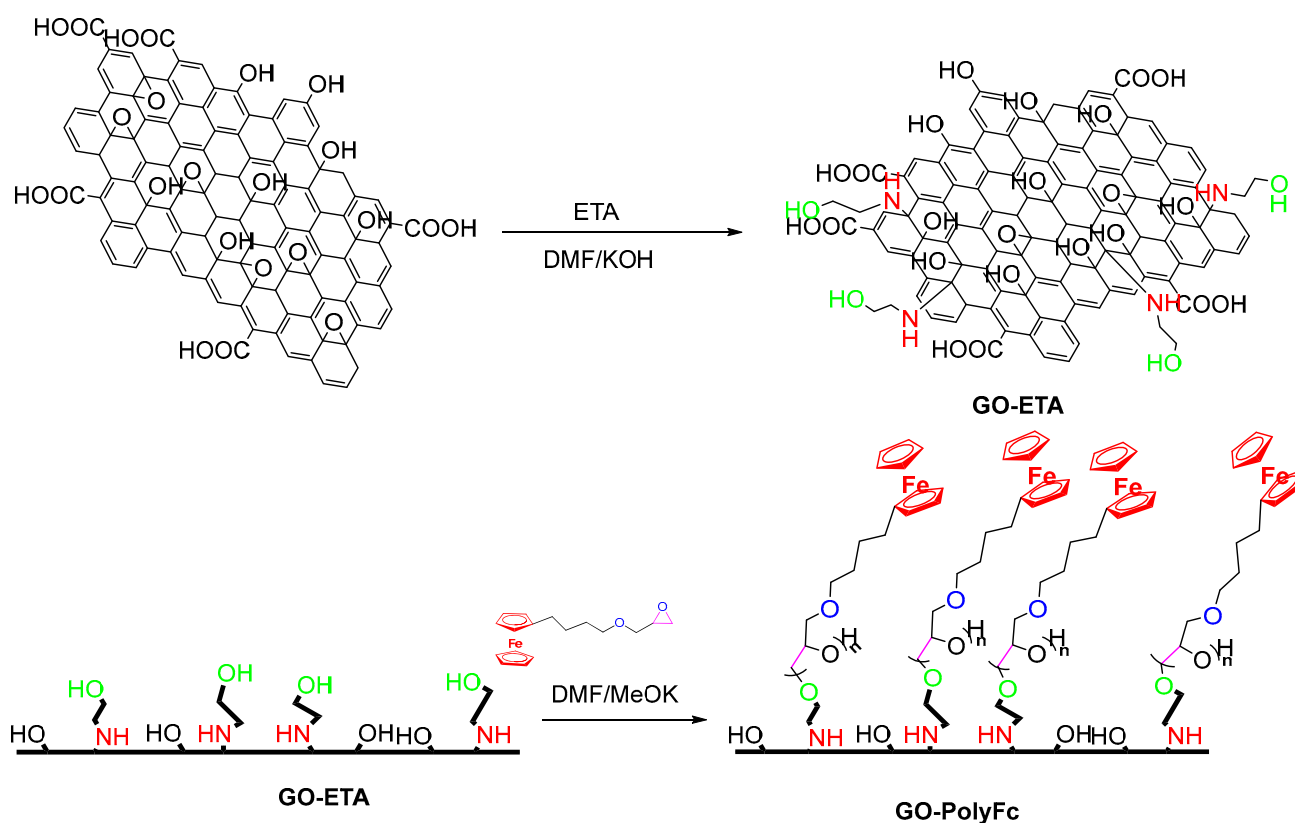


Figure 18. Synthesis of graphene oxide surface-modified ferrocene nanosheets (GO-polyFc).

3.1.10. Uses of Ferrocene in Modern Fuel Cells or Batteries

Ferrocene as an organometallic compound has been investigated as a standard electrode in redox potential measurements because of its excellent redox activity. In this study, the redox activity of ferrocene was utilized to design two ferrocene-functionalized polymers through cheap Schiff base interaction with melamine as the backbone [88]. Destructive distillation of synthesized material produced nano hybrids along with the $\text{Fe}_3\text{C}/\text{Fe}$ moiety. Further, a rechargeable zinc–air battery was constructed by utilizing $\text{Fe}_3\text{C}/\text{Fe}$ as a cathode catalyst which exhibited high power density, a small charge–discharge gap, and remarkable stability with less activity decay, in comparison to Pt/C containing commercial batteries (Figure 19).

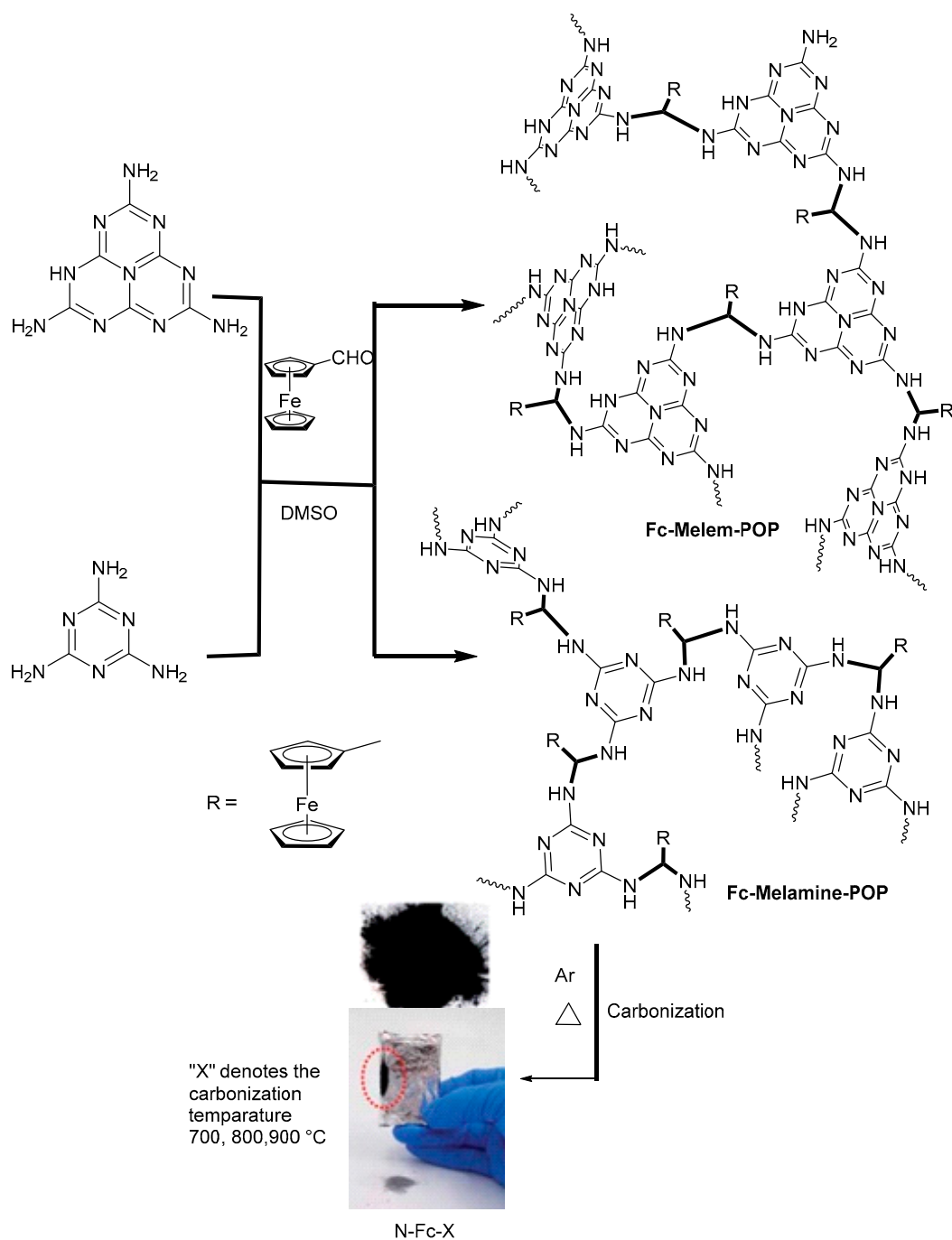


Figure 19. Synthesis of ferrocene-functionalized POPs and nitrogen-doped carbon catalysts.

Liu et al. introduced an efficient ferrocene-based electrode for Li^+ batteries with excellent electrochemical features such as significant reversible power, high charge retention, and remarkable charge–discharge rate capability [89]. XRD and cyclic voltammetry analysis showed that the electrochemical reaction of ferrocene was partially reversible and some metallic iron (Fe) clung to the anode even after de-lithiation. The metallic iron and solid electrolyte interface were amenable to the superb electrochemical properties of the designed electrode.

3.1.11. Redox-Mediating Potential of Ferrocene Derivatives

Among redox-active materials, ferrocene and ferrocene-based polymeric materials are of special interest due to their high stability in redox reactions and facile derivative syntheses. For example, an array of redox poly-(2-methacryloyloxy) and light-sensitive polymers based on ferrocenyl carboxylate-Co-4-methylacrylamino-4-nitroazobenzene (P (FcEMA-MAAZoo)s) were synthesized through free radical oligomerization protocol [90]. Light-responsive potential and redox properties of these polymers were evaluated via spectroscopy and cyclovoltammetric analysis. These polymeric slides were thought to have vital applications in a potentially high-information storehouse, and their mechanism of information storage is described in Figure 20.

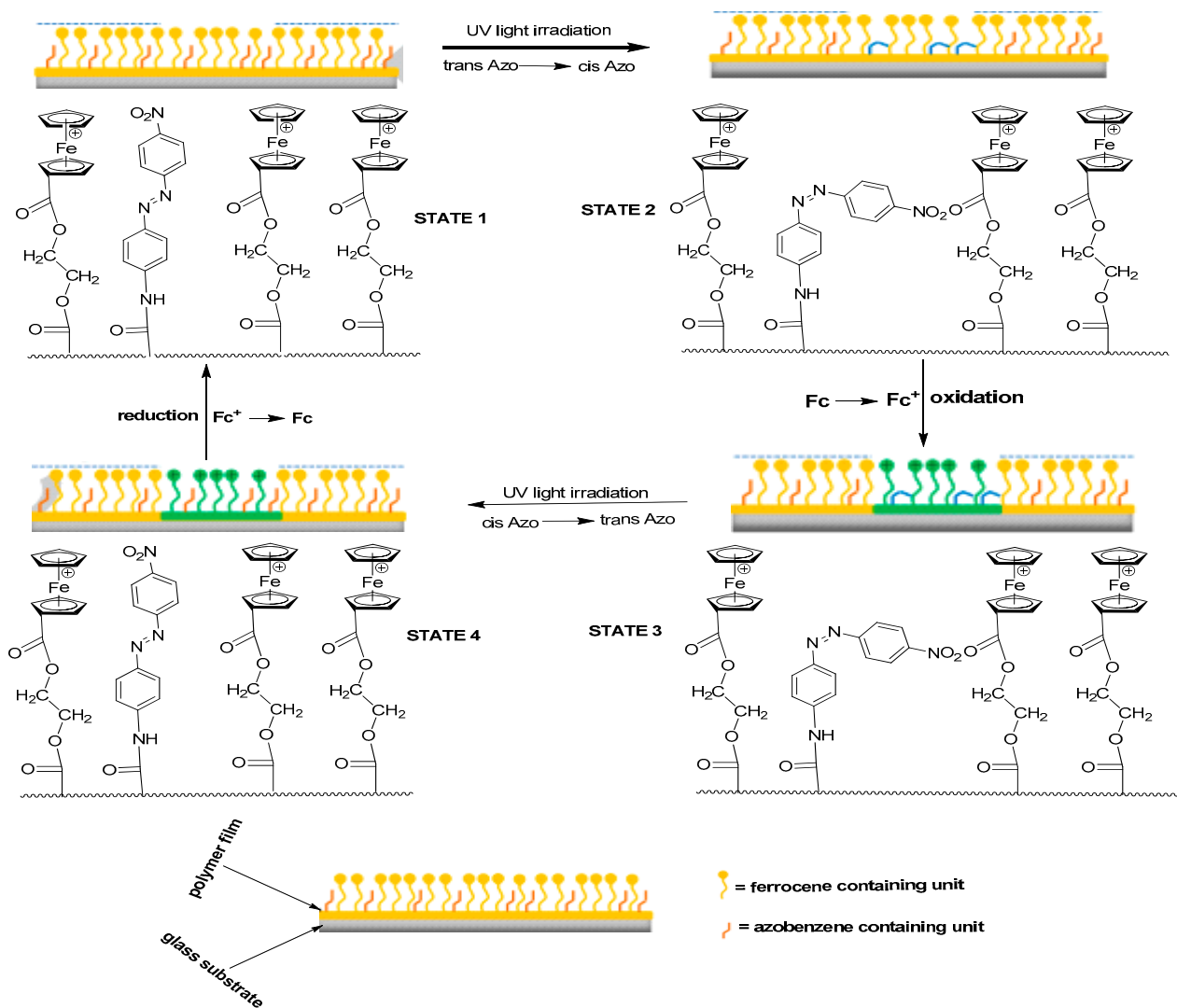


Figure 20. Mechanism of multi-state information storage on (P (FcEMA-MAAZoo)s)-based polymers.

3.1.12. Application in Photo-Induced Electron Transfer: Cascaded Molecular Logic

Karmakar and co-workers combined the redox activity of ferrocene with the photo-physical properties of coumarin and quinoline through the development of a molecular tool that turned on luminescence through the photo-induced electron transfer (PET) phenomenon with d^{10} metal ions [91]. Further, this research group also fabricated a probe (a), which behaved differently with various metal ions through fluorescent expression. Taking the edge of the differential selectiveness of this probe, binary basic logic circuits “INHIBIT” and “OR” were designed, which were used in biosensing applications with slight modifications (Figure 21).

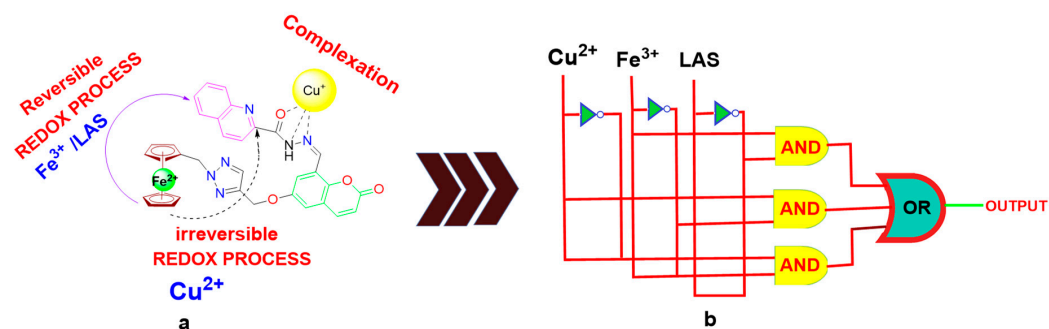


Figure 21. (a) Ferrocene-appeended coumarin–quinoline probe. (b) Combinational logic constructed with Cu^{2+} , Fe^{3+} , and LAS as inputs.

3.1.13. Role of Ferrocene in Catalytic Graphitization

In laboratory-prepared, modified novolak phenolic resins, graphitization was induced using ferrocene (PR). A recent study described the morphological and structural differences in the intermediate carbon structures containing iron throughout the graphitization process, obtained after several steps of heat treatment from 200 to 1000 °C. The presence of ferrocene (a catalyst and carbon source) and the reducing environment are both responsible for the induction of phenolic resin graphitization in onion-like hollow carbon. The hollow onion-shaped material facilitated 96% elimination in 5 min in the photocatalytic research of the pesticide atrazine (ATZ) in an aqueous medium and affected the mechanism of ATZ degradation and the synthesis of atrazine-2-hydroxy (HAT) in various reactors (Figure 22) [92].

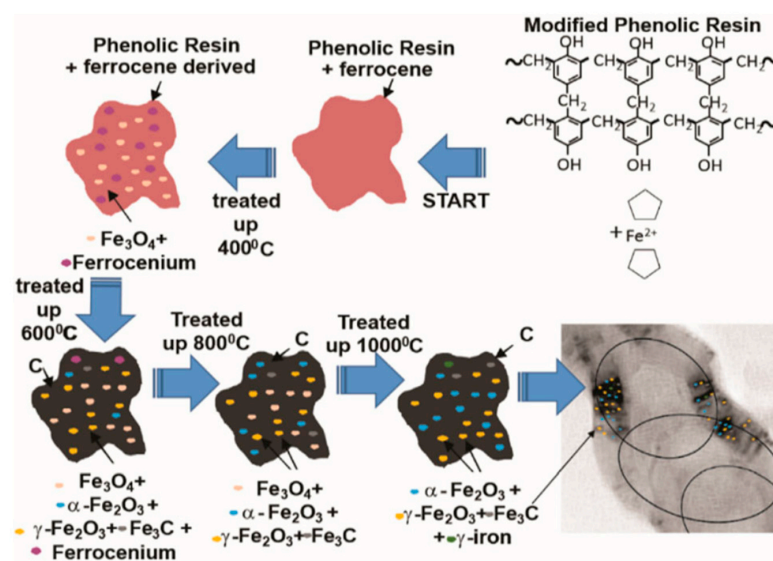
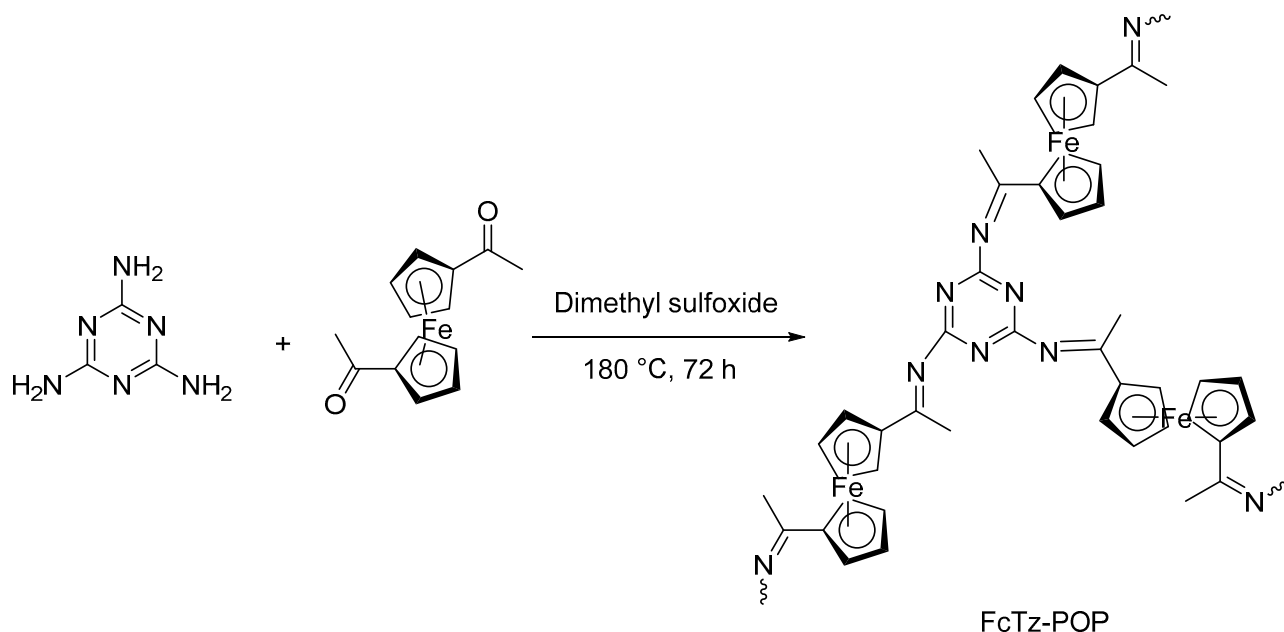


Figure 22. Magnetic nanoparticle formation during phenolic resin catalytic graphitization/ferrocene thermal decomposition process.

3.1.14. Ferrocene-Based Polymer as a Scavenger for Radioiodine

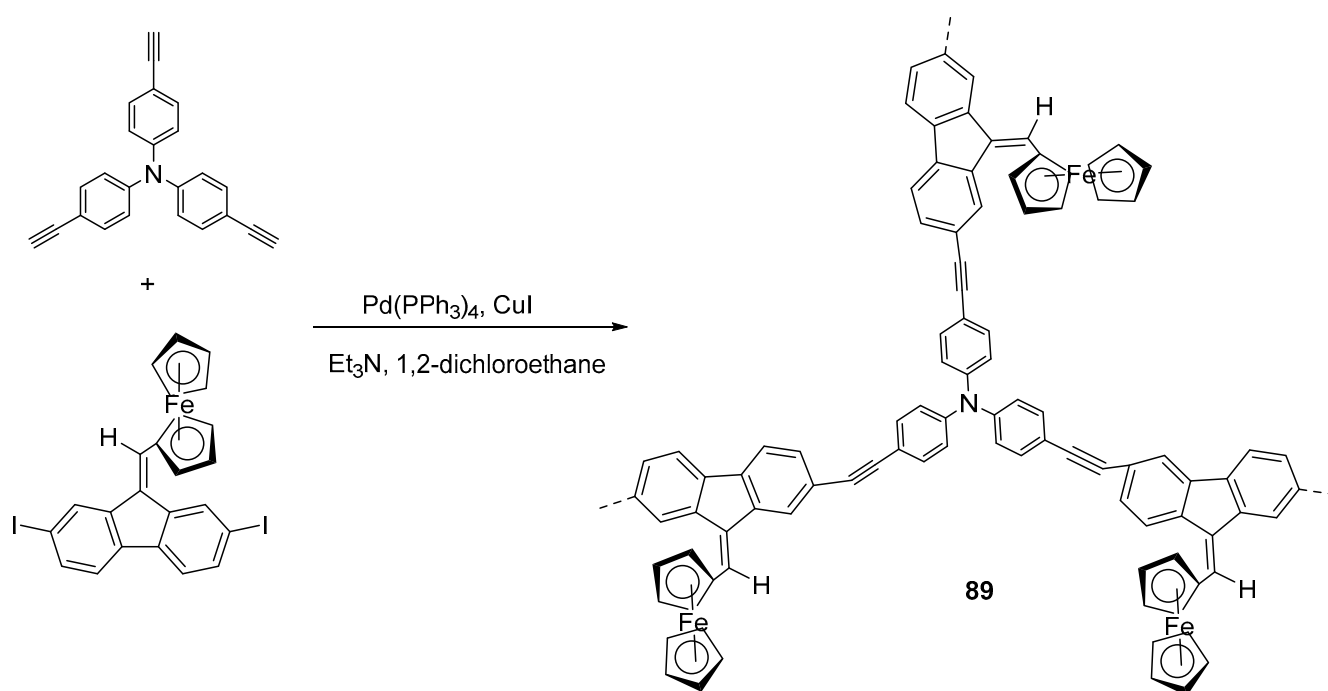
By using the Schiff base reaction, the porous ferrocene-linked organic polymer (FcTz-POP) was synthesized and exhibited a high iodine vapor capacity, 1.8 times that of a reference material without ferrocene (BpTz-POP). FcTz-POP exhibits a rapid rate of I₂ adsorption and a relatively high affinity due to the abundance of ferrocene blocks with a high electron density (Scheme 42). The iodine capturing for FcTzPOP, which is substantially higher than that of ferrocene-free BpTz-POP, can reach up to 396 wt% at 348 K and atmospheric pressure by integrating ferrocene building blocks. This is mostly due to the cyclopentadienyl group, which interacts with the iodine molecule more strongly than the benzene ring, and the Fe²⁺ on ferrocene, which may electrostatically bind negatively charged polyiodides [93].



Scheme 42. Synthesis of ferrocene-linked organic polymer (FcTz-POP) for iodine removal.

3.1.15. Ferrocene-Based Hyperbranched Polymers as Electroactive Materials

Using the Sonogashira coupling reaction, Wei et al. developed a ferrocene-based hyperbranched metallopolymer (**89**), incorporating the alternate units of TPA and fluorene as the main skeleton. An efficient method of controlling their morphology was successfully demonstrated to produce uniform nanostructures as spheres and hollow polyhedrons for specific applications (Scheme 43). When built into laser-induced breakdown spectroscopy (LIBs), the spherical polymer (SP) with a microporous structure had remarkable redox performances and displayed high capacity, large cycle stability, and better rate capability. The analogous HP provided rising BET surface areas of 1195 m² g⁻¹ in the precursor-derived ceramics by merging the intrinsic micropore of the organic frameworks and the macropore from the hollow polyhedron, and the as-made carbon materials were further applicable to remove water [94].



Scheme 43. Ferrocene–fluorene-appended branched polymer.

3.2. Applications in Catalysis

Because of their accessibility, novel stereochemical characteristics, the extensive variability of co-ordination approaches and options for the modification of the steric hindrance, thermal stability and tolerance to oxygen and water, serene derivatization, and electronic properties, ferrocene-grafted ligands created a large number of multipurpose ligand architectures in the recent trend of asymmetric catalysis.

3.2.1. Ferrocene-Functionalized Phosphine Ligand

The chemistry of the di- and polyphosphine ferrocene-based ligands in catalytic cross-coupling is detailed in carbon–carbon, carbon–nitrogen, and carbon–oxygen bond-forming reactions. Recently, an efficient ferrocene-grafted bi-functional phosphine-catalyzed enantioselective cycloaddition reaction of oxo-allenes with a large number of ketones was reported in order to prepare substituted dihydropyran derivative (90) [95]. Mechanistic study revealed that multifunctional phosphine catalyst containing ferrocene moiety (P_5), had excellent stereoselectivity in Rauhut Currier reaction, allylation, and chiral cycloaddition reaction, among all other ferrocene-functionalized phosphine ligands (Figure 23a). Because of ferrocene's strong electron-donating nature as well as its distinctive structure, chiral compounds based on ferrocene played important roles in asymmetric processes. Today, a wide range of chiral ferrocenyl ligands are known. Ferrocenyl chiral ligands have been exercised for ruthenium (II)-catalyzed asymmetric transfer hydrogenation of acetophenone using $\text{HCOOH}/\text{Et}_3\text{N}$ azeotrope as the hydrogen source. When (RC, SFc)-1-(Diphenylphosphino)-2-[1-N-(3-methylpyridin-2-ylmethyl) ethyl] ferrocene (L1) was employed, a moderate chemical yield of 1-phenylethanol with 83% ee was produced (Figure 23b) [96].

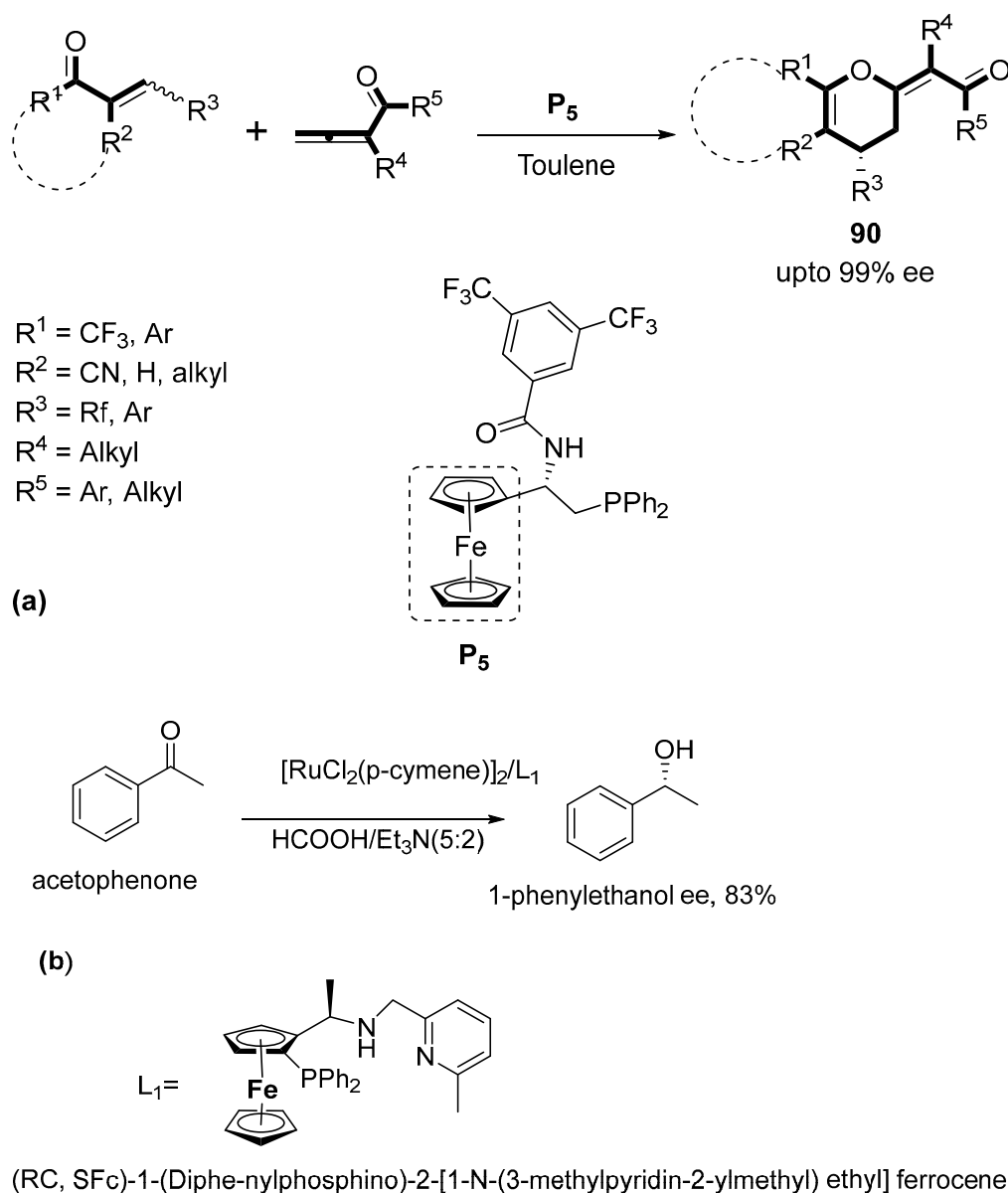


Figure 23. (a) Phosphine-catalyzed cycloaddition reactions of α -substituted allenes, (b) asymmetric synthesis of 1-phenylethanol (ee) from acetophenone using ferrocenyl chiral ligand.

3.2.2. Ferrocene-Appended Thiazolidine Ligand Framework

Ferrocene derivatives bearing donating groups exhibit a large variety of applications, especially in metal-catalyzed modern organic reactions. Based on the impetus provided using thiazoline–oxazoline ligands (**91a–d**), the investigations directed towards the synthesis of asymmetric disubstituted ferrocenyl ligands functionalized on the thiazolidine framework were carried out. The ability of these new bidentate [N, S]-ferrocene ligands to act in Pd-assisted asymmetric allylation had also been described and comes with their oxazoline counterparts (Figure 24). Further, the ortho-directing property of thiazolidine moiety for stereoselective ortho-lithiation reaction was also observed to always give an endoselective product [97].

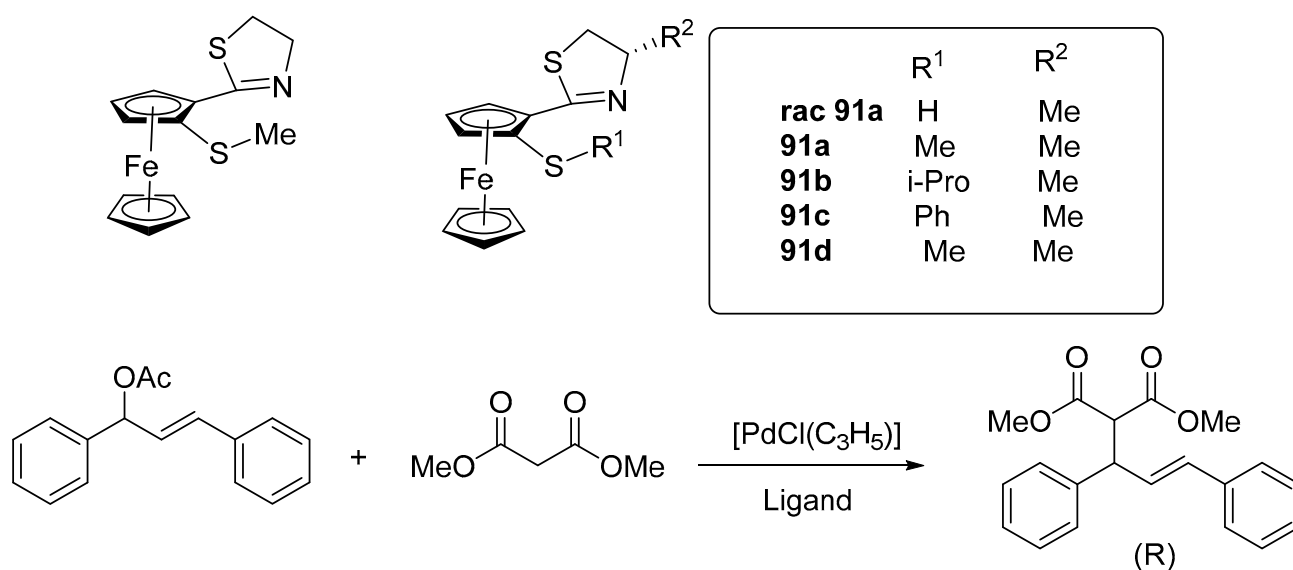


Figure 24. Chiral bidentate [N, S]-ferrocene ligands based on thiazoline used in palladium-catalyzed asymmetric allylic alkylation.

3.2.3. Chiral Oxazolinyl Hydroxyl-Clubbed Ferrocene in Asymmetric Reactions

Chiral oxazolinyl hydroxyl ferrocenes have been reported in the literature, particularly the most recent developments in enantioselective applications of ferrocene derivatives and diastereoselective production. Due to the successful functionalization of the aromatic C_p ring over the past few decades, chiral ferrocene structural variety has increased. Accordingly, multiple research groups have created sophisticated examples of synthetic procedures for N,O bidentate ferrocene moieties (**92a–c**) that have mostly been used as chiral catalysts in zinc-mediated nucleophilic addition reactions to carbonyl compounds. The mechanism subsumes freshly designed competitive catalysts in alkyl and aryl transfers to aldehydes (Figure 25) [98].

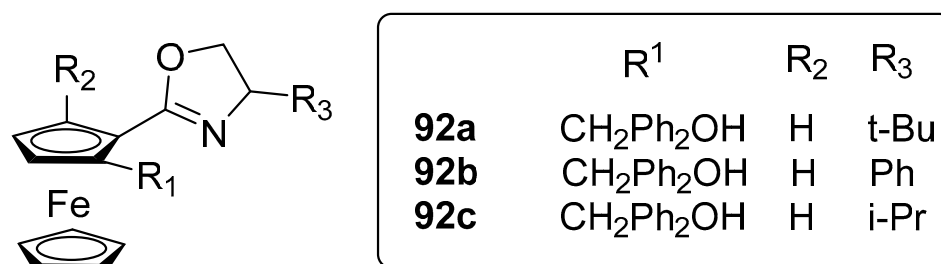
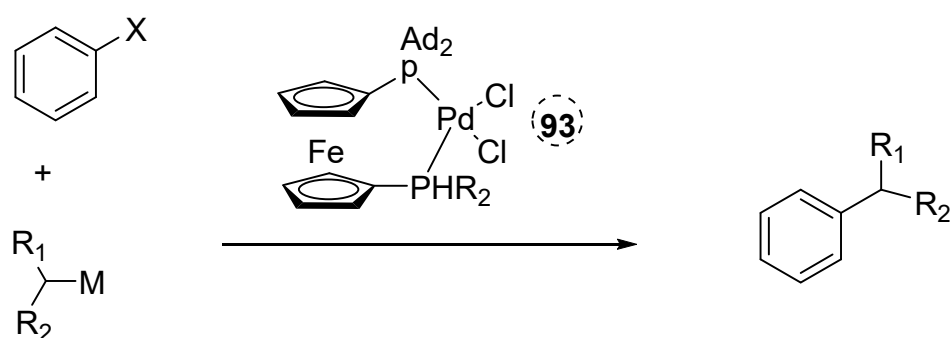


Figure 25. Chiral oxazolinyl hydroxyl ferrocene ligands.

3.2.4. Ferrocene Ligand in sp²–sp³ Coupling Reactions

In an advanced work, Xu and coworkers designed a series of novel ferrocene-based bidentate ligands (**93**) with di(1-adamantyl)phosphine as an anchoring group. After a complete characterization of the ligand structure through XRD, the group applied synthesized chelating catalysts in many C_{sp2}–C_{sp3} coupling reactions such as Murahashi–Feringa, Kumada–Corriu, Negishi, and Suzuki–Miyaura, with good to excellent yields. The devised method was employed for the synthesis of nine drug-like molecules in active pharmaceutical ingredient (API) synthesis (Figure 26) [99].



M= Li, Mg, Zn, B

Figure 26. Catalysis by ferrocene ligands bearing a bulky di-1-adamantylphosphino motif.

3.2.5. Applications of Ferrocene-Based Diols in Hetero Diels Alder Reactions

In a completely different work, Cunningham and Guiry reported a synthetic procedure for novel library synthesis of various ferrocene-functionalized diols (**94a–h**) with applications in hetero Diels Alder reactions. The stereoselectivity of the prepared ligands was maintained carefully and crystallographic data of such components were reported to confirm their structure. XRD study also revealed that these ligands exhibited both intricate inter- and intramolecular hydrogen bonding, along with uncommon, bifurcated hydrogen bonding interactions (Figure 27) [100].

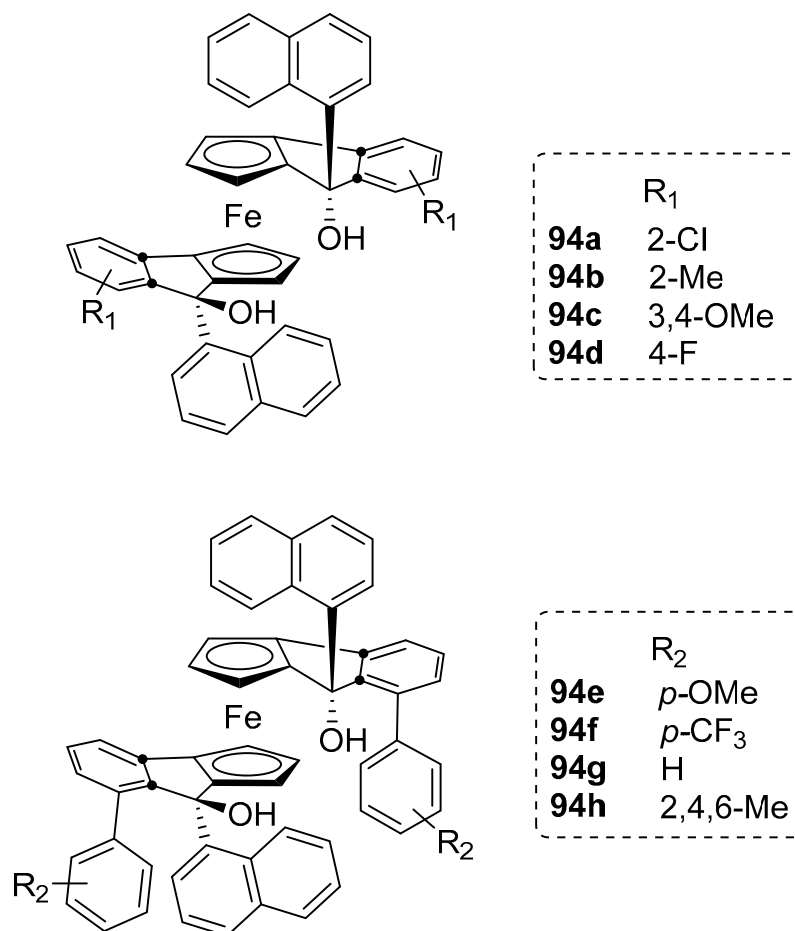


Figure 27. Ferrocene-fused nitrogen heterocycles.

3.3. Industrial Applications

Ferrocene chemistry crisscrossed discipline lines and had a significant part in organic, inorganic, biochemistry, materials science, chemical engineering, etc. These ferrocenyl compounds have recently been developed for industrial use, including in agrochemicals, additives for protective coatings to reduce rusting, fire retardants, rocket propellants, burning rate modifiers, water purification, etc.

3.3.1. Chromatographic Applications

A recent study reported the novel brush-like chiral immobilized stationary phase based on benzoyl-substituted N-ferrocenyl diphenyl ethyl alcohol installed on the surface of silica xerogel [101]. The newly synthesized compound (NF_CBF_S) **95** was used in HPLC and the synthesis employed γ -glycidoxypropyl trimethoxysilane as a binding agent. Amazing separation among the mixture of aromatic amines, hydrocarbon, substituted phenols, isoquinolines, pyrimidines, imidazole, and other aromatic systems was observed (Figure 28).

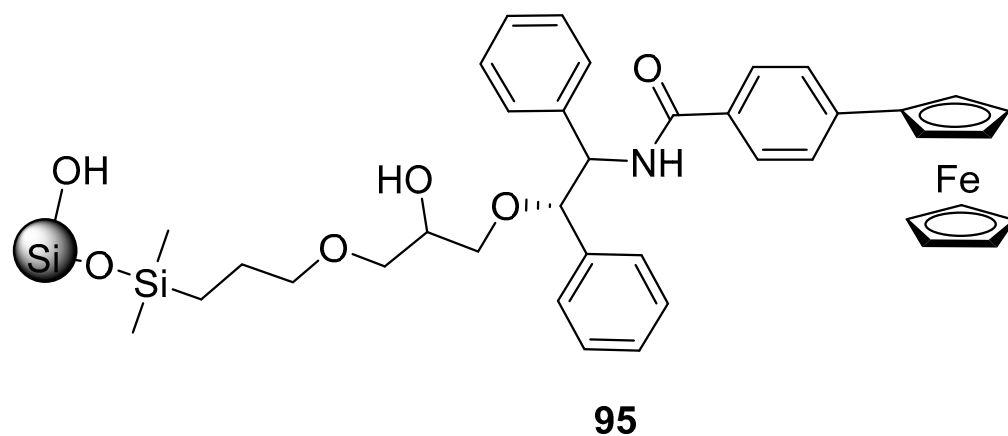
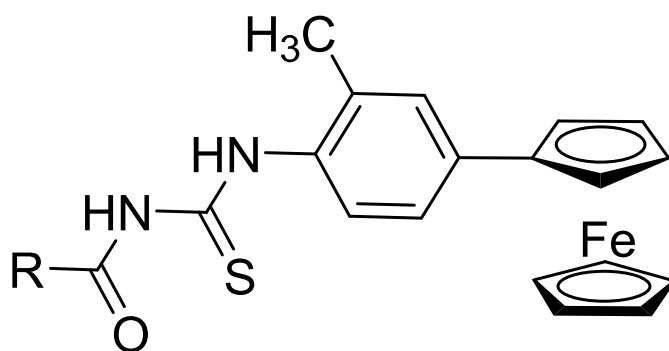


Figure 28. Structure of ferrocene-functionalized stationary phase.

In the same way, Wang and partners developed a non-conventional ferrocene-modified monolith that had a complex structure and was prepared through free radical elongation of vinyl ferrocene inside a stainless-steel column [102]. Proteins and other biological composites were separated by applying monolithic column chromatography. The fabricated porous structure displayed high mechanical strength, high adsorption, and low pressure. The different fractions of proteins were separated, and a highly efficient severance of small molecules was attained.

3.3.2. Corrosion Inhibition Potential

Novel ferrocene-graded thiourea derivatives with a smaller value of carboxymethyl starch (CMS) inhibition were reported as side-chain dependent [103]. These synthesized compounds (**96a–c**) were efficient corrosion inhibitors for mild carbon steel (MCS) in 1M aggressive hydrochloric acid solution, and their masking ability increased with temperature, concentration, and side-chain length (Figure 29). Results of the degraded product of two sample solutions with or without an inhibitor in HCl solution further confirmed the corrosion inhibition potential of the synthesized compounds.



$R = C_{11}H_{22}$ (**96a**) , $C_{13}H_{27}$ (**96b**), $C_{17}H_{35}$ (**96c**)

Figure 29. Ferrocene-based corrosion inhibitor motifs.

Ferrocene-based Schiff bases (**97a–c**) with an extended aromatic system and a large superficial zone have been recently reported (Figure 30). These manufactured bis-ferrocenyl Schiff bases were considered virtuous anticorrosive ingredients for aluminum AA2219-T6 alloy in 0.1 M HCl solution [104]. Further, electron-donating groups OCH_3 and OC_2H_5 bonded to Fcub and Fcuc, consequential in advanced inhibition competence.

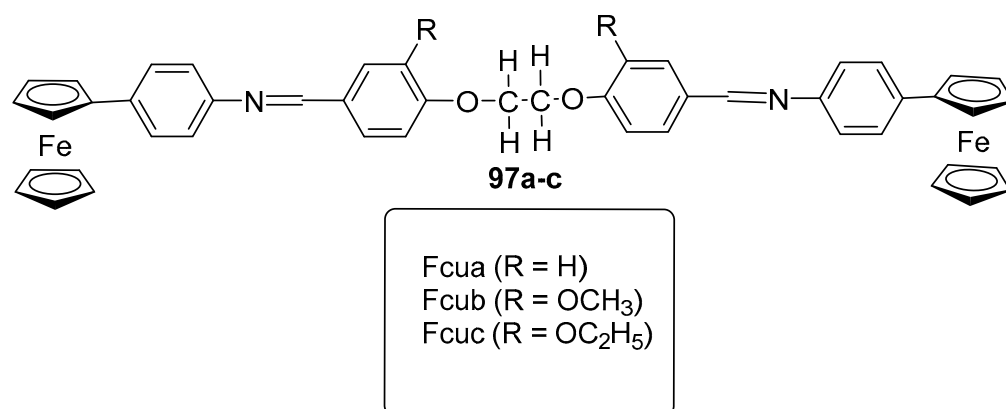


Figure 30. Structure of ferrocenyl Schiff bases (Fcua, Fcub, Fcuc).

3.3.3. Water Treatment

Traditional methods of water purification by chlorine are commonly used but have serious side effects [105]. One method to resolve these problems was the development of novel eco-friendly water disinfectants based on ferrocenylamine compounds, namely, 4-ferrocenylaniline (**98**), N-(3-bromo-2-hydroxybenzylidene)-4-ferrocenylimine (**99**), and N-(3-bromo-5-chlorosalicyl)-4-ferrocenylimine (**100**) [104]. The antibacterial activity of these ferrocene derivatives was evaluated against twelve diverse bacterial strains by applying the micro-dilution approach (Figure 31). In vitro bacterial analysis affirmed that the ferrocenylamine species had more remarkable antibacterial activity than its precursor ferrocene and could be used to eradicate bacteria from the aqueous media.

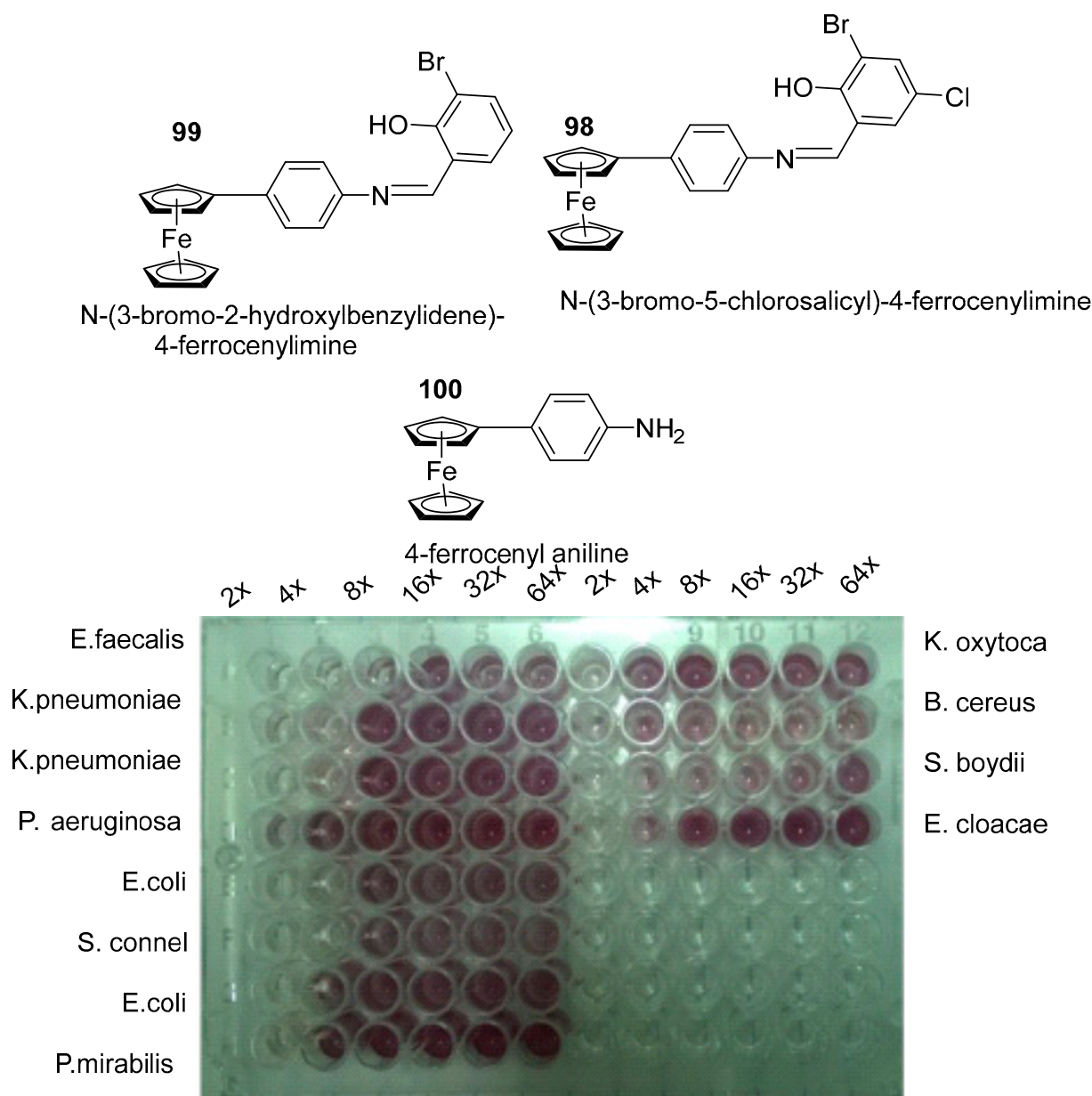


Figure 31. The 96-well microtiter plate layout for the testing of ferrocenylimine compounds.

Metalocene, especially ferrocene, can encapsulate organic contaminants efficiently as it has a cavity between two cyclopentadienyl rings and the Fe^{2+} center, but its solubility in aqueous media is a notorious drawback. An advanced article reported the solution to this issue via the preparation of novel ferrocene-functionalized organosilica nanoparticles and investigated them for sewage water treatment (Figure 32). The fabricated MONs manifested great absorption power for PO_4^{3-} within the range of 729, 1299, and 835 mg^{-1}/g , and the adsorption capacity for Congo red and Pb^{2+} was also measured and compared with reference $\text{SiO}_2\text{-Fe}$. This comparison confirmed the strong adsorption potential of MONs, and with further modifications, these materials could be used to resolve the issue of water treatment [106].

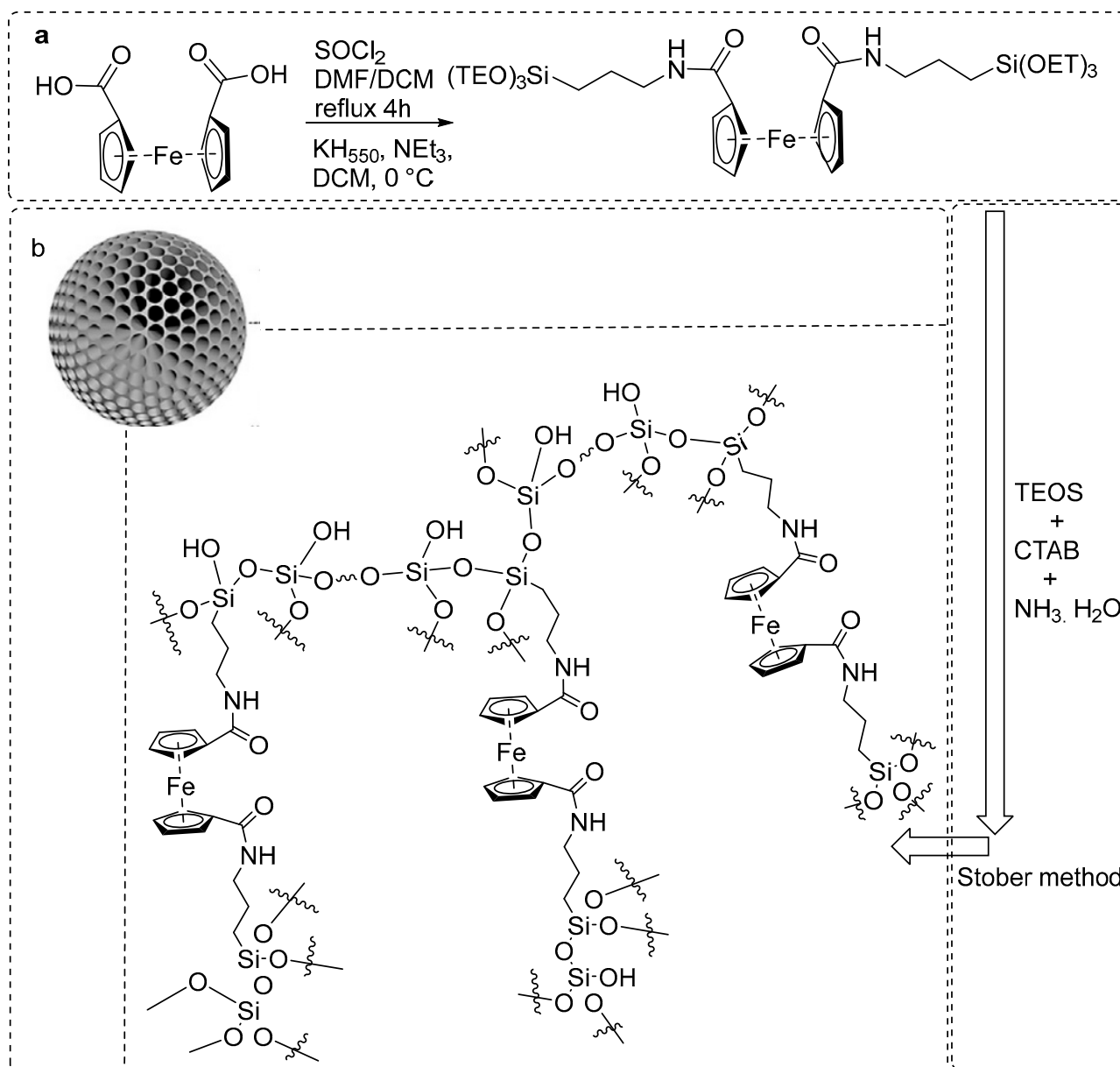


Figure 32. (a) Synthetic routes of ferrocene-containing organo-alkoxysilanes and (b) schematic illustration of MONs.

Yang and co-authors reported a synthesis of two permeable cross-polymers denoted as DPPF-HPP and DPPOF-HPP with excellent surface areas and comparable stoma structures of the concomitant micropores and mesopores [107]. They exhibited excellent adsorption of various colors with reported adsorption dimensions of 2280 mg g^{-1} and 1440 mg g^{-1} for Congo Red and Crystal Violet, respectively. Also, such materials exhibited no mark of degradation under repeated cycles and offered a remarkable potential for wastewater treatment (Figure 33).

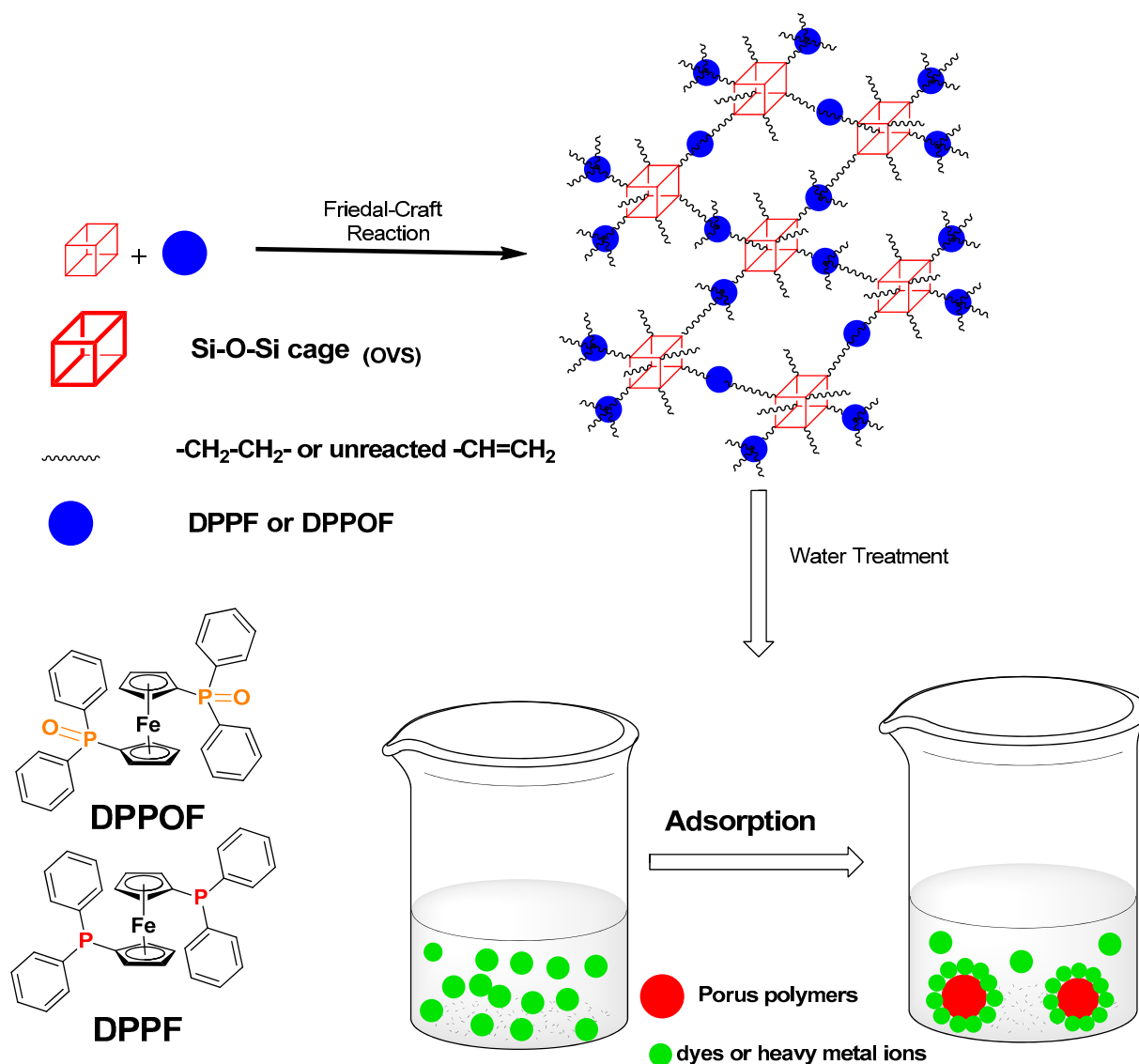
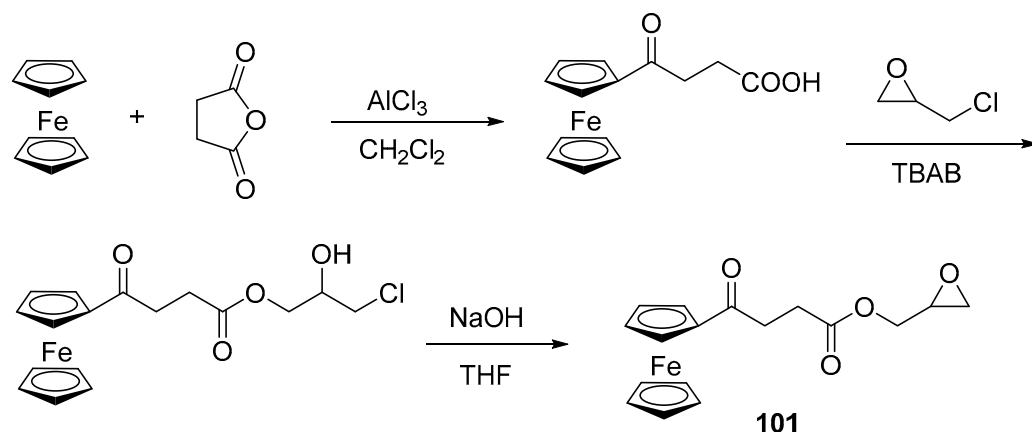


Figure 33. Schematic representation of water treatment through synthesized porous materials.

3.3.4. Use in Rocket Propellants

The addition of Fc-based BRCs to the propellant system enhances the combustion process and lowers the pressure exponents because of their better ignitability, excellent compatibility, reversible redox behavior, and thermal stability. In this regard, new ferrocene-grafted BRCs, named 3-(ferrocenylcarbonyl) propionic acid diglycidyl ester, were synthesized and their electrochemical properties were extensively studied (Scheme 44). Fc-PADE exhibited remarkable performance in the catalytic decomposition of inorganic oxidizer ammonium perchlorate (AP) and compromising anti-locomotory potential [108]. The novel ferrocene-based epoxy compound (101) also had compatible properties for burning rate catalysis in ammonium-perchlorate-based propellant [109].



Scheme 44. Synthesis of 3-(ferrocenylcarbonyl) propionic acid diglycidyl ester.

The inclusion of ferrocene in highly branched structures enhanced the catalytic behavior of BRCs and can mitigate controlled migratory problems. Using the same concept, Wang's group reported the synthesis of ethylene-diamine-based ferrocene-terminated dendrimers (0 G, 1 G, 2 G, and 3 G) and evaluated their electrochemical properties (Figure 34). The burning rate catalytic action of all synthesized dendrimers on the thermal breakdown of AP was inspected by TGA and differential thermogravimetry (DTG) techniques. Further anti-locomotory analysis revealed that first, second, and third generations of synthesized materials expressed upgraded anti-migration behavior in the ammonium-perchlorate-based propellant [110].

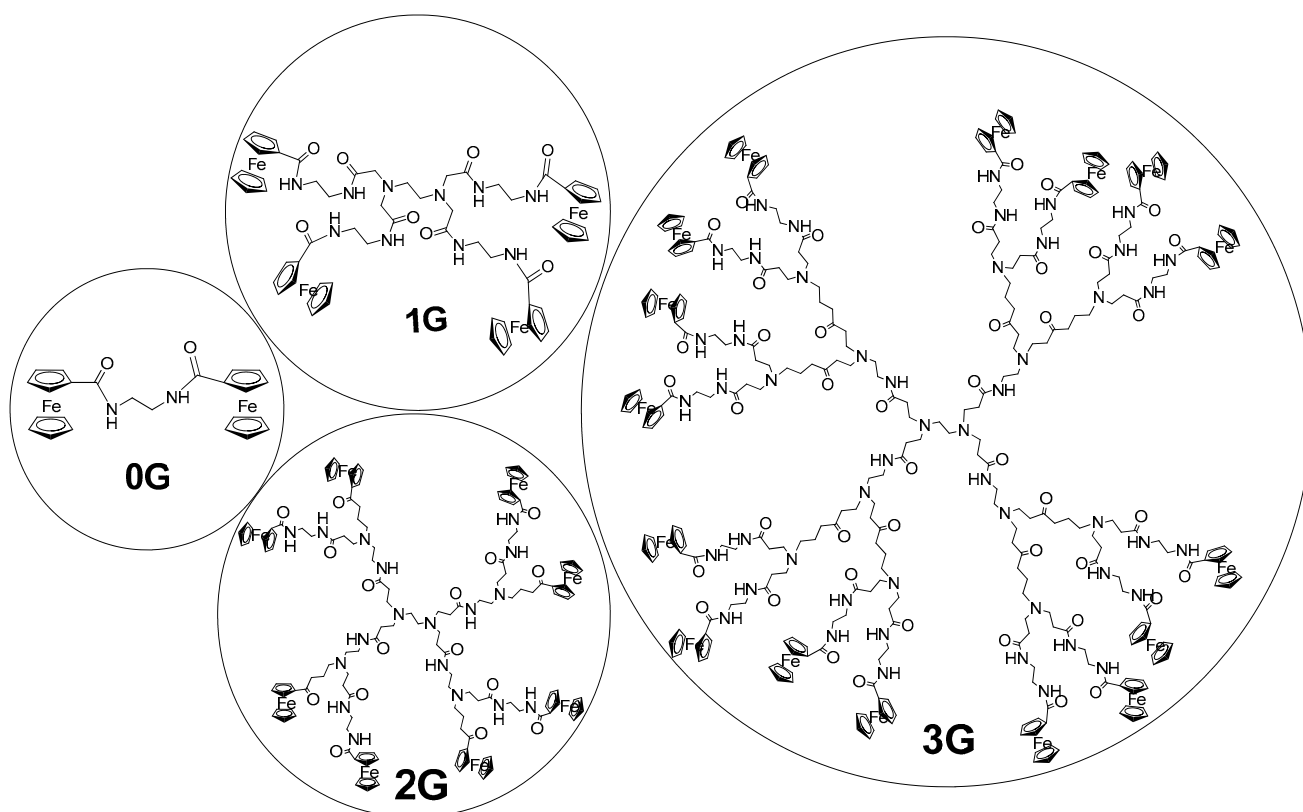


Figure 34. The 0–3G ethylene-diamine-based ferrocene-terminated dendrimers.

Cheng and co-workers blended ferrocene-grafted triazolyl compounds (F_c-TAZ_5) and characterized their structure through spectroscopic studies (Figure 35). Anti-locomotion

and stability aspects of all $Fc-TAZ_5$ were investigated, compared with catocene, and evaluated for their ignition capacity towards the thermal degradation of oxidizing agents [111]. Further, it was observed that the shear degradation potential of ammonium perchlorate could be upgraded by utilizing the triazolyl derivatives **102e**, **102g**, and **102k**.

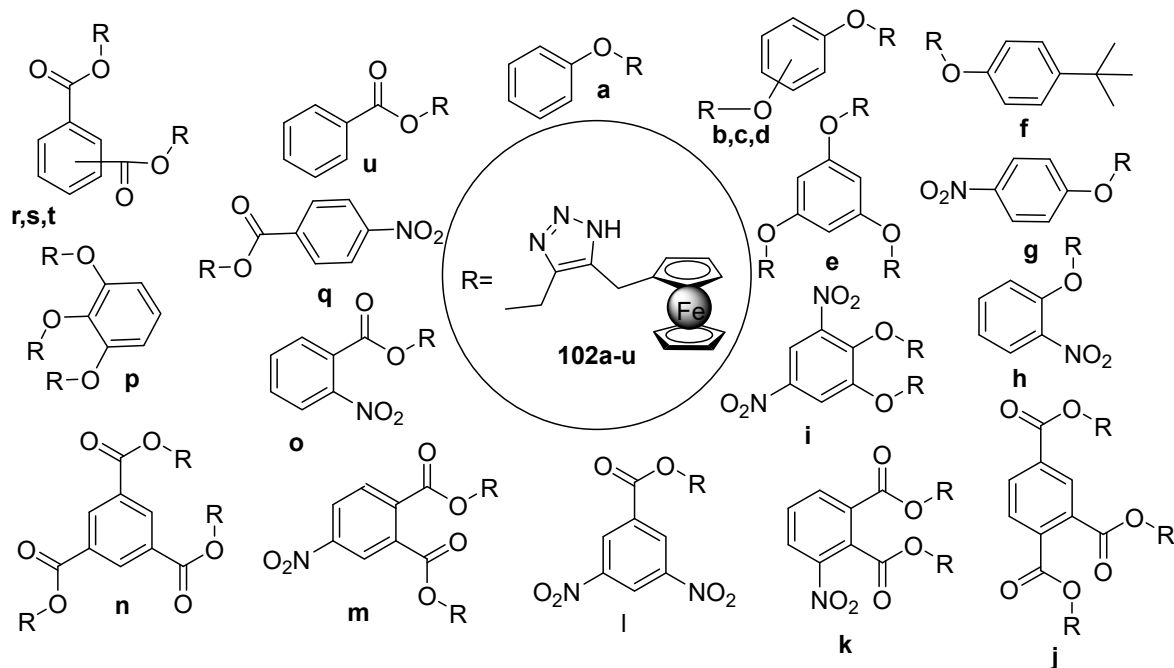
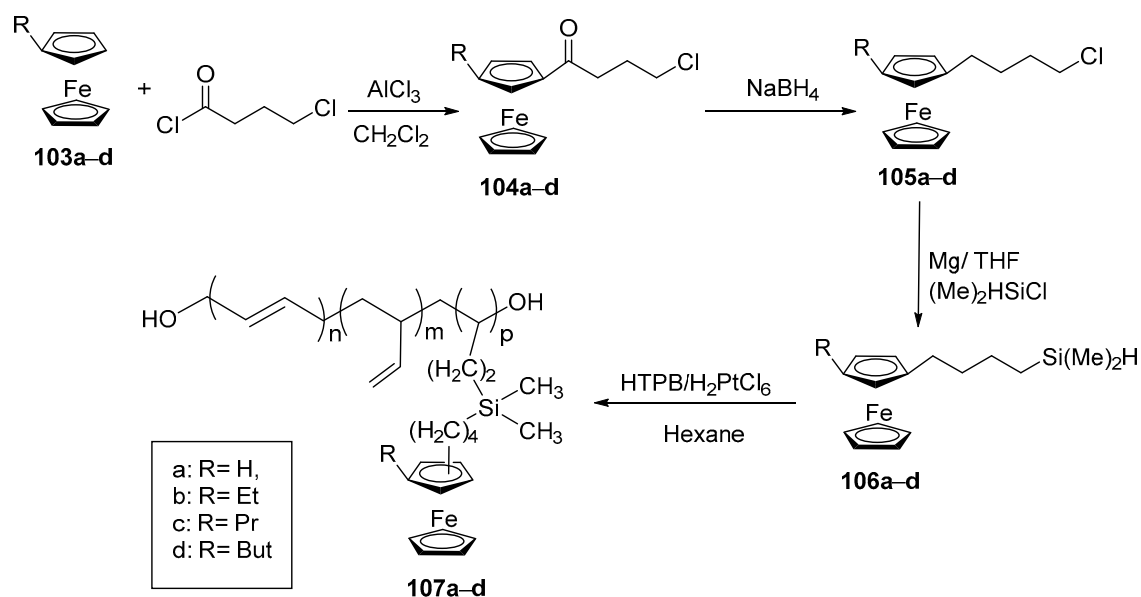


Figure 35. Structures of all ferrocene-grafted triazolyl compounds ($Fc-TAZ_5$).

3.3.5. Applications in BR Catalysis

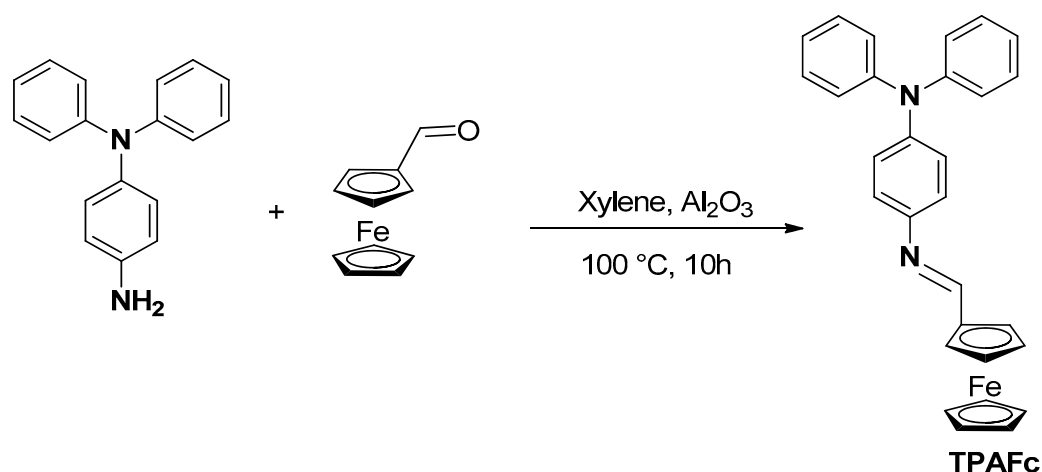
In a recent article, Keshver reported a synthesis of ferrocene-based hydroxyl-terminated polybutadiene conjugates **107(a–d)** through Friedel Crafts acylation reaction and their thermal-stability-related features were studied via thermo-gravimetric experiments (Scheme 45). Various other features like viscosity iron percentage and glass transition temperature confirmed HTPB as a superb burning rate accelerator catalyst for the construction of a composite gas generator [112].



Scheme 45. Synthesis of [4-(Dimethylsilyl)butyl] alkylferrocene-appended HTPBs.

3.3.6. Use in Electrochromic Appliances

Ferrocene (Fc) is widely used as an organometallic functional group owing to its easy modification, excellent electron-donating ability, and single-electron reversible redox reaction potential. A research group performed a synthesis of ferrocene-based triphenylamine derivative (*E*)-*N*-(4-(Diphenylamino) phenyl)-formimidoyl ferrocene (TPAFc) and carried out CV analysis that confirmed a coupling reaction between TPA units and the formation of an electroactive polymer film during successive scans (Scheme 46). These PTPAFc films displayed reversible electrochromic potential, excellent display, and quick switching response, which qualified these materials as an efficient contributor to the operation of electrochromic appliances [113].



Scheme 46. Chemical structure and synthesis route of TPAFc.

3.3.7. Modified Voltammetric Sensors with Ferrocene

Beitollahi et al. developed modified sensor and biosensor designs. Due to ferrocene's benefits, numerous electrochemical sensors and biosensors with favorable analytical properties have been developed (Figure 36). The enhanced electrochemical sensitivity is connected to surface fouling resistance, which calls for excellent stability [114].

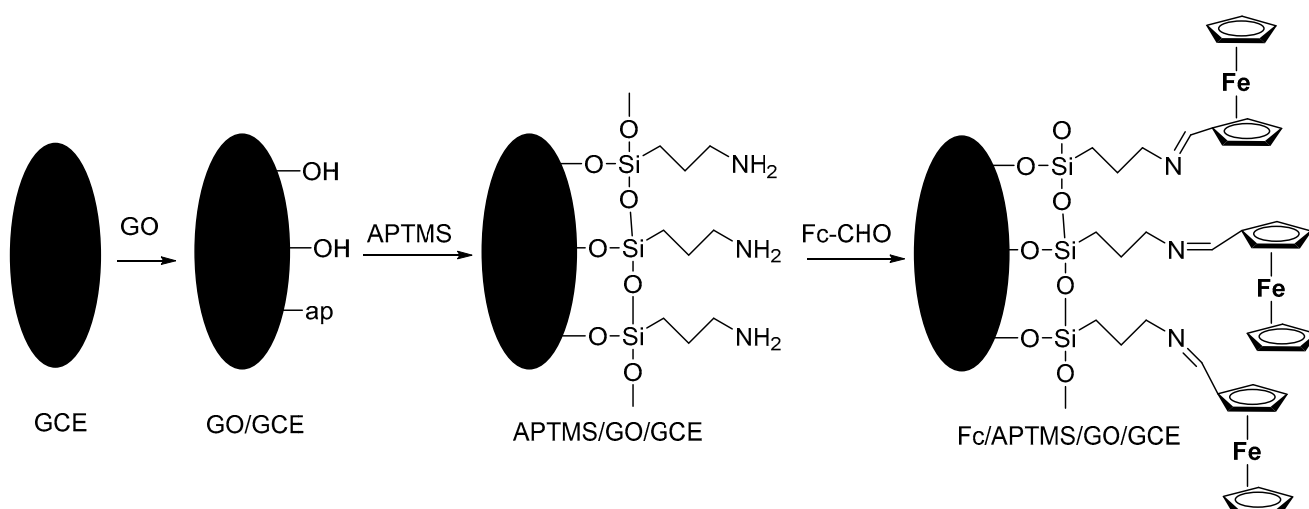


Figure 36. Fabrication of a glassy carbon electrode modified with graphene oxide which was then silanized with (3-aminopropyl) trimethoxysilane and ferrocene carboxaldehyde.

3.3.8. Application of Ferrocene in Aqueous Redox Flow Battery Suitable for High Temperatures

Using free radicals, the ferrocene monomer was successfully copolymerized with a water-soluble co-monomer. The redox potential of the ferrocene polymer ($E_{1/2} = 0.52$ V) in an aqueous environment is marginally higher than that of the low-molar-mass ferrocene derivatives previously disclosed, according to electrochemical characterization (Figure 37). Testing on batteries showed that the polymer exhibited consistent cycling behavior through 100 cycles of charging and discharging at room temperature and 60 °C, with an average Coulombic efficiency of over 99.8% throughout all cycling trials. Investigations into the active materials' temperature stability showed that they can not only endure high temperatures with ease, but that they actually facilitate the electrochemical reactions. As a result, costly cooling solutions are no longer essential, and the environmental effects can be carefully considered [115].

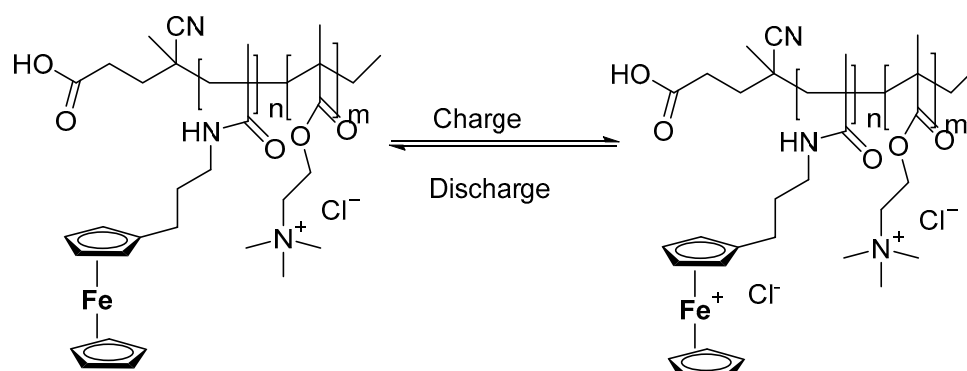


Figure 37. Ferrocene copolymer charging and discharging in redox flow battery.

3.3.9. Ferrocene-Based Non-Enzymatic Hydrogen Peroxide Sensors

In a recent study, novel ferrocene-based naphthaquinone structures 2,3-diferrocenyl-1,4-naphthoquinone (107a) and 2-bromo-3-ferrocenyl-1,4-naphthoquinone (107b) were synthesized through the combination of 2,3-Dibromo-1,4-naphthoquinone with ferrocene boronic acid [115]. Additionally, electrochemical characterization methods such as CV, CA, DPV, and EIS were used to examine the H₂O₂ detection capabilities of ferrocene-based naphthaquinone derivatives. The voltammetric behavior of H₂O₂ at 2-bromo-3-ferrocene-1,4-naphthoquinone in PBS has been studied under ideal conditions (Figure 38) [116].

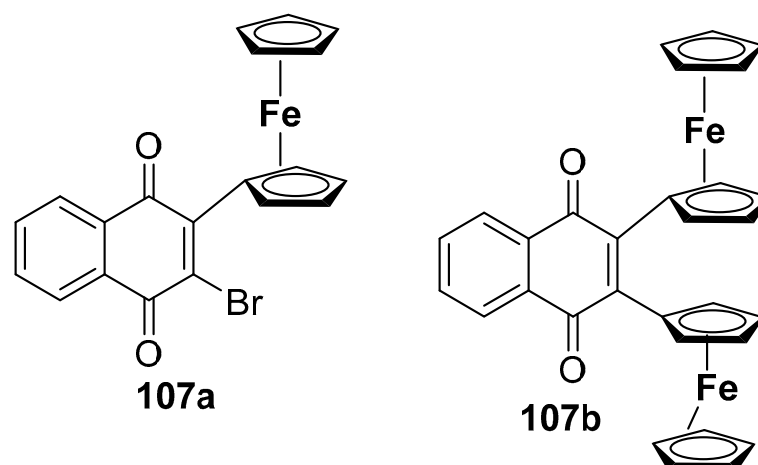
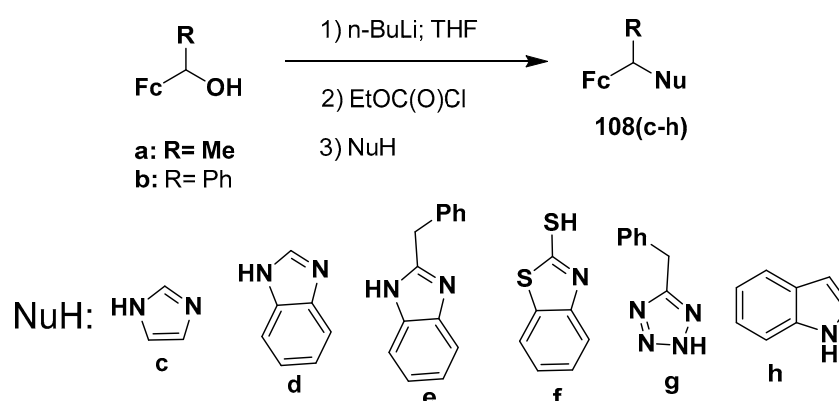


Figure 38. Ferrocene-based naphthoquinone as H₂O₂ sensor.

3.4. Agricultural Applications

3.4.1. Herbicide and Pesticide Safeners

In an auspicious work, ferrocene-functionalized heterocycles **108(c–h)** were prepared by treating α -ferrocene alcohol with azole or sulfur nucleophiles in acid-free conditions and investigated for their plant growth regulation effect (Scheme 47). These prepared azole derivatives showed plant vegetation potential and herbicidal findings of growth modulation, and the herbicide antitoxin properties of synthesized azoles were controlled by taking maize seeds and a reference herbicide (60% metasulfuron-methyl). After a comprehensive study, these ferrocene derivatives were considered efficient plant growth activators with herbicide safeness [117].



Scheme 47. One-pot α -ferrocenylalkylations with α -ferrocenols.

It is worth mentioning that ferrocenes proved to be useful in evidencing the redox properties of Fe(II) adsorbed onto mineral surfaces. To give an example, an exceptional electrochemical sensor was developed based on graphitic carbon–nitride and graphene oxide nanocomposites covalently linked with a ferrocene scaffold (Figure 39). The synthesized chemosensor exhibited a very low value of the limit of detection for Metolcarb which proved its superiority. The practical use of this sensitive material was found in many fruit and vegetable samples and attained satisfactory results with high precision [118].

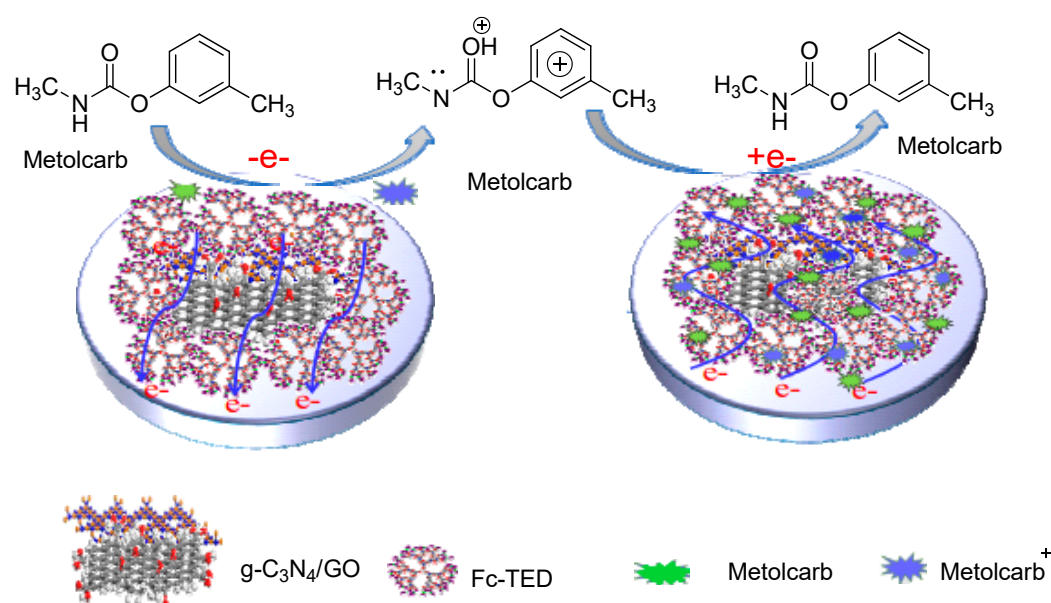
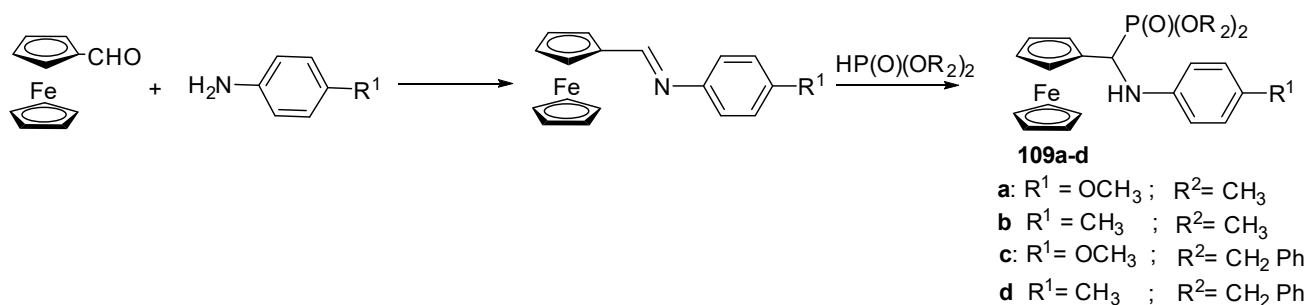


Figure 39. Mechanistic model of the sensor response to Metolcarb.

3.4.2. Plant Growth Activators

Lewkoweski and co-workers synthesized ferrocene-appended α -amino-phosphonates separated in the form of crystals with a remarkable yield of 50–70% (Scheme 48). Toxicity assay of compound **109c** was evaluated and described as less harmful for radish and oat plants while **109a** exhibited activity against *Vibrio fischeri*. Among all derivatives, **109d** displayed exceptional behavior, totally harmless to oat seedlings and thought to be the best contender for further investigation with respect to its expected application as a herbicide [119].



Scheme 48. Synthesis of N-aryl amino(ferrocenyl)methylphosphonates.

3.4.3. Solid-Phase Microextraction for the Determination of Iron Organic Compounds in Seawater and Soil

In an article, direct immersion of solid-phase microextraction (DI-SPME) and gas chromatography coupled to microwave-induced plasma with atomic emission detection (GC-MIP-AED) were used for the determination of five ferrocene derivatives (1,1'-dimethylferrocene, ferrocene carboxaldehyde, acetylferrocene, ferroceneacetonitrile, and benzoylferrocene) in seawater and soil. For this purpose, commercial fibers made of attached divinylbenzene and polydimethylsiloxane with good extraction efficiency were used in the DI mode. The reported detection limits (DLs) for soil and seawater were 0.9–4 ng g⁻¹ and 3–110 pg mL⁻¹, respectively (Figure 40) [120].

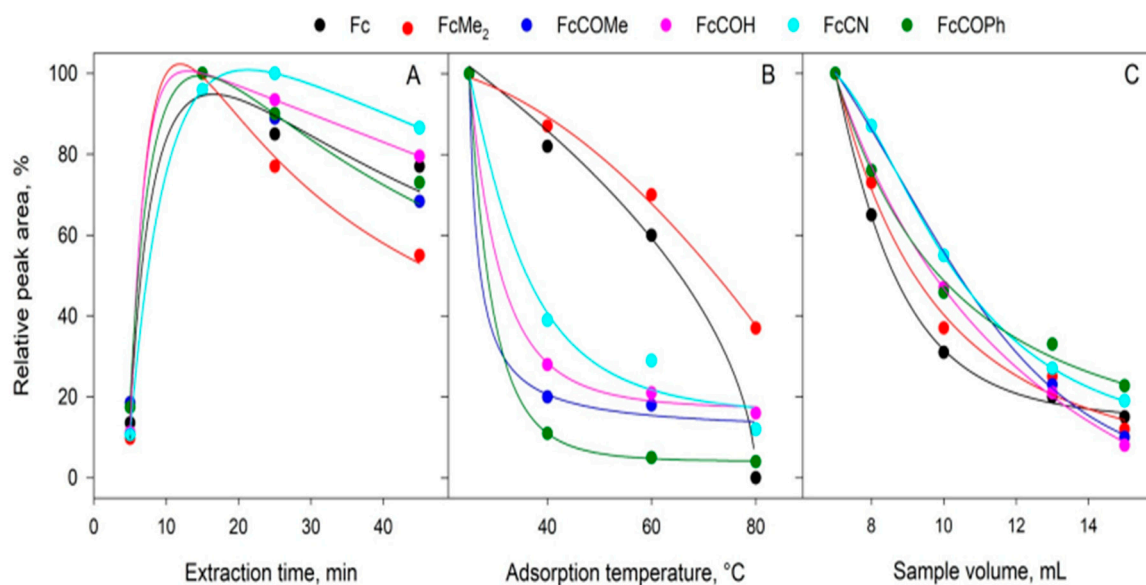


Figure 40. Influence of (A) extraction time, (B) extraction temperature, and (C) sample solution volume on the sensitivity.

3.4.4. A Probe-Free Electrochemical Immunosensor for Methyl Jasmonate

Methyl jasmonate, an endogenous plant hormone that is crucial to the creation of food, was identified by a unique probeless electrochemical immunosensor accomplished by Xing and coworkers. The procedure includes the attachment of ferrocene with carboxylated graphene (COOH-GR) and multi-walled carbon nanotubes (COOH-MWNT) to produce a composite that was further processed to afford screen-printed electrodes (SPE). The conductivity and catalytic activity of the sensor were enhanced by the application of COOH-GR and COOH-MWNT while keeping the MeJA antibody fixed. As a result, MeJA can be detected using the immunosensor without the use of an external redox probe solution with a very low detection limit, such as 31.26 fM (Figure 41) [121].

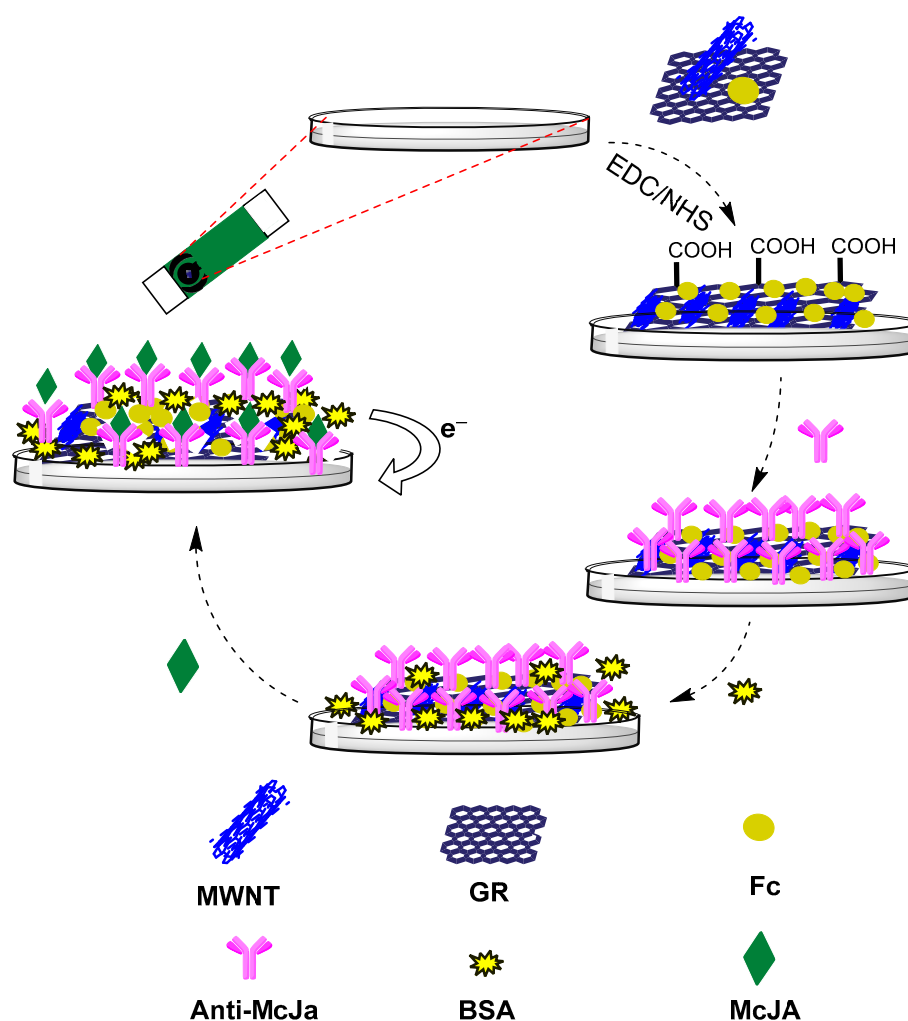
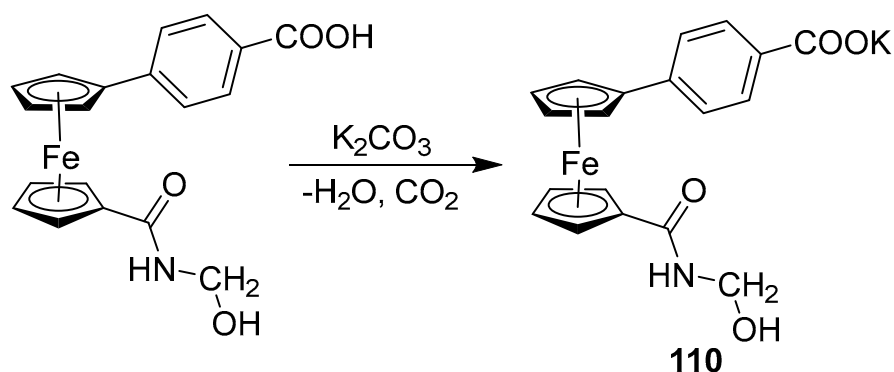


Figure 41. Schematic illustration of the construction process of the electrochemical immunosensor of MeJA.

3.4.5. Ferrocene-Containing Nitrogen Fertilizers

A recent survey reported liquid nitrogen fertilizers containing some derivatives of ferrocene, detailing their use, importance in agriculture, and spectral analysis. Experimental studies revealed that cotton and wheat have better retention of yield elements than control when applying a new Ferben–potassium nitrogen liquid fertilizer during the application period. The final result reported a surge in the yield of cotton by 5–6 ts/ha and wheat by 10–16 ts/ha, indicating high economic efficiency (Scheme 49) [122].



Scheme 49. Synthesis of Ferben–potassium fertilizer.

3.5. Biological Applications

Biochemical uses of ferrocene derivatives are typified by a wealth of contributions. In advanced research, Jolly and group members reported the progress of a vastly penetrating double-mode electrochemical podium for the recognition of microRNAs, which was a significant tool in gene expression activity. The platform was industrialized by consuming peptide nucleic acids as probes on gold electrode surfaces to capture target miRNAs, and thiolated ferrocene offered a harmonizing detection approach by elevating miRNA concentration (Figure 42) [123]. The electrochemical platform could also be readily extended to other miRNA/DNA detection along with the preparation of microarray platforms.

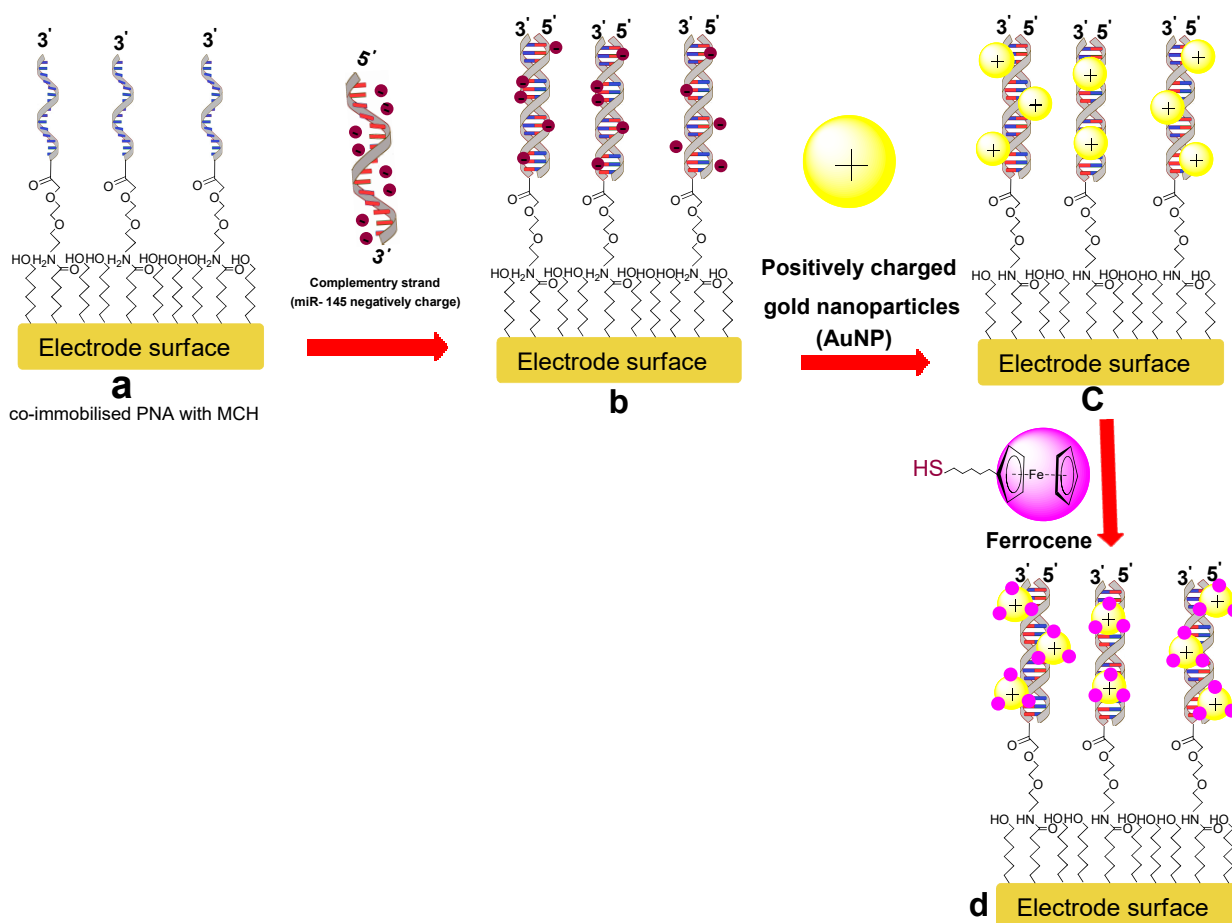


Figure 42. Schematic representation of microRNA detection strategy.

Another handy piece of work described the fabrication protocol of a trifle electrochemical immunosensor for the hypersensitive identification of the Avian Leukosis virus subgroup (Alv-J) using β -cyclodextrin, gold nanoparticles, and ferrocene group host–guest composite as marked and GR-PTCA provide the sensor surface (Figure 43). Impairment of composite material directly onto the surface of the secondary antibody (ab_2) confirmed its powerful binding affinity to the host. Moreover, it was reported that the immunosensor had higher receptiveness, remarkable reliability, and reusability, recommended for the computable diagnosis of ALv-5 during clinical trials [124].

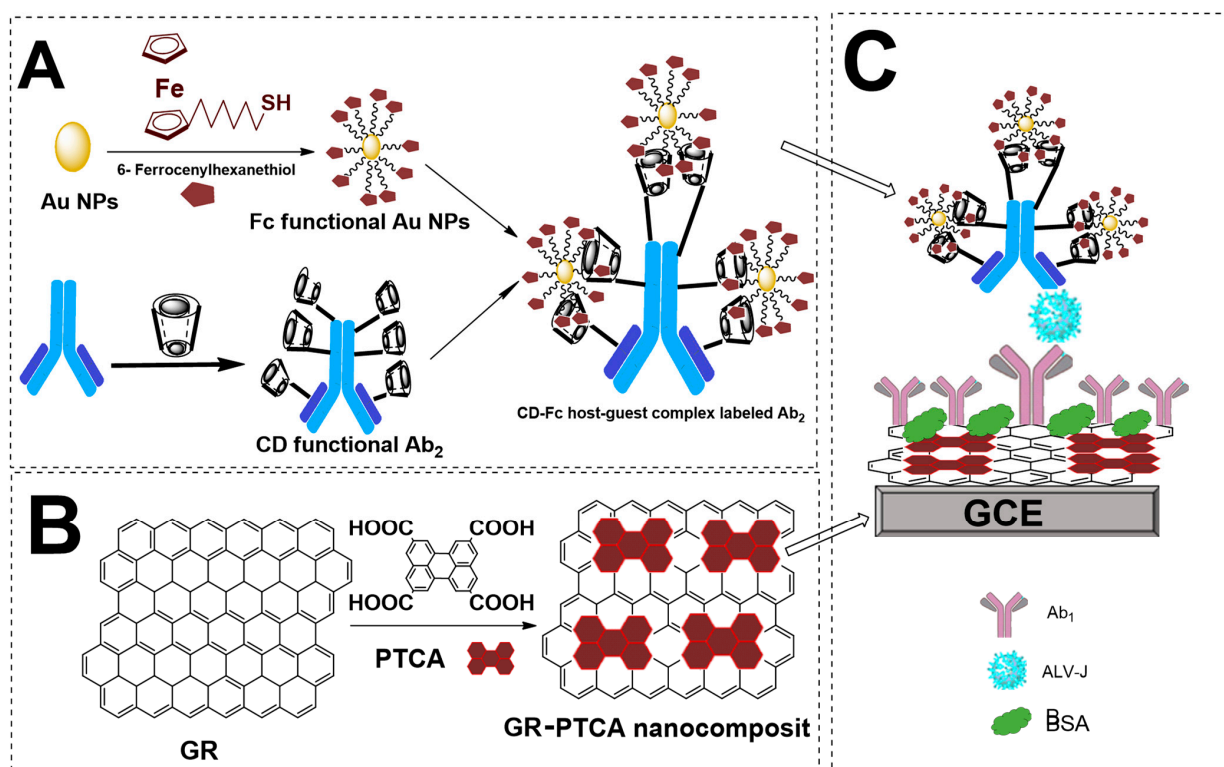


Figure 43. Schematic illustration of the preparation of Fc-AuNP-b-CD-Ab₂ (A), GR-PTCA (B), and the assembly of the electrochemical immunosensor (C).

The DNA–drug complex has attracted great attention recently and the linkage of ferrocene-functionalized drugs with nucleic acids seems to be a “cherry on the top” in the field of medicinal chemistry. In a comprehensive study, a synthetic protocol for the synthesis of a new guanine-rich DNA ligand based on naphthalene diimide (NDI) linked with ferrocene was reported, and the redox potential was analyzed using guanine-rich DNA-immobilized gold electrodes [125]. The redox activity of these ligands was evaluated, and the electrode surface was modified for DNA binding. Moreover, CV analysis described greater selectivity of **111** and **113** for G-quadruplex and realized the anticancer activity of these compounds with a low value of cytotoxicity for normal cells (Figure 44).

In a different work, Jia’s group synthesized three ferrocene-based naphthalimides and evaluated their attaching abilities with DNA using ethidium bromide displacement techniques [126]. Among all derivatives, **115** exhibited the highest binding potential for DNA strands with remarkable activity against four different human cancerous cells, evaluated by cytotoxicity tests. The synchronizing potential of the ferrocene nucleus was responsible for the upgradation of cytotoxicity that was linked to the damaged DNA of the cancer cell (Figure 45).

An array of ferrocenyl chalcones was investigated for their binding affinities with calf thymus DNA and bovine serum albumin, inspected by UV–visible, circular dichroism, and phosphorescence spectroscopy [127]. Likewise, topoisomerase retardation analysis

Ferrocene derivatives have quickly received significant interest in drug delivery research due to their unique structure, redox character, and hydrophobicity, as they could be transformed into a hydrophilic ferrocenium cation in the presence of a mild oxidizing agent [128]. In this regard, a significant effort was made to design hydrophilic ferrocene tetradecyl units to build up cationic micelles through self-assembly, and the detailed mechanism is described in Figure 47. Micelles were then converted with hyaluronic acid to obtain the HA-Fe-C₁₄ complex. These micelles were used for the delivery of Adriamycin drugs, released under a higher GSH environment. The synthesized micelles were concentrated inside tumor cells and revealed highly efficient antitumor potential in both primary and secondary biological screening tests [129].

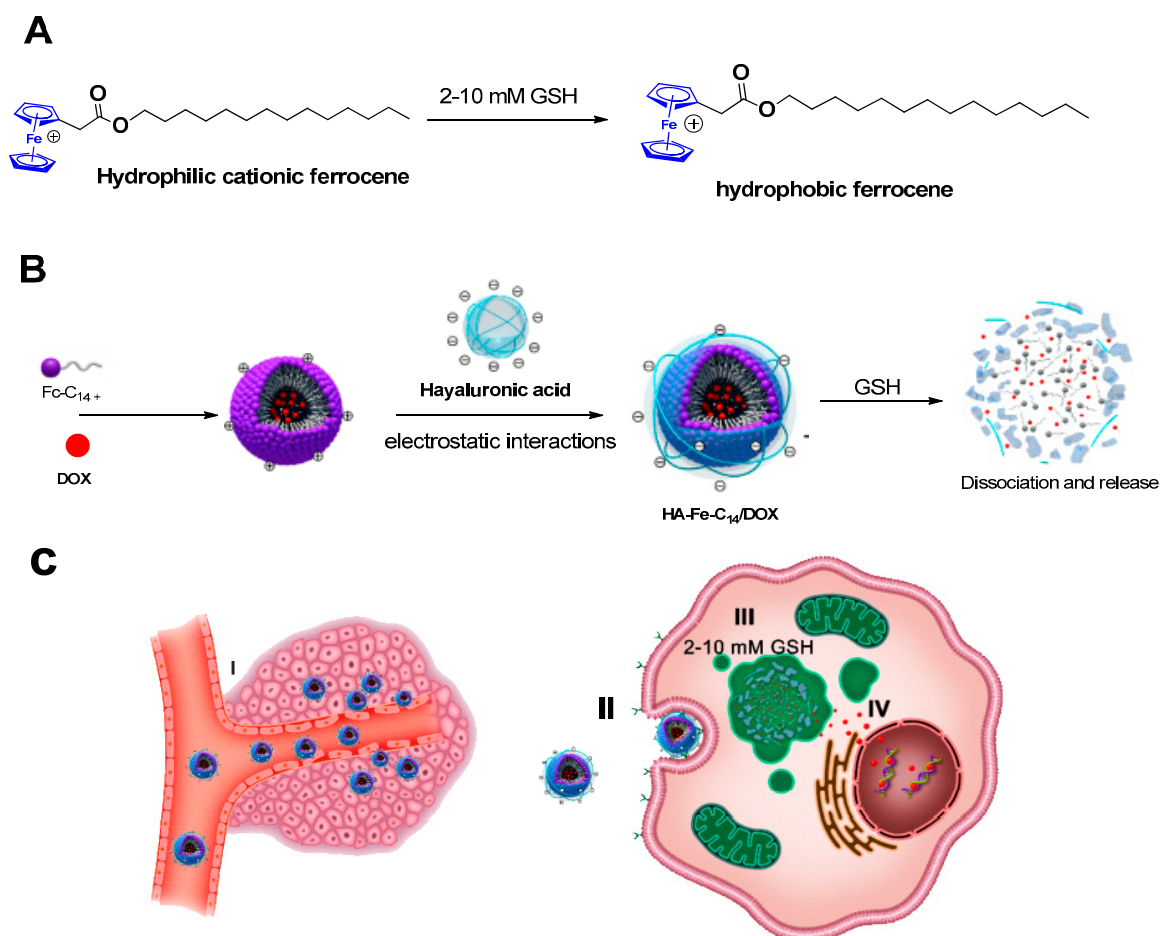
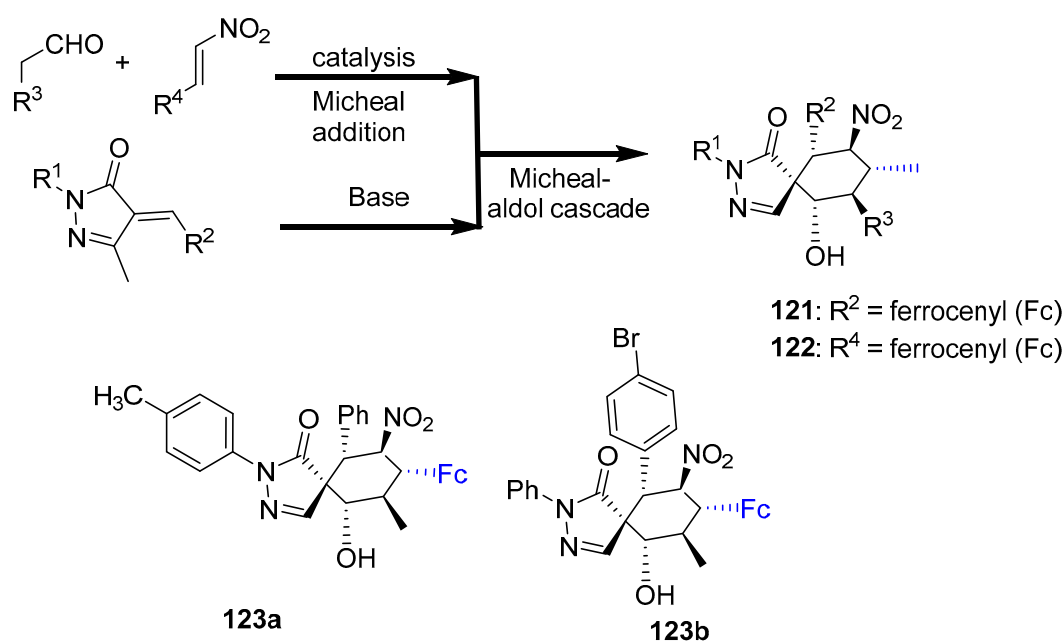


Figure 47. The detailed mechanism of Adriamycin delivery.

Recently, poly-functionalized chiral spiro-pyrazoline–ferrocene hybrids were synthesized through asymmetric organic catalysis and screened for their RalA inhibition potential (Scheme 50) [130]. Among all synthesized compounds, **123a** exhibited powerful RalA inhibition and led to the accretion of RSO and passive spread of pancreatic cancer cells via tempted mitochondrial damage and apoptosis in pancreatic tumor cells. This was a competent application of asymmetric organic catalysis in organometallic bio-organometallic chemistry.



Scheme 50. Asymmetric synthesis of chiral spirocyclic pyrazolone ferrocene hybrids.

3.6. Medicinal Applications

Organometallic compounds like ferrocene have unique properties like low toxicity, low oxidizing potential, water and air stability, and electrochemical aspects that allow them to have wide applications in medicinal chemistry. Nowadays, ferrocene derivatives have found their way into pharmacology as potent HIV, anti-cancer, anti-trypanosomal, antimalarial, anti-diabetic, and antiviral agents, among others. These potent ferrocene-based drugs were either prepared through organic synthesis or developed from already-recommended drugs via drug reprofiling or repurposing strategies in which the structural variation of established drugs with ferrocene scaffolds was reported [131,132].

3.6.1. Anticancer Activity

Ferrocene derivatives have been reported to display anti-proliferative activity against several tumor cell lines with less toxic effects in comparison to known anticancer drugs. Since 1970, several types of ferrocenyl compounds were synthesized and subjected to anticancer studies because of their remarkable electrochemical properties and lower toxicity. Ahmad et al. carried out the synthesis of four newly modified Mannich bases of Lawsone that accommodated the Ferrocene units. Lawsone contains a naphthoquinone nucleus whose drug properties were already reported [133]. The biological study showed that compound **124a** is the most active member among a series of four compounds that had maximum antiproliferative activity and it could be a promising lead for the development of ligands that could be used for the treatment of hormone-refractory prostate carcinomas and MDR tumors (Figure 48).

Numerous ferrocene conjugates, including the new N-(*p*-chlorophenyl)-carboxamido ferrocene (**125–131**), were synthesized and their antitumor activity was explored in detail [134]. Among these ligands, **126** and **128** with benzimidazole mainstay were potent against HeLa cells, attaining IC₅₀ values of ~5 μM and ~6 μM, respectively. Complex **130**, also bearing a benzimidazole support, presented somewhat higher values (~11 μM). These complex mechanisms were thought to be related to a more operative cytotoxic potential (Figure 49).

Sonia and Martina synthesized ferrocenyl conjugates of clotrimazole by replacing one of the aryl rings with ferrocene in the triphenylmethane system (Figure 50). Biological screening tests of these derivatives on two different human prostate cells were carried out and compared with the parent drug that exhibited a twofold increment in the cytotoxicity of

these ferrocenyl conjugates on HT29 colorectal carcinoma cells. Moreover, commensurable activity was shown against MCF-7 breast cancer cells [135].

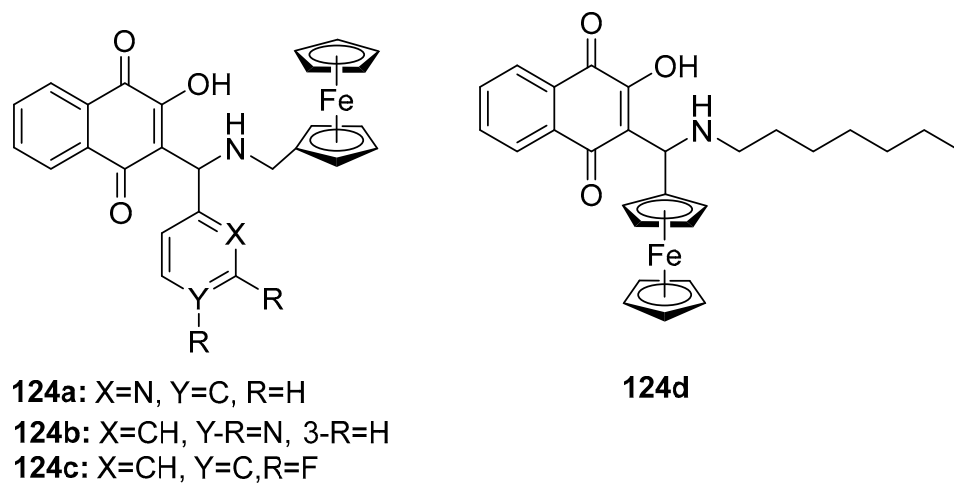


Figure 48. Ferrocene-based Mannich bases derived from Lawsone.

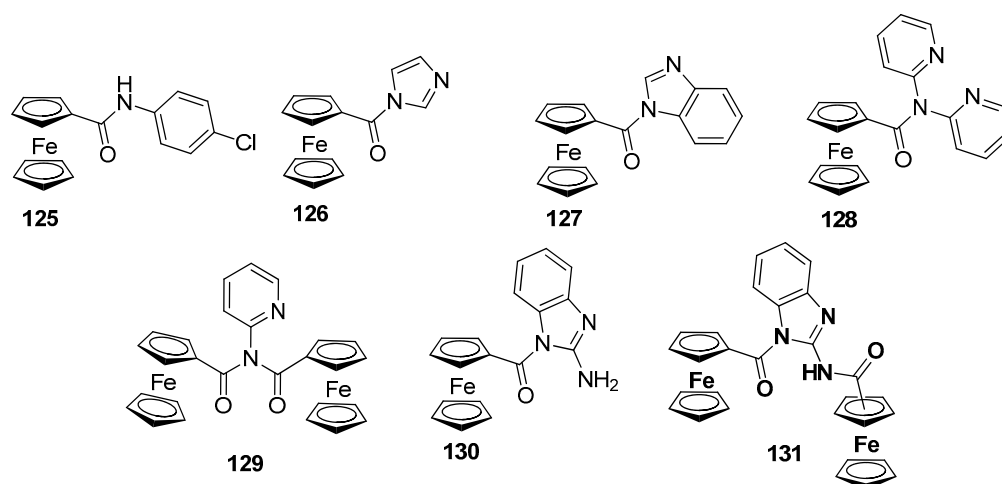


Figure 49. Structures of ferrocene-appended anticancer ligands.

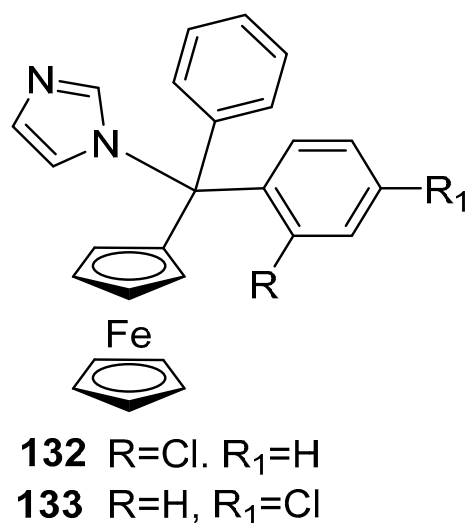
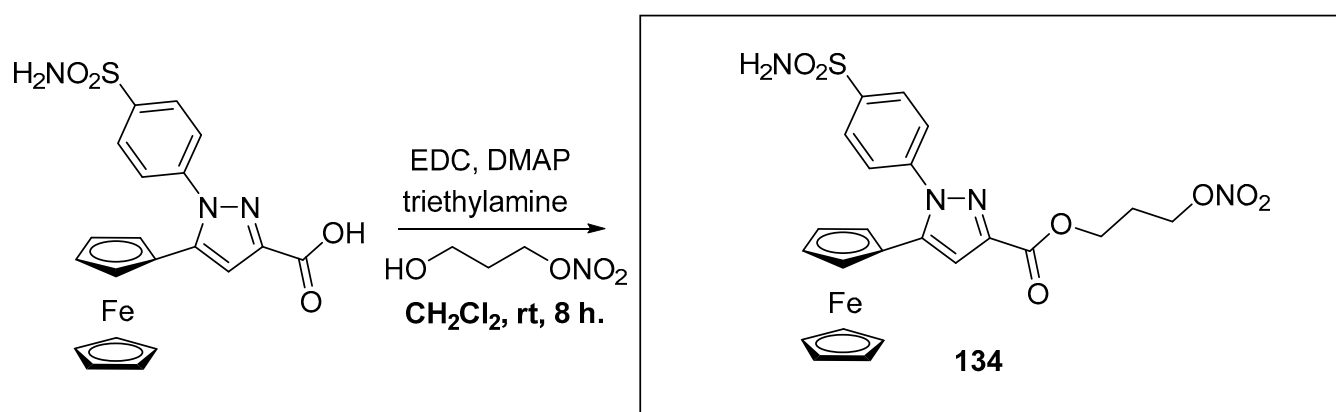


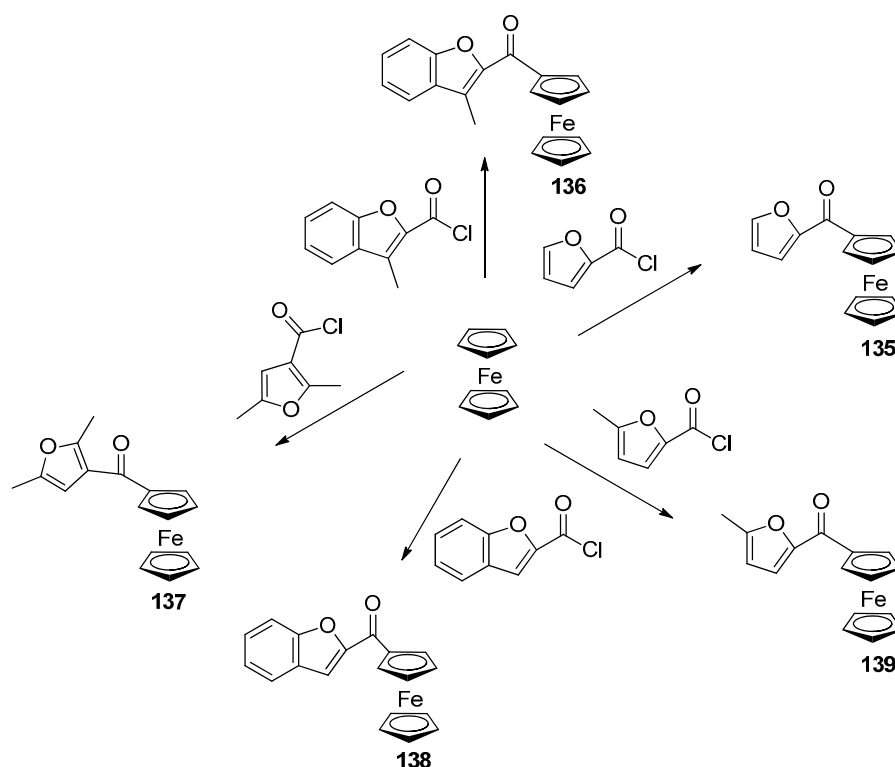
Figure 50. Clotrimazole ferrocene conjugates.

In an advanced work, unique nitric oxide accommodating pyrazole–ferrocene conjugates were synthesized and reported as COX-2 suppressors [136]. Bioassay analysis of the synthesized compound confirmed the potency of **134** which was the highest among all the synthesized compounds (Scheme 51) and had the maximum anti-propagative capacity and could be destroyed by depolarization of the cell's powerhouse, and discharge took place not inside HeLa cells. This phenomenon was harmonized with the antiproliferative potential for **134** which is thought to be a suitable drug for cancer therapy.



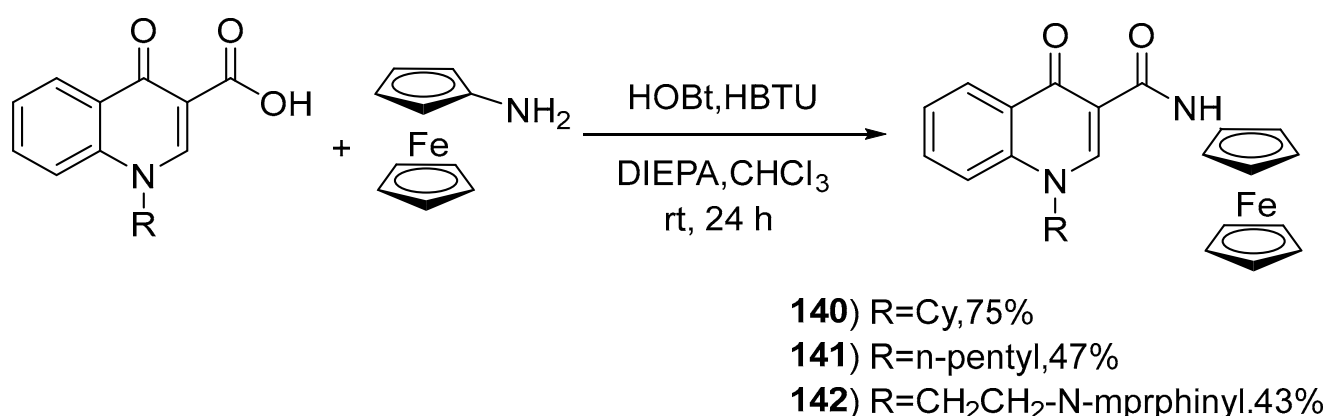
Scheme 51. Synthesis of nitric-oxide-bearing pyrazole–ferrocene conjugate.

Ferrocene and furan derivatives have long been known to be some of the most biologically active compounds [137,138]. Herein, five ferrocenyl furan analogs were prepared through EAS reaction using AlCl₃–EtAlCl₂ Lewis acids (Scheme 52). Though toxicity is directly linked to concentration, at a 100 mg/mL concentration, the protection of cell viability was observed to be 70%. For compounds **135–139**, the necrotic effects were found to be between 21% and 39% at a 50 mg/mL concentration [139].



Scheme 52. AlCl₃–EtAlCl₂-catalyzed ferrocenyl furan derivative synthesis.

Combinatorial synthesis of ferrocene-linked amides was performed by Sansook and co-workers through an amide coupling reaction (Scheme 53). Three final ferrocene-grafted conjugates were characterized in the solid form by X-ray crystallography and exhibited hydrogen bonding as found in NH---C=O N-methylation of the amide, which was used to carry out a pharmacophore identification study. These synthesized ligands are realized as effective-cannabinoid receptor (CB₁, and CB₂) agonists, representing single-digit nanomolar potency [140].



Scheme 53. Synthesis of ferrocene-functionalized amide derivatives.

Realizing the anticancer potential of quinoline scaffolds, Maracic and colleagues synthesized novel O-substituted and N-substituted 4-quinoline conjugates having ferrocene scaffolds [141]. In vitro analysis exhibited that the N-substituted compound displayed cytostatic activity on selective cancerous cells. Among all N-alkylated derivatives, **145** showed remarkable activity against acute leukemia in blast crisis, whereas **146c** realized a selective inhibitory effect on Raji cells without harming the normal cell (Figure 51).

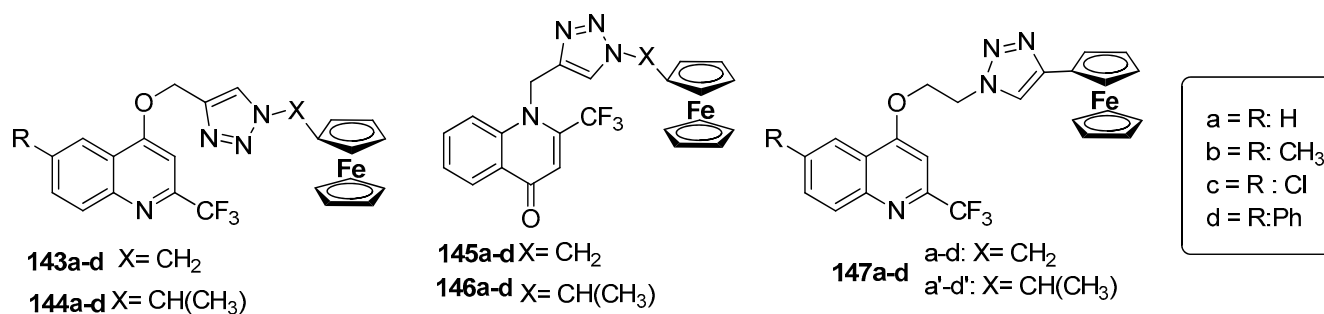
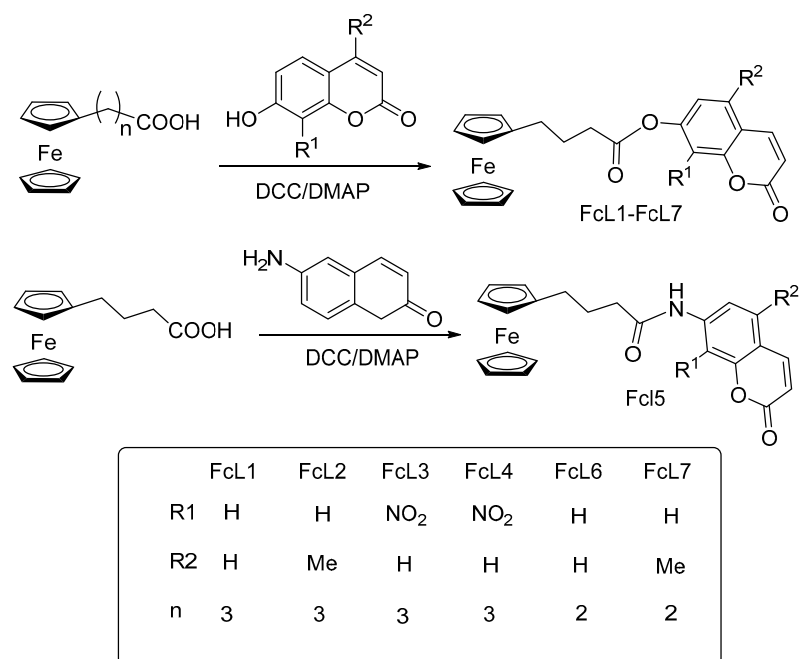


Figure 51. Structures of ferrocene-quinoline conjugates with different O and N substitutions.

In a different work, a group of Wei and coworkers synthesized a series of seven Ferrocene-based coumarin conjugates and performed their biological screening, with the conclusion that **FcL₁** and **FcL₅** showed excellent anticancer potential due to the small value of formal potential E^o, and the latter exhibited promising activity against SGC line cells [142]. Exceptionally, **FcL₄** displayed well-marked cytotoxicity against cancer cells with an IC₅₀ value of 1.09 μmol·L⁻¹, comparable to Adriamycin (Scheme 54).



Scheme 54. Synthesis of ferrocenyl-substituted coumarin derivatives.

3.6.2. Antimalarial Agents

Polymeric conjugates, introduced by Ringsdorf, have several benefits over non-polymeric agents due to their high molecular mass and drug release can be delayed, therefore improving drug bioavailability and thus allowing the administration of smaller doses over larger intervals of time. Using the same concept, Mukaya synthesized two groups of polymeric co-conjugates, one bearing ferrocene and the other containing a neridronate moiety, and evaluated their antimalarial activity by secondary bioassay analysis [143]. Among the two groups of drugs, ferrocene-grafted derivatives proved active against a chloroquine-resistant strain of malarial agent, and especially **148e**, along with its co-conjugate, expressed outstanding antimalarial activity. Blood component analysis revealed the selectiveness of these compounds for erythrocytic parasites without harming the host's red blood cells (Figure 52).

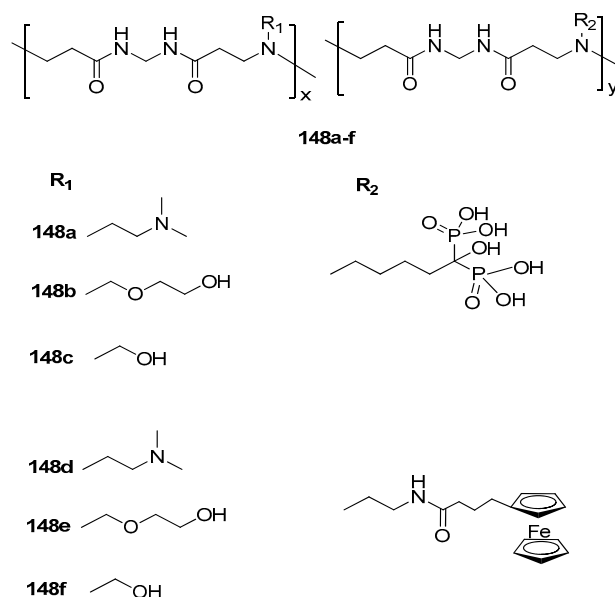


Figure 52. Structure of ferrocene- and neridronate-based conjugates.

Several drugs have been repurposed through ferrocene inclusion, and the most outstanding compound reported so far is ferro-chloroquine, with notable in vitro antimalarial activity against CQ-resistant plasmodium falciparum strains. Recently, a research group reported the synthesis of an unusual ferrocene-functionalized artemisinin ligand through a piperazine bridge and subjected it to biological screening tests on chloroquine cognizant (NF54) and chloroquine refractory strains of the malarial causative agents [144]. Cytotoxicity tests were carried out on fetus kidney cells and they concluded that amino artemisinin derivatives with a ferrocene scaffold exhibited differential activity towards malarial parasites in the company of normal cells (Figure 53).

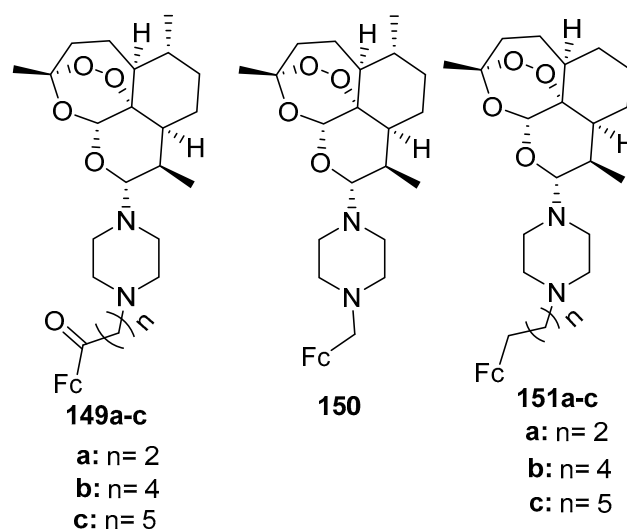


Figure 53. Structure of ferrocene-appended artemisinin conjugates.

An array of advanced cathomycin conjugates was contrived with compromising product amounts by Mbaba and co-authors [145]. Primary biological screening analysis confirmed the antimalarial activity of the target compound **152** towards the falciparum pathogen. It was observed that the ferrocene scaffold elevated the potency of novobiocin derivatives against plasmodium strains. Moreover, a secondary bioassay proved the inhibition face behavior of these conjugates for heat shock proteins Hsp90 (Figure 54).

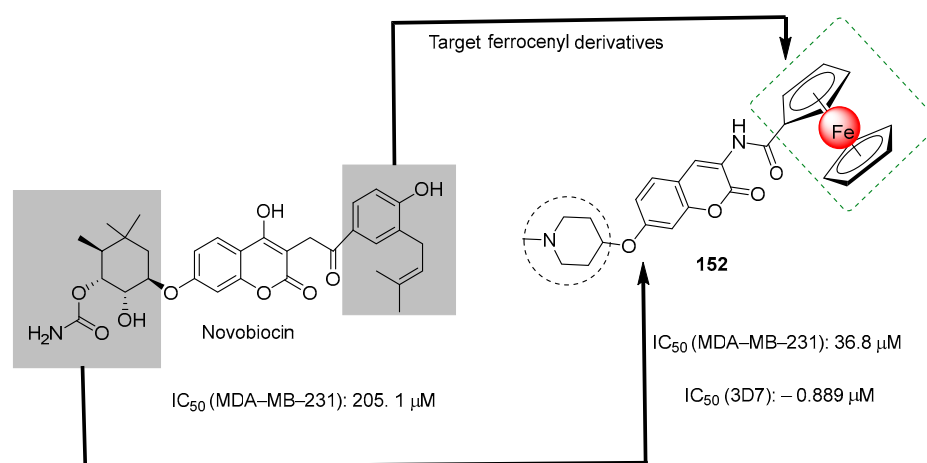


Figure 54. Chemical structures of novobiocin and its ferrocenyl derivative.

Synthesis of three groups of new quinoline-based ferrocenyl conjugates through an easy and effective study was performed by Minic's group, and they evaluated their antimalarial activity through a secondary bioassay [146]. It was realized that all three derivatives showed little micro-molar potential towards the chloroquine-effective strain

of *P. falciparum*, whereas **154** and **155** also expressed their sub-molecular activity towards the chloroquine-ineffective strain of *P. falciparum*, making them leads for future malarial investigation studies (Figure 55).

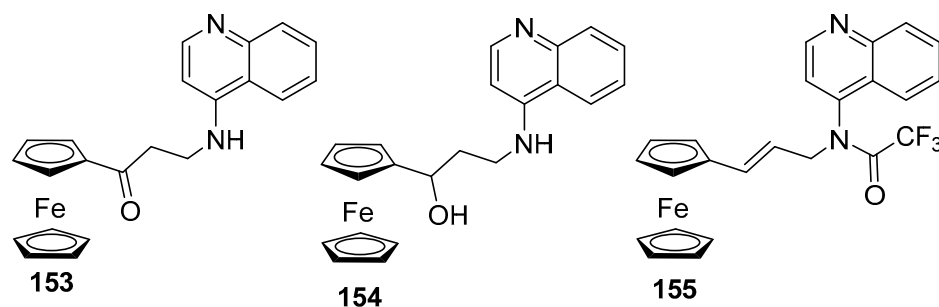


Figure 55. Structures of ferrocene-functionalized quinoline derivatives.

3.6.3. Antioxidant Activity

Ferrocene and adamantane are chemically very different but are quite similar in size and hydrophobicity, and the results obtained in these studies open wide possibilities for applications of adamantly ferrocene derivatives. In an article, Stimac and colleagues synthesized and reported the antioxidant potential of ferrocene derivatives through the DPPH free radical scavenging method [147]. The percentage of DPPH quenching in the presence of Fc-COOH and all prepared compounds was measured and shown in a graph exposing that monosubstituted compounds **156** and **158** exhibited better antioxidant potential than disubstituted compounds **157** and **159** (Figure 56). Further, an IC₅₀ value of **159** was the minimum among all synthesized ligands, which further confirmed its antioxidant potential.

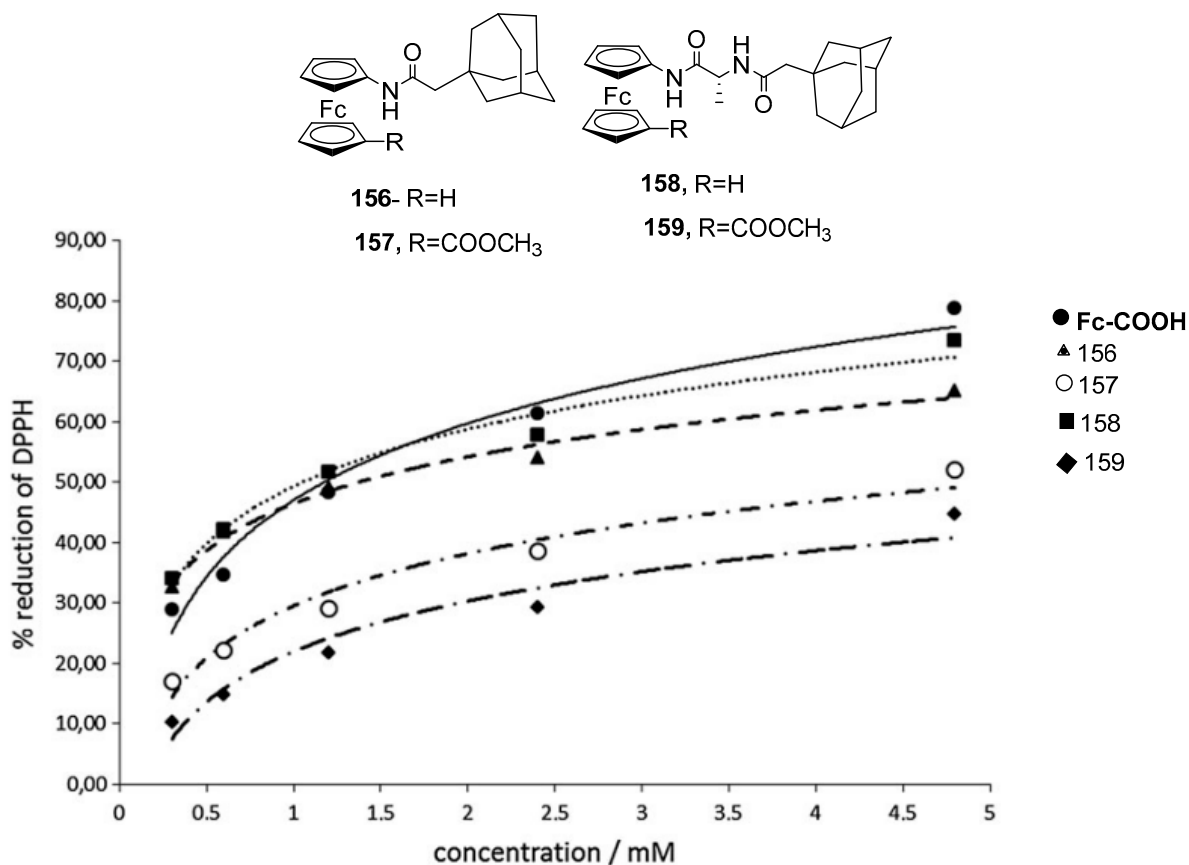


Figure 56. Structure of adamant ferrocene derivatives.

3.6.4. Antidiabetic Agents

The group of Bano and Khan recently conducted a detailed study of ferrocene-grafted acyl urea derivatives and homoleptic carboxylates through in silico and in vivo analysis and evaluated their antidiabetic potential [148]. All examined scaffolds showed large binding interactions for target sites, including receptors and enzymes, i.e., aldose reductase, glucokinase, $C\alpha$ glycosides, etc. In vivo analysis of these compounds on alloxan-coaxed mice confirmed that DPC1 (**160**) and DPAA (**161**) decreased the blood glucose level of the host body mass and dose-dependently (mg/kg) reduced the level of glycosylated hemoglobin in the diabetic host (Figure 57).

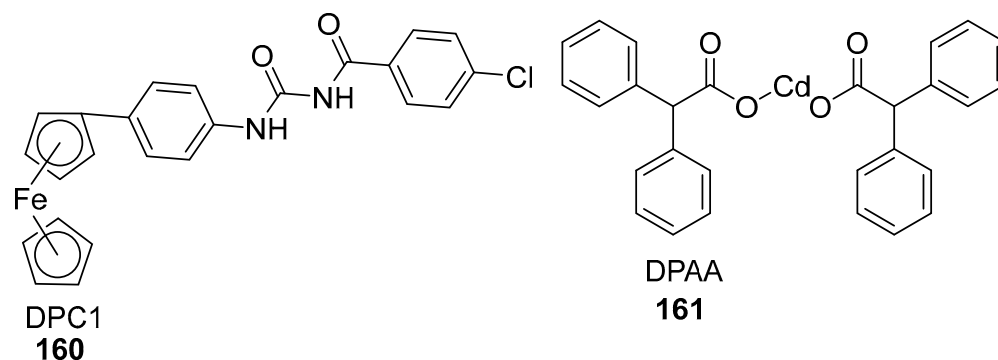
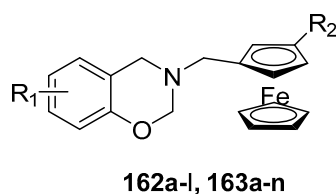


Figure 57. Structure of ferrocene-appended antidiabetic scaffolds.

3.6.5. Ferrocene-Grafted Anti-Trypanosomal Agents

In another interesting example of drug repurposing, Mbaba and assistants developed novel ferrocene 1,3-benzoxazine conjugates by applying a drug reprofiling strategy and carried out their biology screening tests to confirm their anti-trypanosomal activity [149]. The remarkable medicinal potential of these compounds was observed against *T. Brucei*-infected strains with an IC_{50} value of 0.15–38.6 μ M. Moreover, compound **163c** showed maximum efficacy due to the side-chain $CH_2NMC_2O_4$, and a 20-fold rise in the potency of the reprofiled drug was observed (Figure 58).



| $R_2 = H$ | $R_2 = CH_2NMe_2$ |
|------------------------------|------------------------------|
| 162a : $R_1 = H$ | 163a : $R_1 = H$ |
| 162b : $R_1 = 6-Me$ | 163b : $R_1 = 6-Me$ |
| 162c : $R_1 = 6-Cl$ | 163c : $R_1 = 6-Cl$ |
| 162d : $R_1 = 6-Br$ | 163d : $R_1 = 6-Br$ |
| 162e : $R_1 = 6-OMe$ | 163e : $R_1 = 6-OMe$ |
| 162f : $R_1 = 6-NO_2$ | 163f : $R_1 = 6-NO_2$ |
| 162g : $R_1 = 7-Me$ | 163g : $R_1 = 5/7-Me$ |
| 162h : $R_1 = 7-Br$ | 163h : $R_1 = 7-Br$ |
| 162i : $R_1 = 7-F$ | 163i : $R_1 = 7-F$ |
| 162j : $R_1 = 5-Br$ | 163j : $R_1 = 5-Br$ |
| 162k : $R_1 = 5-F$ | 163k : $R_1 = 5-F$ |
| 162l : $R_1 = naph$ | 163l : $R_1 = naph$ |
| | 163m : $R_1 = 6-Cl$ |
| | 163n : $R_1 = 6-NO_2$ |

Figure 58. Structure of reprofiled ferrocene-based benzoxazines.

Using a different protocol, Paucar and co-researchers developed new ferrocenyl Mannich bases and carried out artificial insemination tests to check out their inhibitory potential toward sleep sickness parasites [150]. Compound **164** showed superior suppressing capacity among all conjugates and the calculated IC_{50} value was also high, reaching the maximum for the Arequipa strain. Further, this compound also minimized many damaged cells through a genotoxic phenomenon. In the end, molecular docking was also performed to find the binding capacities of the examined compound with Fe-SOD enzymes (Figure 59).

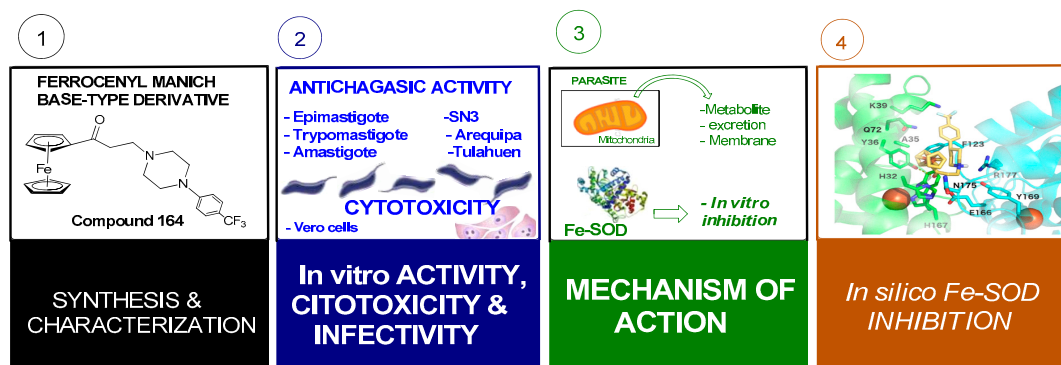


Figure 59. Synthesis, cytotoxicity assay, mode of action, and computational analysis of compound **164**.

3.6.6. Antimicrobial Agent

Antimicrobial agents have been effectively applied to treat patients with micro-organism diseases, but the major problem is that their causative agents have become immune to these drugs. Many drugs that are based on metallocene, especially ferrocene, possess modified pharmacological and toxicological characteristics compared to their original characteristics when administered as metal-based compounds.

Parveen et al. explored the synthesis of new pyrazoline-appended ferrocenyl quinoline compounds **165a–f** and checked out their antimicrobial potential [151]. Fifteen bacterial and fungal strains were exposed to these derivatives via the Broth micro-dilution method, and the compounds exhibited extraordinary MIC values against the examined stains. Among all samples, ligands **165d** exhibited remarkable antimicrobial activity by measuring MIC value within the range of 8–32 Hg/mol. These organometallic compounds could be used as part of a two-in-one strategy to synthesize potential antimicrobials (Figure 60).

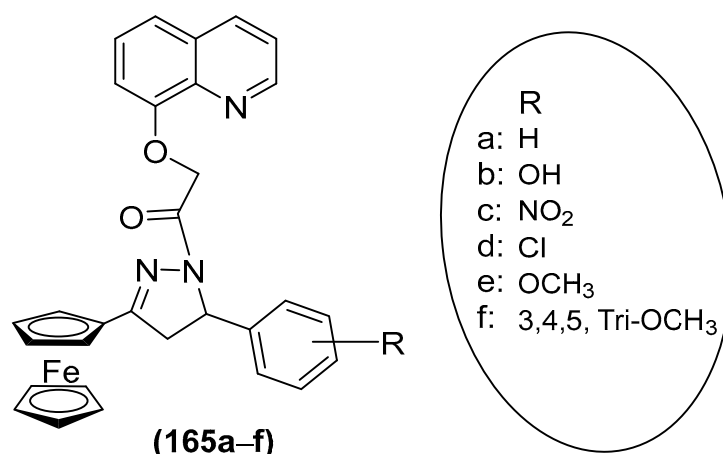


Figure 60. Chemical structure of ferrocene-grafted pyrazoline conjugated.

3.6.7. Ferrocene Hybrids as BET Bromodomain Inhibitors

Hassell's group synthesized a wisely intended bromodomain inhibitor **166b** that was a rationally designed ferrocene conjugate of the BET bromodomain (BRD) probe molecule **166a** [152]. The newly developed probe **166b** displayed excellent BRD affinity in

biochemical assays as well as in pharmacokinetic studies, and a slight rise in cell potency was observed when the same molecule was converted to a purported Fe (III) species in cells after exposure to sodium nitroprusside. The metabolism of the synthesized structure calls for an extensive study of its metabolism in metal-comprising compounds, which may improve their application in clinical settings (Figure 61).

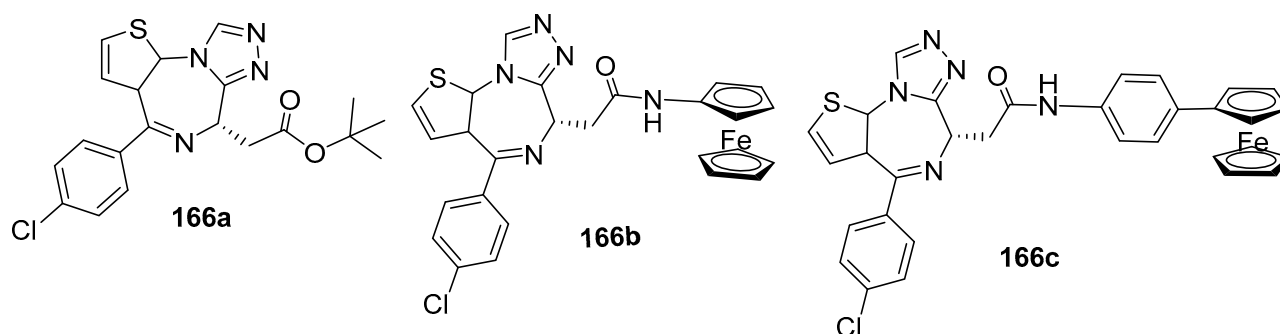
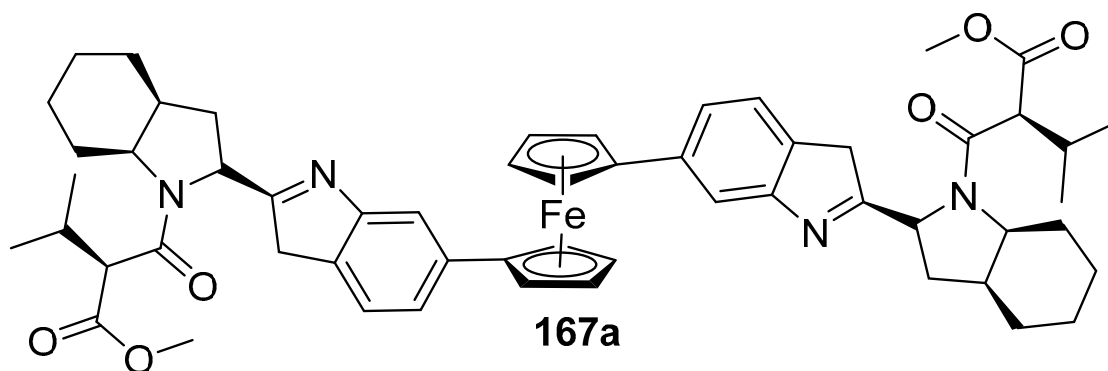


Figure 61. Ferrocene-based BET bromodomain inhibitors.

3.6.8. Antiviral Agent

The synthesis of 1,1-ferrocenediyl conjugates and their HCV GT-1a and GT-1b replicons has been extensively studied by Gadachanda's group by exploiting the versatility of ferrocene chemistry [153]. Among all reported compounds, **167a** offered a fragile rotary component that bargains extra conformational flexibility to provide promising affinities with the marked NS5A protein. The QSAR derived after these organometallic materials opened an influential door for the groundbreaking design of the geometrically associated, and favorably pursued, biplanar organic analog Odalasvir (Figure 62).



HCV GT-1a = 15pM

HCV GT- 1b = 2pM

Rat hepatocytotoxicity CC_{50} = 72 μ M

Rat oral PK (10 mg) F = 38%

Figure 62. Structures of ferrocene-based HCV NS5A inhibitors.

3.7. Electrochemical Insulin Detection

Using an advanced methodology, a stepwise fabrication process of the electrochemical sensor based on a polyfunctional fullerene/BSA-luminol nanocomposite, Fc-aptamer **II**, and a sandwich-like ECL detector was reported and subjected to insulin detection (Figure 63). Ferrocene, with remarkable conductivity and promising catalytic accomplishment for H_2O_2 , was employed to inactivate aptamer **II** with the maximum capability,

and the corresponding ferrocene-grafted aptamer II acted as a seizure probe to characterize insulin with greater specificity. Additionally, the constructed ECL aptasensor represented a sensitivity range of 0.0001–1000 ng/mL and a low limit of detection of 0.04 pg./mL (S/N = 3) for insulin [154].

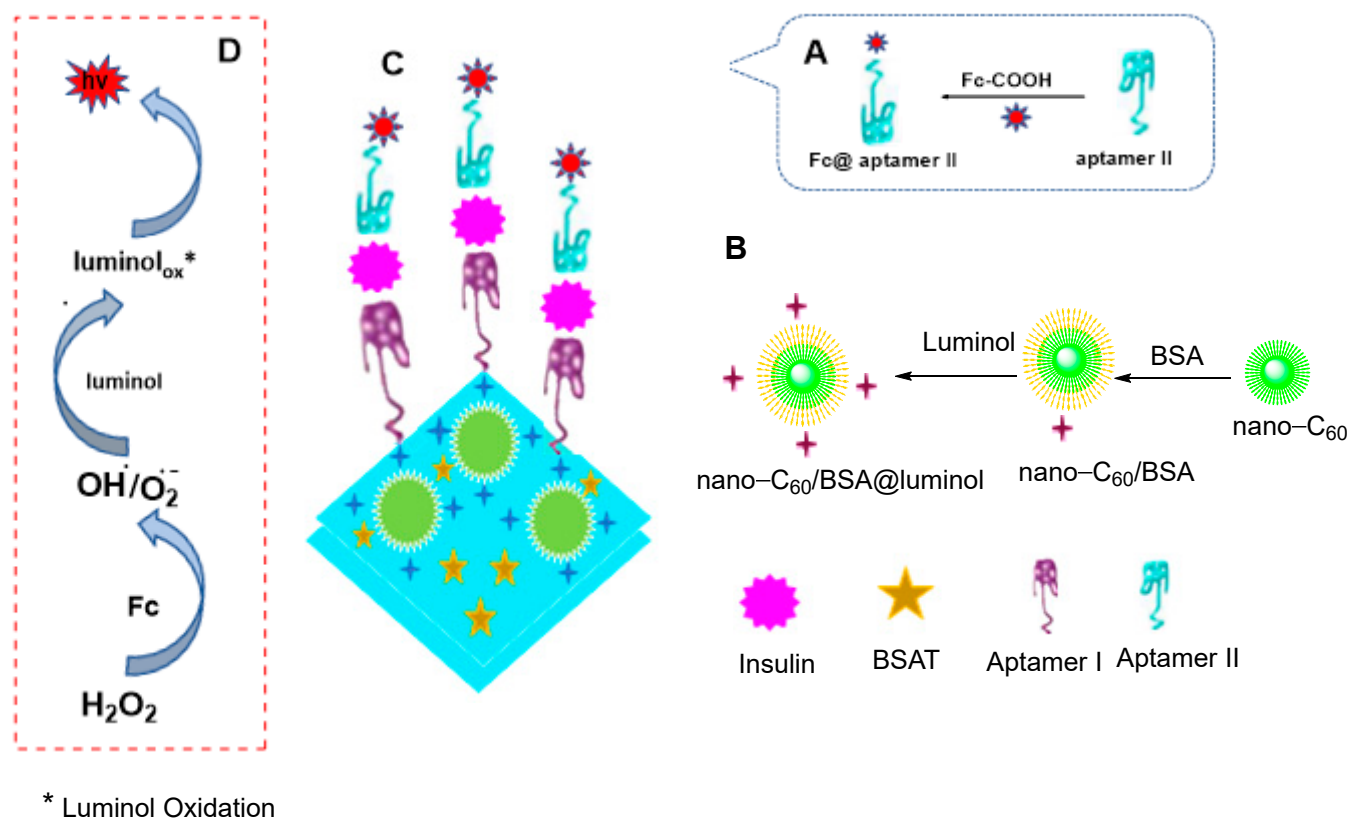


Figure 63. Representative illustration of design, strategy, and fabrication process of the sandwiched ECL sensing platform. (A) Formation of Aptamer II from ferrocene-grafted aptamer II, (B) Formation of BSA-luminol nanocomposite, (C) Fabrication of the insulin targeted ECL aptasensor, (D) The possible reaction mechanism of ECL aptasensor.

An electrochemical immunosensor was selected as an efficient analytical technique to assess the ultra-sensitive detection of neuron-specific enolase (NSE) in human serum. During the experiment, it was discovered that DPV significantly altered the peak value signals of Cu-MOFs-Au and Fc-L-Cys at potentials of 0.20 V and 0.20 V, respectively. As a result, a ratiometric electrochemical immunosensor for the quantitative determination of NSE was created using Fc-L-Cys as the label for Ab2 and Cu-MOFs-Au as the electrode-sensing surface. DPV tested and examined the immunosensor's data and performance results. Cu-MOFs can deposit Au nanoparticles on a greater number of sites because they have a large specific surface area in addition to offering the immunosensor the signal it needs. L-cysteine (L-Cys) can significantly reduce Fc-COOH leakage, allowing Fc⁺ to steadily deliver the additional signal that is needed. Cu-MOFs-redox Au's peak fell while Fc-L-Cys' redox peak rose as the NSE concentration was increased. At a specific range of values, the ratio ($I = I_{Cu}/I_{Fc}$) of two distinct signals was linear with the logarithm of NSE concentration. In short, the immunosensor demonstrated good performance in the concentration range of 1 pg/mL to 1 g/mL, and the detection limit was 0.011 pg/mL, under the optimal experimental conditions. It demonstrated an unexpectedly high sensitivity when compared to other immunosensors. Also, this technique offered a fresh concept for the highly precise quantitative detection of other biomarkers [155].

4. Conclusions

This review provides insight into a wide range of aspects regarding the synthesis of organic conjugates functionalized with ferrocene motifs and their multidisciplinary applications. Ferrocene derivatives constitute an important class of organometallic compounds with an extensive range of applications due to the inspiring chemistry of the iron (II) center and the adamancy in aqueous and aerobic media integrated with aromaticity. This recapitulation not only gives access to a great heterogeneity of ferrocene derivatives but also highlights the ability of these derivatives to endure simplistic iron oxidation, which makes them mesmerizing targets in numerous disciplines like materials science, agriculture, industry, electrochemistry, bio-organometallic chemistry, catalysis, and pharmacological applications. The content of this review article is confined to the literature published from 2016 to the start of 2023.

Author Contributions: A.S. and F.A.: Conceptualization, Investigation, Supervision, review & editing. U.R. and S.B.: Writing and Arrangement; G.S.: Review, writing and Editing; F.A: Financial Assistance. All authors have read and agreed to the published version of the manuscript.

Funding: This research received no external funding.

Institutional Review Board Statement: Not applicable.

Informed Consent Statement: Not applicable.

Data Availability Statement: Not applicable.

Conflicts of Interest: The authors declare no conflict of interest.

References

1. Heinze, K.; Lang, H. Ferrocene beauty and function. *Organometallics* **2013**, *32*, 5623–5625. [[CrossRef](#)]
2. de Souza, A.; Pires, A.; Soldi, V. Thermal stability of ferrocene derivatives and ferrocene-containing polyamides. *J. Therm. Anal. Calorim.* **2002**, *70*, 405–414. [[CrossRef](#)]
3. Fery-Forgues, S.; Delavaux-Nicot, B. Ferrocene and ferrocenyl derivatives in luminescent systems. *J. Photochem. Photobiol. A* **2000**, *132*, 137–159. [[CrossRef](#)]
4. Saleem, M.; Yu, H.; Wang, L.; Khalid, H.; Akram, M.; Abbasi, N.M.; Huang, J. Review on synthesis of ferrocene-based redox polymers and derivatives and their application in glucose sensing. *Anal. Chim. Acta* **2015**, *876*, 9–25. [[CrossRef](#)] [[PubMed](#)]
5. Astruc, D. Why is ferrocene so exceptional? *Eur. J. Inorg. Chem.* **2017**, *2017*, 6–29. [[CrossRef](#)]
6. Atkinson, R.C.; Gibson, V.C.; Long, N.J. The syntheses and catalytic applications of unsymmetrical ferrocene ligands. *J. Chem. Soc. Rev.* **2004**, *33*, 313–328. [[CrossRef](#)]
7. Hudson, R.D. Ferrocene polymers: Current architectures, syntheses and utility. *J. Organomet. Chem.* **2001**, *637*, 47–69. [[CrossRef](#)]
8. Herrmann, W.A. Ferrocene as a gasoline and fuel additive. In *Applied Homogeneous Catalysis with Organometallic Compounds*; Cornils, P., Mult., H.C., Herrmann, W.A., Eds.; John Wiley & Sons, Ltd.: Hoboken, NJ, USA, 2002; pp. 586–590, ISBN 9783527328970.
9. Al-Khalidi, U.K.; Al-Lami, H.S. Ferrocene as accelerator for free radical copolymerization of methyl methacrylate/methacrylic acid monomers. *Iraqi J. Polym.* **2015**, *18*, 65–70.
10. Alvarez, J.; Ren, T.; Kaifer, A.E. Redox potential selection in a new class of dendrimers containing multiple ferrocene centers. *Organometallics* **2001**, *20*, 3543–3549. [[CrossRef](#)]
11. Gao, J.M.; Wang, L.; Yu, H.J.; Xiao, A.G.; Ding, W.B. Recent research progress in burning rate catalysts. *Propellants Explos. Pyrotech.* **2011**, *36*, 404–409. [[CrossRef](#)]
12. Singh, A.; Lumb, I.; Mehra, V.; Kumar, V. Ferrocene-appended pharmacophores: An exciting approach for modulating the biological potential of organic scaffolds. *Dalton Trans.* **2019**, *48*, 2840–2860. [[CrossRef](#)]
13. Mathi, S.; Gupta, P.K.; Kumar, R.; Nagarale, R.K.; Sharma, A. Ferrocenium ion confinement in polyelectrolyte for electrochemical nitric oxide sensor. *ChemistrySelect* **2019**, *4*, 3833–3840. [[CrossRef](#)]
14. Dakmouche, M.; Saidi, M.; Hadjadj, M.; Yousfi, M.; Rahmani, Z. Enhancement of the Inhibitor efficiency of 4-phenyl-1, 2-dithiol-3-thione on corrosion of mild steel for 20% sulphuric acid. *Asian J. Chem.* **2012**, *24*, 4887.
15. Tan, J.; Li, H.; Hu, X.; Abdullah, R.; Xie, S.; Zhang, L.; Zhao, M.; Luo, Q.; Li, Y.; Sun, Z. Size-tunable assemblies based on ferrocene-containing DNA polymers for spatially uniform penetration. *Chem* **2019**, *5*, 1775–1792. [[CrossRef](#)]
16. Chakraborty, A.K.; Mallik, B. Anomalous photoconductivity of ferrocene. *Synth. Met.* **1995**, *73*, 239–245. [[CrossRef](#)]
17. Mamane, V. Metal-catalyzed cross-coupling reactions for ferrocene functionalization: Recent applications in synthesis, material science and asymmetric catalysis. *Mini Rev. Org. Chem.* **2008**, *5*, 303–312. [[CrossRef](#)]
18. Yang, X.; Wang, Y.; Qi, W.; Su, R.; He, Z. Bioorganometallic ferrocene-tripeptide nanoemulsions. *Nanoscale* **2017**, *9*, 15323–15331. [[CrossRef](#)]

19. Falcone, N.; Kraatz, H.-B. Ferrocene peptide-based supramolecular gels: Current trends and applications. In *Advances in Bioorganometallic Chemistry*; Hirao, T., Moriuchi, T., Eds.; Elsevier: Amsterdam, The Netherlands, 2019; pp. 57–74, ISBN 9780128141977.
20. Larik, F.A.; Saeed, A.; Fattah, T.A.; Muqadar, U.; Channar, P.A. Recent advances in the synthesis, biological activities and various applications of ferrocene derivatives. *Appl. Organomet. Chem.* **2017**, *31*, e3664. [[CrossRef](#)]
21. Zhai, X.; Yu, H.; Wang, L.; Deng, Z.; Abdin, Z.U.; Tong, R.; Yang, X.; Chen, Y.; Saleem, M. Recent research progress in the synthesis, properties and applications of ferrocene-based derivatives and polymers with azobenzene. *Appl. Organomet. Chem.* **2016**, *30*, 62–72. [[CrossRef](#)]
22. Wu, J.; Wang, L.; Yu, H.; Khan, R.U.; Haroon, M. Ferrocene-based redox-responsive polymer gels: Synthesis, structures and applications. *J. Organomet. Chem.* **2017**, *828*, 38–51. [[CrossRef](#)]
23. Khan, A.; Wang, L.; Yu, H.; Haroon, M.; Ullah, R.S.; Nazir, A.; Elshaarani, T.; Usman, M.; Fahad, S.; Haq, F. Research advances in the synthesis and applications of ferrocene-based electro and photo responsive materials. *Appl. Organomet. Chem.* **2018**, *32*, e4575. [[CrossRef](#)]
24. Patra, M.; Gasser, G. The medicinal chemistry of ferrocene and its derivatives. *Nat. Rev. Chem.* **2017**, *1*, 0066. [[CrossRef](#)]
25. Hassan, A.S.; Hafez, T.S. Antimicrobial activities of ferrocenyl complexes: A review. *J. Appl. Pharm. Sci.* **2018**, *8*, 156–165.
26. Gao, C.; Chang, L.; Xu, Z.; Yan, X.-F.; Ding, C.; Zhao, F.; Wu, X.; Feng, L.-S. Recent advances of tetrazole derivatives as potential anti-tubercular and anti-malarial agents. *Eur. J. Med. Chem.* **2019**, *163*, 404–412. [[CrossRef](#)]
27. Ludwig, B.S.; Correia, J.D.; Kühn, F.E. Ferrocene derivatives as anti-infective agents. *Coord. Chem. Rev.* **2019**, *396*, 22–48. [[CrossRef](#)]
28. Oparina, L.A.; Kolyvanov, N.A.; Tarasova, O.A.; Albanov, A.I.; Tantsyrev, A.P.; Trofimov, B.A. Nucleophilic Addition of 1, 1'-Bis (hydroxymethyl) ferrocene to Alkynes: Synthesis of ferrocene diethenyl ethers. *Synthesis* **2020**, *52*, 320–326. [[CrossRef](#)]
29. Korb, M.; Lang, H. Multi-ferrocenyl aryl ethers—applying nucleophilic aromatic substitution reactions to aryl fluorides. *Eur. J. Inorg. Chem.* **2017**, *2017*, 276–287. [[CrossRef](#)]
30. Soni, A.; Upadhyay, Y.; Srivastava, A.K.; Sharma, C.; Joshi, R.K. A facile synthesis of ferrocene functionalized vinyl ethers and their application as optical sensors for Cu²⁺ ions detection. *Inorganica Chim. Acta* **2023**, *548*, 121371. [[CrossRef](#)]
31. Abbasi, H.; Teimuri-Mofrad, R. Synthesis and characterization of novel ferrocenyl glycidyl ether polymer, ferrocenyl poly (epichlorohydrin) and ferrocenyl poly (glycidyl azide). *Appl. Organomet. Chem.* **2020**, *34*, e5270. [[CrossRef](#)]
32. Li, G.; Liu, Q.; Liao, B.; Chen, L.; Zhou, H.; Zhou, Z.; Xia, B.; Huang, J.; Liu, B. Synthesis of novel ferrocene-based conjugated microporous polymers with intrinsic magnetism. *Eur. Polym. J.* **2017**, *93*, 556–560. [[CrossRef](#)]
33. Mattoussi, M.; Matoussi, F.; Raouafi, N. Non-enzymatic amperometric sensor for hydrogen peroxide detection based on a ferrocene-containing cross-linked redox-active polymer. *Sens. Actuators B Chem.* **2018**, *274*, 412–418. [[CrossRef](#)]
34. Mato, M.; Pérez-Caaveiro, C.; Sarandeses, L.A.; Perez Sestelo, J. Ferrocenylindium reagents in palladium-catalyzed cross-coupling reactions: Asymmetric synthesis of planar chiral 2-aryl oxazolyl and sulfanyl ferrocenes. *Adv. Synth. Catal.* **2017**, *359*, 1388–1393. [[CrossRef](#)]
35. Schmiel, D.; Butenschön, H. Directed iron-catalyzed ortho-alkylation and arylation: Toward the stereoselective catalytic synthesis of 1, 2-disubstituted planar-chiral ferrocene derivatives. *Organometallics* **2017**, *36*, 4979–4989. [[CrossRef](#)]
36. López, E.; Suárez, T.; Ballesteros, A.; López, L.A. Gold (I)-catalyzed reaction of ferrocene and propargylic esters: Synthesis of functionalized ferrocene derivatives. *Eur. J. Inorg. Chem.* **2017**, *2017*, 225–228. [[CrossRef](#)]
37. Jawaria, R.; Khan, M.U.; Hussain, M.; Muhammad, S.; Sagir, M.; Hussain, A.; Al-Sehemi, A.G. Synthesis and characterization of ferrocene-based thiosemicarbazones along with their computational studies for potential as inhibitors for SARS-CoV-2. *J. Iran. Chem. Soc.* **2021**, *19*, 839–846. [[CrossRef](#)]
38. Ochiai, K.; Fujii, S. Structure-property and structure–activity relationships of phenylferrocene derivatives as androgen receptor antagonists. *Bioorganic Med. Chem. Lett.* **2021**, *46*, 128141. [[CrossRef](#)]
39. Amin, B.U.; Yu, H.; Wang, L.; Nazir, A.; Fahad, S.; Haq, F.; Mahmood, S.; Liang, R.; Uddin, M.A.; Lin, T. Recent advances on ferrocene-based compounds and polymers as a burning rate catalysts for propellants. *J. Organomet. Chem.* **2020**, *921*, 121368. [[CrossRef](#)]
40. Sattar, M.; Kumar, S. Palladium-catalyzed removable 8-aminoquinoline assisted chemo- and regioselective oxidative sp²-C–H/sp³-C–H cross-coupling of ferrocene with toluene derivatives. *Org. Lett.* **2017**, *19*, 5960–5963. [[CrossRef](#)]
41. Kumar Sikder, B.; Naidu Ganivada, M.; Jana, T. Functional alkyl-ferrocene grafted hydroxyl terminated polybutadiene. *Chemistry-Select* **2021**, *6*, 8058–8062. [[CrossRef](#)]
42. Chen, Q.; Li, Y.; Liu, Y.; Sun, P.; Yang, Z.; Xu, T. Designer ferrocene Catholyte for aqueous organic flow batteries. *ChemSusChem* **2021**, *14*, 1295–1301. [[CrossRef](#)]
43. Wang, S.-B.; Gu, Q.; You, S.-L. Cp* Co (III)-catalyzed ortho C–H amidation of 2-pyridinyl ferrocenes with 1, 4, 2-dioxazol-5-ones. *J. Catal.* **2018**, *361*, 393–397. [[CrossRef](#)]
44. Ravutsov, M.; Dobrikov, G.M.; Dangalov, M.; Nikolova, R.; Dimitrov, V.; Mazzeo, G.; Longhi, G.; Abbate, S.; Paoloni, L.; Fusè, M. 1, 2-Disubstituted planar chiral ferrocene derivatives from sulfonamide-directed ortho-lithiation: Synthesis, absolute configuration, and chiroptical properties. *Organometallics* **2021**, *40*, 578–590. [[CrossRef](#)]
45. Yao, Y.; Xu, H.; Tian, Z.; Zhang, J.; Zhan, F.; Yan, M.; Jia, C. Simple-synthesized sulfonated ferrocene ammonium for aqueous redox flow batteries. *ACS Appl. Energy Mater.* **2021**, *4*, 8052–8058. [[CrossRef](#)]

46. Yadav, R.; Singh, S.; Trivedi, M.; Kociok-Köhn, G.; Rath, N.P.; Köhn, R.D.; Muddassir, M.; Kumar, A. New main-group ferrocenyldithiocarbamates and conversion to ferrocene oxazolidine-2-thione and-2-one. *New J. Chem.* **2020**, *44*, 3268–3277. [[CrossRef](#)]
47. Gao, X.; Gong, G.; Zhang, Z.; Du, G.; Cao, Y.; Zhao, G. A novel cyclopalladated ferrocene derivative: Synthesis, single crystal structure and evaluation of in vitro antitumor activity. *J. Mol. Struct.* **2020**, *1200*, 127077. [[CrossRef](#)]
48. Sayed, F.N.; Mohamed, G.G. Newly synthesized lanthanides complexes of ferrocene-based Schiff base with high biological activities and improved molecular docking data. *J. Organomet. Chem.* **2022**, *977*, 122450. [[CrossRef](#)]
49. Zhang, Z.; Du, G.; Gong, G.; Sheng, Y.; Lu, X.; Cai, W.; Wang, F.; Zhao, G. A novel ferrocene-palladium metal complex: Synthesis, single crystal structure, in vitro cytotoxicity study and molecular docking. *J. Mol. Struct.* **2021**, *1232*, 130021. [[CrossRef](#)]
50. Liu, Y.; Dang, Y.; Yin, D.; Yang, X.; Yang, L.; Zou, Q. One-pot, multi-component synthesis of 3, 4-dihydropyrimidin-2 (1H)-one derivatives containing ferrocenyl. *Res. Chem. Intermed.* **2020**, *46*, 547–555. [[CrossRef](#)]
51. Minić, A.; Pešić, M.S.; Novaković, S.B.; Bogdanović, G.A.; Todosijević, A.; Komatina, D.I.; Stevanović, D. Synthesis, structural and electrochemical characterization of novel ferrocene-containing tetrahydropyrimidin-2 (1H)-ones. *J. Organomet. Chem.* **2020**, *923*, 121422. [[CrossRef](#)]
52. Minić, A.; Novaković, S.B.; Bogdanović, G.A.; Bugarinović, J.P.; Pešić, M.S.; Todosijević, A.; Komatina, D.I.; Damjanović, I.; Stevanović, D. Synthesis and structural characterizations of novel atropisomeric ferrocene-containing six-membered cyclic ureas. *Polyhedron* **2020**, *177*, 114316. [[CrossRef](#)]
53. Li, H.; Chi, W.; Liu, Y.; Yuan, W.; Li, Y.; Li, Y.; Tang, B.Z. Ferrocene-based hyperbranched polytriazoles: Synthesis by click polymerization and application as precursors to nanostructured magnetoceramics. *Macromol. Rapid Commun.* **2017**, *38*, 1700075. [[CrossRef](#)]
54. Maračić, S.; Jakopec, S.; Piškor, M.; Leventić, M.; Lapić, J.; Djaković, S.; Raić-Malić, S. Mechanochemical synthesis and antiproliferative activity of novel ferrocene quinoline/quinolone hybrids. *J. Organomet. Chem.* **2023**, *37*, e7124. [[CrossRef](#)]
55. Panda, K.N.; Thorat, K.G.; Ravikanth, M. Covalently linked meso-tetraaryl triphyrin (2.1. 1)-ferrocene (s) conjugates: Synthesis and properties. *Org. Biomol. Chem.* **2019**, *17*, 5066–5074. [[CrossRef](#)]
56. Snegur, L.V.; Lyapunova, M.V.; Verina, D.D.; Kachala, V.V.; Korlyukov, A.A.; Ilyin, M.M., Jr.; Davankov, V.A.; Ostrovskaya, L.A.; Bluchterova, N.V.; Fomina, M.M. Nitro-imidazoles in ferrocenyl alkylation reaction. Synthesis, enantiomeric resolution and in vitro and in vivo bioeffects. *J. Organomet. Chem.* **2018**, *871*, 10–20. [[CrossRef](#)]
57. Zhang, W.; Xu, W.; Ma, C.; Li, Y. Synthesis of ferrocene-based polysubstituted pyrrolidines. *Chem. Heterocycl. Compd.* **2019**, *55*, 939–942. [[CrossRef](#)]
58. Prabu, S.; David, E.; Viswanathan, T.; Thirumoorthy, K.; Panda, T.; Dragonetti, C.; Colombo, A.; Marinotto, D.; Righetto, S.; Roberto, D. NLO-active Y-shaped ferrocene conjugated imidazole chromophores as precursors for SHG polymeric films. *Dalton Trans.* **2020**, *49*, 1854–1863. [[CrossRef](#)]
59. Liu, Y.; Xin, H.; Yin, J.; Yin, D. Microwave-assisted synthesis of 3-substituted-6-ferrocene methylene-1, 2, 4-triazolo [3, 4-b]-1, 3, 4-thiadiazoles. *Transit. Met. Chem.* **2018**, *43*, 381–385. [[CrossRef](#)]
60. Khan, S.A.; Asiri, A.M.; Zayed, M.E.; Parveen, H.; Aqlan, F.M.; Sharma, K. Microwave-assisted synthesis, characterization, and density functional theory study of biologically active ferrocenyl bis-pyrazoline and bis-pyrimidine as organometallic macromolecules. *J. Heterocycl. Chem.* **2019**, *56*, 312–318. [[CrossRef](#)]
61. Shibata, T.; Uno, N.; Sasaki, T.; Kanyiva, K.S. Pt-catalyzed enantioselective cycloisomerization for the synthesis of planar-chiral ferrocene derivatives. *J. Org. Chem.* **2016**, *81*, 6266–6272. [[CrossRef](#)]
62. Jia, L.; Liu, X.; Zhang, A.-A.; Wang, T.; Hua, Y.; Li, H.; Liu, L. Synthesis of planar chiral ferrocenes via a Pd (0)-catalyzed syn-carbopalladation/asymmetric C–H alkenylation process. *Chem. Commun.* **2020**, *56*, 1737–1740. [[CrossRef](#)]
63. Rozhkova, Y.S.; Plekhanova, I.V.; Gorbunov, A.A.; Stryapunina, O.G.; Chulakov, E.N.; Krasnov, V.P.; Ezhikova, M.A.; Kodess, M.I.; Slepukhin, P.A.; Shklyav, Y.V. Synthesis of novel racemic 3, 4-dihydroferroceno [c] pyridines via the Ritter reaction. *Tetrahedron Lett.* **2019**, *60*, 768–772. [[CrossRef](#)]
64. Kameoka, A.; Tsuchiya, K. Influence of ferrocene on engine and vehicle performance. *SAE Int. J. Engines* **2006**, *1*, 34–48.
65. Janecki, H. Ferrocene derivatives in boundary lubrication. *Tribol. Lett.* **2006**, *24*, 99–103. [[CrossRef](#)]
66. Apreutesei, D.; Lisa, G.; Scutaru, D.; Hurduc, N. Investigations on thermal stability of some ferrocene liquid crystals bearing azo, ferrocenyl and cholesteryl units. *J. Optoelectron. Adv. Mater.* **2006**, *8*, 737–740.
67. Yousefinejad, S.; Honarasa, F.; Solhjo, A. On the solubility of ferrocene in nonaqueous solvents. *J. Chem. Eng. Data* **2016**, *61*, 614–621. [[CrossRef](#)]
68. Saleem, M.; Yu, H.; Wang, L.; Khalid, H.; Akram, M.; Abbasi, N.M.; Chen, Y. Study on synthesis of ferrocene-based boronic acid derivatives and their saccharides sensing properties. *J. Electroanal. Chem.* **2016**, *763*, 71–78. [[CrossRef](#)]
69. Rabti, A.; Mayorga-Martinez, C.C.; Baptista-Pires, L.; Raouafi, N.; Merkoçi, A. Ferrocene-functionalized graphene electrode for biosensing applications. *Anal. Chim. Acta* **2016**, *926*, 28–35. [[CrossRef](#)]
70. Dong, W.; Wang, K.; Chen, Y.; Li, W.; Ye, Y.; Jin, S. Construction and characterization of a chitosan-immobilized-enzyme and β -cyclodextrin-included-ferrocene-based electrochemical biosensor for H₂O₂ detection. *Materials* **2017**, *10*, 868. [[CrossRef](#)]
71. Lu, X.; Wen, X.; Fan, Z. A sensitive biosensor based on a ferrocene-marked adapter for the fluorescence detection of platelet-derived growth factor BB. *J. Lumin.* **2020**, *221*, 117042. [[CrossRef](#)]

72. Singh, G.; Arora, A.; Rani, S.; Kalra, P.; Kumar, M. A click-generated triethoxysilane tethered ferrocene-chalcone-triazole triad for selective and colorimetric detection of Cu^{2+} ions. *ChemistrySelect* **2017**, *2*, 3637–3647. [[CrossRef](#)]
73. Liu, Y.; Hu, J.; Teng, Q.; Zhang, H. Ferrocenyl-based thioethers and sulphones as optical, and electrochemical sensors for the differential detection of Hg^{2+} and Cu^{2+} ions. *Sens. Actuators B Chem.* **2017**, *238*, 166–174. [[CrossRef](#)]
74. Zhou, Y.; Cao, Y.; Gong, G.; Zhang, Y.; Zhao, H.; Gao, X.; Zhao, G. A simple but effective ferrocene derivative as a redox, and fluorescent receptor for highly selective recognition of Al^{3+} ions. *Inorg. Chem. Commun.* **2018**, *96*, 170–174. [[CrossRef](#)]
75. Atasen, S.K.; Alcaay, Y.; Yavuz, O.; Yucel, B.; Yilmaz, I. Beryllium ion sensing through the ion pair formation between the electrochemically reduced ferrocenyl naphthoquinone radicals and Be^{2+} ions. *J. Chem. Sci.* **2019**, *131*, 41. [[CrossRef](#)]
76. Hosseinzadeh, R.; Maliji, F.; Golchoubian, H.; Bekhradnia, A. A novel ferrocene-based calix [4] arene as an efficient optical and electrochemical sensor for highly selective fluoride recognition. *ChemistrySelect* **2019**, *4*, 3914–3920. [[CrossRef](#)]
77. Wu, P.; Wang, G.; Zhou, L.; Lu, J.; Wang, J. The first colorimetric receptor for the $\text{B}_4\text{O}_7^{2-}$ anion based on nitro substituted phenanthroimidazole ferrocene derivatives. *RSC Adv.* **2018**, *8*, 3782–3788. [[CrossRef](#)]
78. Feng, X.-Z.; Ferranco, A.; Su, X.; Chen, Z.; Jiang, Z.; Han, G.-C. A facile electrochemical sensor labeled by ferrocenoyl cysteine conjugate for the detection of nitrite in pickle juice. *Sensors* **2019**, *19*, 268. [[CrossRef](#)]
79. Boink, A.; Speijers, G. Health effects of nitrates and nitrites, a review. *Acta Hort.* **1999**, *563*, 29–36. [[CrossRef](#)]
80. Zaleskaya, M.; Jaglenieć, D.; Karbarz, M.; Dobrzycki, Ł.; Romański, J. Squaramide based ion pair receptors possessing ferrocene as a signaling unit. *Inorg. Chem. Front.* **2020**, *7*, 972–983. [[CrossRef](#)]
81. Reddy, P.G.; MG, M.; Joseph, A.M.; Nandi, S.; Ghosh, S.; Pradeep, C.P.; Sharma, S.K.; Gonsalves, K.E. Ferrocene bearing non-ionic poly-aryl tosylates: Synthesis, characterization and electron beam lithography applications. *J. Photopolym. Sci. Technol.* **2018**, *31*, 669–678. [[CrossRef](#)]
82. Shi, Y.; Xiao, L.; Wu, D.; Li, F.; Li, D.; Zhang, J.; Li, S.; Zhou, H.; Wu, J.; Tian, Y. Synthesis, crystal structure, electrochemistry and third-order nonlinear optical properties of two novel ferrocene derivatives. *J. Organomet. Chem.* **2016**, *817*, 36–42. [[CrossRef](#)]
83. Pielak, K.; Bondu, F.; Sanguinet, L.; Rodriguez, V.; Castet, F.; Champagne, B. Acid-triggered switching of the second-order nonlinear optical properties of a ferrocenyl-containing indolino-oxazolidine derivative. *Dyes Pigm.* **2019**, *160*, 641–646. [[CrossRef](#)]
84. Singh, A.; Singh, P.; Kociok-Köhn, G.; Trivedi, M.; Kumar, A.; Chauhan, R.; Rane, S.B.; Terashima, C.; Gosavi, S.W.; Fujishima, A. 1, 1'-Bis (diphenylphosphino) ferrocene-appended nickel (ii) dithiolates as sensitizers in dye-sensitized solar cells. *New J. Chem.* **2018**, *42*, 9306–9316. [[CrossRef](#)]
85. Liu, H.; Wu, Y.; Wu, F.-Y.; Liu, J.-C. New type of ferrocene group substituted porphyrin axial coordinate self-assembly for dye-sensitized solar cells. *Org. Electron.* **2019**, *71*, 290–295. [[CrossRef](#)]
86. Rajak, R.; Saraf, M.; Mohammad, A.; Mobin, S.M. Design and construction of a ferrocene based inclined polycatenated Co-MOF for supercapacitor and dye adsorption applications. *J. Mater. Chem. A* **2017**, *5*, 17998–18011. [[CrossRef](#)]
87. Teimuri-Mofrad, R.; Abbasi, H.; Hadi, R. Graphene oxide-grafted ferrocene moiety via ring opening polymerization (ROP) as a supercapacitor electrode material. *Polymer* **2019**, *167*, 138–145. [[CrossRef](#)]
88. Zhou, B.; Liu, L.; Cai, P.; Zeng, G.; Li, X.; Wen, Z.; Chen, L. Ferrocene-based porous organic polymer derived high-performance electrocatalysts for oxygen reduction. *J. Mater. Chem. A* **2017**, *5*, 22163–22169. [[CrossRef](#)]
89. Liu, Z.; Feng, L.; Su, X.; Qin, C.; Zhao, K.; Hu, F.; Zhou, M.; Xia, Y. Micro-sized organometallic compound of ferrocene as high-performance anode material for advanced lithium-ion batteries. *J. Power Sources* **2018**, *375*, 102–105. [[CrossRef](#)]
90. Xia, X.; Yu, H.; Wang, L.; Deng, Z.; Shea, K.J. Preparation of redox- and photo-responsive ferrocene- and azobenzene-based polymer films and their properties. *Eur. Polym. J.* **2018**, *100*, 103–110. [[CrossRef](#)]
91. Karmakar, M.; Bhatta, S.R.; Giri, S.; Thakur, A. Oxidation-induced differentially selective turn-on fluorescence via photoinduced electron transfer based on a ferrocene-appended coumarin–quinoline platform: Application in cascaded molecular logic. *Inorg. Chem.* **2020**, *59*, 4493–4507. [[CrossRef](#)]
92. Renda, C.G.; Contreras Medrano, C.P.; Costa, L.J.D.; Litterst, F.J.; Saitovitch, E.M.B.; Magon, C.J.; Gualdi, A.J.; Venâncio, T.; Bertholdo, R.; Moreira, A.J. Role of ferrocene-derived iron species in the catalytic graphitization of novolak resins. *J. Mater. Sci.* **2021**, *56*, 1298–1311. [[CrossRef](#)]
93. Wang, Y.; Tao, J.; Xiong, S.; Lu, P.; Tang, J.; He, J.; Javaid, M.U.; Pan, C.; Yu, G. Ferrocene-based porous organic polymers for high-affinity iodine capture. *Chem. Eng. J.* **2020**, *380*, 122420. [[CrossRef](#)]
94. Wei, Z.; Wang, D.; Liu, Y.; Guo, X.; Zhu, Y.; Meng, Z.; Yu, Z.-Q.; Wong, W.-Y. Ferrocene-based hyperbranched polymers: A synthetic strategy for shape control and applications as electroactive materials and precursor-derived magnetic ceramics. *J. Mater. Chem. C* **2020**, *8*, 10774–10780. [[CrossRef](#)]
95. Wang, H.; Lu, W.; Zhang, J. Ferrocene derived bifunctional phosphine-catalyzed asymmetric Oxa[4 + 2] cycloaddition of α -substituted allenones with enones. *Chem. Eur. J.* **2018**, *23*, 13587–13590. [[CrossRef](#)]
96. Mo, Y.Z.; Wang, Q.J.; Nie, H.F.; Wang, Q.F. The Application of New Chiral Ferrocene Ligands in Asymmetric Transfer Hydrogenation of Ketones. *Int. J. Org. Chem.* **2018**, *8*, 54–83.
97. Sánchez-Rodríguez, E.; Hochberger-Roa, F.; Corona-Sánchez, R.; Barquera-Lozada, J.; Toscano, R.; Urrutigoity, M.; Gouygou, M.; Ortega-Alfaro, M.; López-Cortés, J. Chiral bidentate [N, S]-ferrocene ligands based on a thiazoline framework. Synthesis and use in palladium-catalyzed asymmetric allylic alkylation. *Dalton Trans.* **2017**, *46*, 1510–1519. [[CrossRef](#)]
98. Xu, D.; Zhang, J.; Dai, L. Chiral oxazolonyl hydroxyl ferrocene catalysts: Synthesis and applications in asymmetric reactions. *ChemistrySelect* **2020**, *5*, 9443–9456. [[CrossRef](#)]

99. Xu, G.; Gao, P.; Colacot, T.J. Tunable unsymmetrical ferrocene ligands bearing a bulky di-1-adamantylphosphino motif for many kinds of csp²–csp³ couplings. *ACS Catal.* **2022**, *12*, 5123–5135. [[CrossRef](#)]
100. Cunningham, L.; Guiry, P.J. Design and synthesis of a ferrocene-based diol library and application in the hetero-Diels-Alder reaction. *Chem. Eur. J.* **2023**, *29*, e202203006. [[CrossRef](#)]
101. Qiao, L.; Zhou, X.; Li, X.; Du, W.; Yu, A.; Zhang, S.; Wu, Y. Synthesis and performance of chiral ferrocene modified silica gel for mixed-mode chromatography. *Talanta* **2017**, *163*, 94–101. [[CrossRef](#)]
102. Wang, Q.; Zhou, X.; Li, Q.; Zhao, P.; Ren, Y.; Jiang, T.; Shen, S. Fabrication of a ferrocene-based monolithic column with a network structure and its application in separation of protein and small molecules. *J. Chromatogr. B* **2019**, *1114*, 71–75. [[CrossRef](#)]
103. Fatima, S.; Sharma, R.; Asghar, F.; Kamal, A.; Badshah, A.; Kraatz, H.-B. Study of new amphiphiles based on ferrocene containing thioureas as efficient corrosion inhibitors: Gravimetric, electrochemical, SEM and DFT studies. *J. Ind. Eng. Chem.* **2019**, *76*, 374–387. [[CrossRef](#)]
104. Nazir, U.; Akhter, Z.; Janjua, N.K.; Asghar, M.A.; Kanwal, S.; Butt, T.M.; Sani, A.; Liaqat, F.; Hussain, R.; Shah, F.U. Biferrocenyl Schiff bases as efficient corrosion inhibitors for an aluminium alloy in HCl solution: A combined experimental and theoretical study. *RSC Adv.* **2020**, *10*, 7585–7599. [[CrossRef](#)] [[PubMed](#)]
105. Nieuwenhuijsen, M.J.; Toledano, M.B.; Eaton, N.E.; Fawell, J.; Elliott, P. Chlorination disinfection byproducts in water and their association with adverse reproductive outcomes: A review. *Occup. Environ. Med.* **2000**, *57*, 73–85. [[CrossRef](#)] [[PubMed](#)]
106. Yang, S.; Chen, S.; Fan, J.; Shang, T.; Huang, D.; Li, G. Novel mesoporous organosilica nanoparticles with ferrocene group for efficient removal of contaminants from wastewater. *J. Colloid Interface Sci.* **2019**, *554*, 565–571. [[CrossRef](#)] [[PubMed](#)]
107. Yang, X.; Liu, H. Diphenylphosphine-substituted ferrocene/silsesquioxane-based hybrid porous polymers as highly efficient adsorbents for water treatment. *ACS Appl. Mater. Interfaces* **2019**, *11*, 26474–26482. [[CrossRef](#)]
108. Zhou, W.; Wang, L.; Yu, H.; Yang, X.; Chen, Q.; Wang, J. Synthesis of a novel ferrocene-based epoxy compound and its burning rate catalytic property. *RSC Adv.* **2016**, *6*, 53679–53687. [[CrossRef](#)]
109. Zhao, L.; Wang, F.; Weng, X.; Li, R.; Zhou, X.; Lin, H.; Yu, H.; Liao, B.-Q. Novel indicators for thermodynamic prediction of interfacial interactions related with adhesive fouling in a membrane bioreactor. *J. Colloid Interface Sci.* **2017**, *487*, 320–329. [[CrossRef](#)]
110. Wang, L.; Yu, H.; Saleem, M.; Akram, M.; Khalid, H.; Abbasi, N.M.; Yang, X. Synthesis of ethylene diamine-based ferrocene terminated dendrimers and their application as burning rate catalysts. *J. Colloid Interface Sci.* **2017**, *487*, 38–51.
111. Cheng, W.; Shi, X.; Zhang, Y.; Jian, Y.; Zhang, G. Novel ferrocene-based 1, 2, 3-triazolyl compounds: Synthesis, anti-migration properties and catalytic effects on oxidizers during combustion. *Inorganica Chim. Acta* **2020**, *502*, 119374. [[CrossRef](#)]
112. Rahimpour, K.; Teimuri-Mofrad, R.; Abbasi, H.; Parchehbaf, M.; Abedinpour, S.; Soleimani, S. Synthesis, characterization and properties investigation of [4-(dimethylsilyl) butyl] alkylferrocene grafted HTPB as novel ferrocene based burning rate accelerator catalysts for composite gas generators. *Polym-Plast. Techn. Mat.* **2019**, *58*, 2056–2065. [[CrossRef](#)]
113. Lv, X.; Huang, C.; Tameev, A.; Qian, L.; Zhu, R.; Katin, K.; Maslov, M.; Nekrasov, A.; Zhang, C. Electrochemical polymerization process and excellent electrochromic properties of ferrocene-functionalized polytriphenylamine derivative. *Dyes Pigm.* **2019**, *163*, 433–440. [[CrossRef](#)]
114. Beitollahi, H.; Khalilzadeh, M.A.; Tajik, S.; Safaei, M.; Zhang, K.; Jang, H.W.; Shokouhimehr, M. Recent advances in applications of voltammetric sensors modified with ferrocene and its derivatives. *ACS Omega* **2020**, *5*, 2049–2059. [[CrossRef](#)]
115. Borchers, P.S.; Strumpf, M.; Friebe, C.; Nischang, I.; Hager, M.D.; Elbert, J.; Schubert, U.S. Aqueous redox flow battery suitable for high temperature applications based on a tailor-made ferrocene copolymer. *Adv. Energy Mater.* **2020**, *10*, 2001825. [[CrossRef](#)]
116. Ertas, N.A.; Kavak, E.; Salman, F.; Kazici, H.C.; Kivrak, H.; Kivrak, A. Synthesis of ferrocene based naphthoquinones and its application as novel non-enzymatic hydrogen peroxide. *Electroanalysis* **2020**, *32*, 1178–1185. [[CrossRef](#)]
117. Shevaldina, E.V.; Opredeleznova, K.A.; Chichvarina, O.A.; Spiridonov, Y.Y.; Smol'yakov, A.F.; Dorovatovskii, P.V.; Moiseev, S.K. One-pot acid-free ferrocenylalkylation of azoles with α -ferrocenyl alcohols: Ferrocene-based plant growth regulators and herbicide safeners. *Appl. Organomet. Chem.* **2019**, *33*, e5228. [[CrossRef](#)]
118. Xiao, F.; Li, H.; Yan, X.; Yan, L.; Zhang, X.; Wang, M.; Qian, C.; Wang, Y. Graphitic carbon nitride/graphene oxide (g-C₃N₄/GO) nanocomposites covalently linked with ferrocene containing dendrimer for ultrasensitive detection of pesticide. *Anal. Chim. Acta* **2020**, *1103*, 84–96. [[CrossRef](#)]
119. Lewkowski, J.; Karpowicz, R.; Morawska, M.; Rychter, P.; Rogacz, D.; Lewicka, K.; Dobrzyński, P. Synthesis and ecotoxicological impact of ferrocene-derived amino-phosphonates using a battery of bioassays. *RSC Adv.* **2017**, *7*, 38399–38409. [[CrossRef](#)]
120. Peñalver, R.; Campillo, N.; López-García, I.; Hernández-Córdoba, M. Solid-phase microextraction for the determination of iron organic compounds in seawaters and soils by gas chromatography coupled to microwave-induced plasma with atomic emission detection spectrometry. *Microchem. J.* **2020**, *154*, 104630. [[CrossRef](#)]
121. Xing, G.; Luo, B.; Qin, J.; Wang, X.; Hou, P.; Zhang, H.; Wang, C.; Wang, J.; Li, A. A probe-free electrochemical immunosensor for methyl jasmonate based on ferrocene functionalized-carboxylated graphene-multi-walled carbon nanotube nanocomposites. *Talanta* **2021**, *232*, 122477. [[CrossRef](#)]
122. Ibrokhim, A.; Dilnoza, K. Synthesis of ferrocene-containing liquid nitrogen fertilizers and study of their biological activity. *Univers. Химия И Биология* **2021**, *9*, 91–94.
123. Jolly, P.; Batistuti, M.R.; Miodek, A.; Zhuravski, P.; Mulato, M.; Lindsay, M.A.; Estrela, P. Highly sensitive dual mode electrochemical platform for microRNA detection. *Sci. Rep.* **2016**, *6*, 36719. [[CrossRef](#)]

124. Ning, S.; Zhou, M.; Liu, C.; Waterhouse, G.I.; Dong, J.; Ai, S. Ultrasensitive electrochemical immunosensor for avian leukosis virus detection based on a β -cyclodextrin-nanogold-ferrocene host-guest label for signal amplification. *Anal. Chim. Acta* **2019**, *1062*, 87–93. [[CrossRef](#)] [[PubMed](#)]
125. Kaneyoshi, S.; Zou, T.; Ozaki, S.; Takeuchi, R.; Udou, A.; Nakahara, T.; Fujimoto, K.; Fujii, S.; Sato, S.; Takenaka, S. Cyclic naphthalene diimide with a ferrocene moiety as a redox-active tetraplex-dna ligand. *Chem. Eur. J.* **2020**, *26*, 139–142. [[CrossRef](#)] [[PubMed](#)]
126. Jia, D.-G.; Zheng, J.-A.; Fan, Y.-R.; Yu, J.-Q.; Wu, X.-L.; Wang, B.-J.; Yang, X.-B.; Huang, Y. Ferrocene appended naphthalimide derivatives: Synthesis, DNA binding, and in vitro cytotoxic activity. *J. Organomet. Chem.* **2019**, *888*, 16–23. [[CrossRef](#)]
127. Konkol'ová, E.; Janočková, J.; Perjési, P.; Vašková, J.; Kožurková, M. Selected ferrocenyl chalcones as DNA/BSA-interacting agents and inhibitors of DNA topoisomerase I and II activity. *J. Organomet. Chem.* **2018**, *861*, 1–9. [[CrossRef](#)]
128. De La Rica, R.; Aili, D.; Stevens, M.M. Enzyme-responsive nanoparticles for drug release and diagnostics. *Adv. Drug Deliv. Rev.* **2012**, *64*, 967–978. [[CrossRef](#)]
129. Mao, H.-L.; Qian, F.; Li, S.; Shen, J.-W.; Ye, C.-K.; Hua, L.; Zhang, L.-Z.; Wu, D.-M.; Lu, J.; Yu, R.-T. Delivery of doxorubicin from hyaluronic acid-modified glutathione-responsive ferrocene micelles for combination cancer therapy. *Mol. Pharm.* **2019**, *16*, 987–994. [[CrossRef](#)]
130. Zhang, Y.; Wang, C.; Huang, W.; Haruehanroengra, P.; Peng, C.; Sheng, J.; Han, B.; He, G. Application of organocatalysis in bioorganometallic chemistry: Asymmetric synthesis of multifunctionalized spirocyclic pyrazolone–ferrocene hybrids as novel RalA inhibitors. *Org. Chem. Front.* **2018**, *5*, 2229–2233. [[CrossRef](#)]
131. Messina, P.; Labbé, E.; Buriez, O.; Hillard, E.A.; Vessières, A.; Hamels, D.; Top, S.; Jaouen, G.; Frapart, Y.M.; Mansuy, D. Deciphering the activation sequence of ferrociphenol anticancer drug candidates. *Chem. Eur. J.* **2012**, *18*, 6581–6587. [[CrossRef](#)]
132. Gulam Farooq, M.; Lokhande, M.V. Synthesis of ferrocene based organometallic compounds & antimicrobial activity. *J. Appl. Chem.* **2014**, *7*, 2278–5736.
133. Ahmad, A.; Mahal, K.; Padhye, S.; Sarkar, F.H.; Schobert, R.; Biersack, B. New ferrocene modified lawsone Mannich bases with anti-proliferative activity against tumor cells. *J. Saudi Chem. Soc.* **2017**, *21*, 105–110. [[CrossRef](#)]
134. Realista, S.; Quintal, S.; Martinho, P.N.; Melato, A.I.; Gil, A.; Esteves, T.; Carvalho, M.D.D.; Ferreira, L.P.; Vaz, P.D.; Calhorda, M.J. Electrochemical studies and potential anticancer activity in ferrocene derivatives. *J. Coord. Chem.* **2017**, *70*, 314–327. [[CrossRef](#)]
135. Pedotti, S.; Ussia, M.; Patti, A.; Musso, N.; Barresi, V.; Condorelli, D.F. Synthesis of the ferrocenyl analogue of clotrimazole drug. *J. Organomet. Chem.* **2017**, *830*, 56–61. [[CrossRef](#)]
136. Ren, S.-Z.; Wang, Z.-C.; Zhu, D.; Zhu, X.-H.; Shen, F.-Q.; Wu, S.-Y.; Chen, J.-J.; Xu, C.; Zhu, H.-L. Design, synthesis and biological evaluation of novel ferrocene-pyrazole derivatives containing nitric oxide donors as COX-2 inhibitors for cancer therapy. *Eur. J. Med. Chem.* **2018**, *157*, 909–924. [[CrossRef](#)]
137. Banerjee, R.; Kumar, H.; Banerjee, M. Medicinal significance of furan derivatives: A review. *Int. J. Res. Phytochem. Pharmacol.* **2015**, *5*, 48–57.
138. Fouda, M.F.; Abd-Elzaher, M.M.; Abdelsamaia, R.A.; Labib, A.A. On the medicinal chemistry of ferrocene. *Appl. Organomet. Chem.* **2007**, *21*, 613–625. [[CrossRef](#)]
139. Tombul, M.; Bulut, A.; Türk, M.; Uçar, B.; Işıl, Ö. Synthesis and biological activity of ferrocenyl furoyl derivatives. *Inorg. Nano-Met. Chem.* **2017**, *47*, 865–869. [[CrossRef](#)]
140. Sansook, S.; Tuo, W.; Lemaire, L.; Tourteau, A.; Barczyk, A.; Dezitter, X.; Klupsch, F.; Leleu-Chavain, N.; Tizzard, G.J.; Coles, S.J. Synthesis of bioorganometallic nanomolar-potent CB₂ agonists containing a ferrocene unit. *Organometallics* **2016**, *35*, 3361–3368. [[CrossRef](#)]
141. Maračić, S.; Lapić, J.; Djaković, S.; Opačak-Bernardi, T.; Glavaš-Obrovac, L.; Vrček, V.; Raić-Malić, S. Quinoline and ferrocene conjugates: Synthesis, computational study and biological evaluations. *Appl. Organomet. Chem.* **2019**, *33*, e4628. [[CrossRef](#)]
142. Wei, J.-N.; Jia, Z.-D.; Zhou, Y.-Q.; Chen, P.-H.; Li, B.; Zhang, N.; Hao, X.-Q.; Xu, Y.; Zhang, B. Synthesis, characterization and antitumor activity of novel ferrocene-coumarin conjugates. *J. Organomet. Chem.* **2019**, *902*, 120968. [[CrossRef](#)]
143. Mukaya, E.H.; Van Zyl, R.; Van Vuuren, N.J.; Yangkou Mbianda, X. Polymeric prodrugs containing neridronate and ferrocene: Synthesis, characterization, and antimalarial activity. *Int. J. Polym. Mater.* **2018**, *67*, 401–409. [[CrossRef](#)]
144. De Lange, C.; Coertzen, D.; Smit, F.J.; Wentzel, J.F.; Wong, H.N.; Birkholtz, L.-M.; Haynes, R.K.; David, D.D. Synthesis, in vitro antimalarial activities and cytotoxicities of amino-artemisinin-ferrocene derivatives. *Bioorganic Med. Chem. Lett.* **2018**, *28*, 289–292. [[CrossRef](#)] [[PubMed](#)]
145. Mbaba, M.; de la Mare, J.-A.; Sterrenberg, J.N.; Kajewole, D.; Maharaj, S.; Edkins, A.L.; Isaacs, M.; Hoppe, H.C.; Khanye, S.D. Novobiocin–ferrocene conjugates possessing anticancer and antiplasmodial activity independent of HSP90 inhibition. *JBIC J. Biol. Inorg. Chem.* **2019**, *24*, 139–149. [[CrossRef](#)] [[PubMed](#)]
146. Minić, A.; Van de Walle, T.; Van Hecke, K.; Combrinck, J.; Smith, P.J.; Chibale, K.; D'hooghe, M. Design and synthesis of novel ferrocene-quinoline conjugates and evaluation of their electrochemical and antiplasmodium properties. *Eur. J. Med. Chem.* **2020**, *187*, 111963. [[CrossRef](#)] [[PubMed](#)]
147. Štimac, A.; Lapić, J.; Blasina, V.; Lukinac, M.; Djaković, S.; Crnolatac, I.; Frkanec, L.; Frkanec, R. Adamantyl ferrocene derivatives: Antioxidant abilities and effects on model lipid membranes. *Appl. Organomet. Chem.* **2018**, *32*, e4042. [[CrossRef](#)]

148. Bano, S.; Khan, A.-U.; Asghar, F.; Usman, M.; Badshah, A.; Ali, S. Computational and pharmacological evaluation of Ferrocene-based acyl ureas and homoleptic cadmium carboxylate derivatives for anti-diabetic potential. *Front. Pharmacol.* **2018**, *8*, 1001. [[CrossRef](#)]
149. Mbaba, M.; Dingle, L.M.; Cash, D.; de la Mare, J.-A.; Laming, D.; Taylor, D.; Hoppe, H.C.; Edkins, A.L.; Khanye, S.D. Repurposing a polymer precursor: Synthesis and in vitro medicinal potential of ferrocenyl 1, 3-benzoxazine derivatives. *Eur. J. Med. Chem.* **2020**, *187*, 111924. [[CrossRef](#)]
150. Paucar, R.; Martín-Escolano, R.; Moreno-Viguri, E.; Cirauqui, N.; Rodrigues, C.R.; Marín, C.; Sánchez-Moreno, M.; Pérez-Silanes, S.; Ravera, M.; Gabano, E. A step towards development of promising trypanocidal agents: Synthesis, characterization and in vitro biological evaluation of ferrocenyl Mannich base-type derivatives. *Eur. J. Med. Chem.* **2019**, *163*, 569–582. [[CrossRef](#)]
151. Parveen, H.; Alatawi, R.A.S.; Alsharif, M.A.; Alahmdi, M.I.; Mukhtar, S.; Khan, S.A.; Hasan, S.; Khan, A.U. Novel pyrazoline-based organometallic compounds containing ferrocenyl and quinoline units: Synthesis, characterization and microbial susceptibilities. *Appl. Organomet. Chem.* **2018**, *32*, e4257. [[CrossRef](#)]
152. Hassell-Hart, S.; Runcie, A.; Krojer, T.; Doyle, J.; Lineham, E.; Ocasio, C.A.; Neto, B.A.; Fedorov, O.; Marsh, G.; Maple, H. Synthesis and biological investigation of (+)-JD1, an organometallic BET bromodomain inhibitor. *Organometallics* **2019**, *39*, 408–416. [[CrossRef](#)]
153. Gadhachanda, V.R.; Eastman, K.J.; Wang, Q.; Phadke, A.S.; Patel, D.; Yang, W.; Marlor, C.W.; Deshpande, M.; Huang, M.; Wiles, J.A. Ferrocene-based inhibitors of hepatitis C virus replication that target NS5A with low picomolar in vitro antiviral activity. *Bioorganic Med. Chem. Lett.* **2018**, *28*, 3463–3471. [[CrossRef](#)]
154. Wang, Y.; Sha, H.; Ke, H.; Xiong, X.; Jia, N. A sandwich-type electrochemiluminescence aptasensor for insulin detection based on the nano-C60/BSA@ luminol nanocomposite and ferrocene derivative. *Electrochim. Acta* **2018**, *290*, 90–97. [[CrossRef](#)]
155. Huang, X.; Miao, J.; Fang, J.; Xu, X.; Wei, Q.; Cao, W. Ratiometric electrochemical immunosensor based on L-cysteine grafted ferrocene for detection of neuron specific enolase. *Talanta* **2022**, *239*, 123075. [[CrossRef](#)]

Disclaimer/Publisher's Note: The statements, opinions and data contained in all publications are solely those of the individual author(s) and contributor(s) and not of MDPI and/or the editor(s). MDPI and/or the editor(s) disclaim responsibility for any injury to people or property resulting from any ideas, methods, instructions or products referred to in the content.